UNIVERSITA' DEGLI STUDI DI PADOVA

Dipartimento di Ingegneria Elettrica

Scuola di Dottorato di Ricerca in Ingegneria Industriale

Indirizzo Energetica

Ciclo XX

SYSTEMATIC INVESTIGATION ON SWEPT AND LEANED TRANSONIC COMPRESSOR ROTOR BLADES

Direttore della Scuola: Prof. Paolo F. Bariani

Supervisore: Prof. Vittorio Quaggiotti

Correlatore: Prof. Ernesto Benini

Dottorando: Roberto Biollo

31 gennaio 2008

INDEX

Sommario

Gli stadi transonici di compressione si stanno diffondendo sempre più nei moderni motori aeronautici a reazione, grazie alla loro capacità di fornire elevati rapporti di compressione (anche doppi rispetto ad un tradizionale stadio subsonico) mantenendo una buona efficienza operativa. Ciò permette la riduzione di pesi e ingombri dell'intero sistema di compressione grazie alla riduzione del numero degli stadi. Attualmente si sta investendo molto nel tentativo di migliorarne ulteriormente le prestazioni, soprattutto in termini di efficienza operativa. Un piccolo incremento del rendimento può avere un impatto notevole sul risparmio di combustibile nelle tratte a lungo raggio, potendo quindi rappresentare un fattore di successo del prodotto.

L'elevato rapporto di compressione fornito dagli stadi transonici è legato all'elevata velocità periferica di cui vengono dotati i relativi rotori. L'elevata velocità periferica dà origine ad un flusso relativo supersonico verso la periferia palare, con conseguente formazione di urti aerodinamici. La presenza dell'urto e la sua interazione con i flussi secondari (strato limite, flussi di estremità palare etc.) complicano notevolmente il campo fluido del rotore, rendendo particolarmente complesso il processo di ottimizzazione dell'intero stadio.

Oggigiorno si stanno studiando soluzioni tecnologiche innovative per migliorare le prestazioni di tali rotori. L'adozione di palettature curve (swept and leaned blades) al posto delle ben più convenzionali palettature a sviluppo radiale, sembra essere una delle soluzioni più promettenti. Tuttavia, l'impatto di una data curvatura palare sul comportamento aerodinamico del rotore non è ancora ben prevedibile, sia per quanto riguarda le caratteristiche interne di flusso sia per quel che concerne le prestazioni complessive. Sulla scia di queste osservazioni, è stata qui condotta con successo un'analisi numerico-sistematica volta a comprendere meglio gli effetti della curvatura palare sull'assetto aerodinamico dei rotori in oggetto, nonché valutare i benefici ottenibili da un tale approccio di ottimizzazione. Il lavoro è stato condotto come di seguito descritto.

E’ stata dapprima valutata l’accuratezza di un noto codice fluidodinamico commerciale (ANSYS CFX) nel simulare il comportamento aerodinamico di un rotore transonico. In sostanza, con tale codice sono stati sviluppati e testati alcuni modelli 3-D (diversi per griglia, schema di discretizzazione, modello di turbolenza etc.) del ben noto NASA Rotor 37 (il rotore di uno stadio di compressione sperimentale ben documentato in letteratura e che ben rappresenta gli intensi fenomeni di flusso che caratterizzano le palettature transoniche). I modelli sono stati testati confrontando le prestazioni complessive e le caratteristiche di flusso calcolate con i dati sperimentali disponibili in letteratura.

Verificata l’attendibilità dei risultati forniti dal codice, i modelli più accurati sono stati utilizzati per valutare l’impatto della curvatura palare sulle performance dello stesso Rotor 37 (dotato di palette a sviluppo pressoché radiale). A partire dal Rotor 37, sono stati modellati nuovi rotori agendo semplicemente sulla forma della linea di incernieramento dei profili, allo scopo di calcolarne il comportamento aerodinamico e confrontarlo con quello del rotore di base. In particolare, sono stati modellati 26 nuovi rotori con palette curvate sul piano meridiano (axial sweep) e 26 nuovi rotori con palette curvate sul piano circonferenziale (tangential lean). In breve, la linea di incernieramento del Rotor 37 è stata ridefinita come una spline passante per tre punti di controllo (posti al 33%, 67% e 100% dell’altezza palare, ovvero dello “span”) e le nuove palettature sono state ottenute muovendo sistematicamente tali punti di controllo da un lato e dall’altro rispetto alla posizione originale (sul piano meridiano nel caso dello sweep e sul piano circonferenziale nel caso del lean), in posizioni opportunamente definite e mantenendo lo stesso livello di span.

Sulla base delle simulazioni condotte e dei risultati ottenuti, per i quali si rinvia alle conclusioni della tesi, il lavoro svolto ha messo in luce quanto segue.

a) Il codice adottato ha mostrato una soddisfacente accuratezza nel predire l’assetto aerodinamico del Rotor 37, sia in termini di prestazioni complessive sia in termini di caratteristiche di flusso, rivelandosi uno strumento di importanza notevole per una migliore comprensione del complesso campo fluido sviluppato dai rotori in oggetto e per un più efficace processo di ottimizzazione.

b) La forma della linea di incernieramento dei profili ha mostrato un considerevole impatto sui vari fenomeni di flusso sviluppati dal rotore (urti aerodinamici, flussi secondari quali scie palari, strato limite, trafilamenti alla periferia palare etc.), con la possibilità di poter ridurre gli effetti negativi ad essi associati (dissipazioni energetiche, blockage, instabilità indotte etc.).

c) Il punto precedente conferma la possibilità di poter migliorare in modo apprezzabile le prestazioni di un rotore transonico agendo sulla curvatura palare (una versione modificata del Rotor 37 simulata in ambiente CFX, ottenuta conferendo alla linea di incernieramento originale un'appropriata curvatura tridimensionale, ha mostrato un incremento dell'efficienza complessiva di 1.2 punti percentuali in prossimità della condizione di progetto e un campo operativo stabile più ampio del 50% rispetto al rotore di partenza).

Gli effetti specifici indotti dalle differenti linee di incernieramento sul campo fluido del Rotor 37 sono stati analizzati nel dettaglio e saranno argomentati minuziosamente, conducendo ad una sintesi degli effetti dello sweep assiale e del lean tangenziale sul comportamento aerodinamico del rotore analizzato e, in linea di principio, dei rotori transonici ad esso non eccessivamente dissimili, fino all'individuazione delle curvature più promettenti. Saranno, inoltre, presentate alcune analisi FEM (Finite Element Method) per valutare l'impatto di una tale soluzione tecnologica sul comportamento strutturale della palettatura.

Summary

In modern high-performance aircraft gas-turbine engines, compressor stages must provide high values of both efficiency and compression ratio. This is important to minimize the fuel consumption (a small increment in efficiency can result in huge savings in fuel costs and determine a key factor) and decrease the engine weight and size thanks to the reduction of number of stages (with a positive impact on investment and operational costs). In response to these requirements, transonic axial-flow compressor stages have been developed for many years and are today widely used in aircraft engines.

Even though the performance of transonic compressors has today reached a high level, engine manufactures are oriented toward increasing it further. At the present, the application of sweep and lean (in other words, the use of a curvilinear blade stacking line) on rotor blades is considered one of the most promising technological evolutions to improve the aerodynamic behavior of such machines. However, the presence of intense shock waves and their interaction with secondary flows (wall boundary layer, tip clearance flows etc.) lead to an extremely complex flow field, making the aerodynamic effects of sweep and lean hardly predictable and the development of three-dimensional shaped transonic rotor blades a difficult task.

In this work, a systematic numerical investigation on the impact of blade stacking line shape ("blade curvature" in the following) on internal flow features and overall performance of transonic compressor rotors was undertaken, with the aim to give the compressor designers a better understanding of sweep and lean effects. The work was carried out as follows.

Initially, the capability of the commercial CFD (Computational Fluid Dynamics) code ANSYS CFX to compute the flow within a transonic rotor was explored in detail. This was done defining a few numerical models (different for grid, discretization scheme, turbulence model etc.) of the well-known NASA Rotor 37 (a test compressor rotor well representative of complex flow structures in transonic bladings) and validating them against experimental data available in literature. The agreement between computed and ex-

perimental results was accurately verified in terms of both overall performance and internal flow features (shock, tip clearance flows, blade wakes etc.).

Then, the “best” models resulting from validation were used to investigate the impact of blade curvature on the performance of Rotor 37 (which is a radially-stacked rotor). Various axially swept and tangentially leaned rotors were developed starting from the Rotor 37 by changing the meridional and circumferential shape of the original stacking line respectively. In short, the original stacking line was considered as a spline passing through three control points, located at 33%, 67% and 100% span from the hub. 26 new swept rotors were obtained moving systematically each control point upstream and downstream the original position (on properly selected axial locations), maintaining the same span level. Similarly, 26 new leaned rotors were obtained by changing systematically the circumferential position of the same control points (both in the direction of rotor rotation and against it). The aerodynamic behavior of all the new rotors was simulated, analyzed in detail and compared to that of baseline rotor.

On the basis of numerical results obtained (see Conclusions for details), the work led to the following.

a) The careful evaluation of code CFD capabilities made it possible the definition of accurate 3-D models for a quite reliable prediction of the aerodynamic behavior of transonic compressor rotors (in terms of both overall performance and internal flow phenomena), providing an important tool for a better understanding of complex flow structures which take place in these machines (shock, shock-tip endwall flows interactions, shock-boundary layer interaction etc.) and to give insights on possible optimization techniques.

b) Blade curvature showed a considerable influence on shock waves and secondary flows, leading to the possibility to reduce the entropy generation and aerodynamic losses associated with them.

c) The previous point confirms the possibility to improve the overall performance of a transonic compressor rotor using blade curvature concept (a new version of Rotor 37, obtained by giving the blade a proper 3-D curvature and simulated using CFX, gave an efficiency of about 1.2% higher than that of baseline rotor near the design condition, as well as a stable working range of about 50% wider).

The changes in the flow field of Rotor 37 due to the use of different stacking lines will be argued accurately, as well as the effects of induced flow changes on the overall performance, leading to a helpful synthesis of the impact of axial sweep and tangential lean on the aerodynamic behavior of the rotor (and, presumably, on the aerodynamic behavior of all the transonic compressor rotors similar to the Rotor 37). FEM analyses will be also carried out to evaluate the impact of sweep and lean on the structural behavior of the blade, with the aim to verify the practical feasibility of curved blades in transonic compressor rotors.

Notation

k	specific heat capacity ratio
p	absolute static pressure
t	absolute static temperature
P	absolute total pressure
T	absolute total temperature

Acronyms

CFD	Computational Fluid Dynamics
RANS	Reynolds-Averaged Navier-Stokes
UDS	Upwind Differencing Scheme
LPS	Linear Profile Scheme
PAC	Physical Advection Correction
SST	Shear Stress Transport
FEM	Finite Element Method
TE	Trailing Edge
PS	Pressure Side
SS	Suction Side

Introduction

Transonic axial-flow compressor rotors are today widely used in aircraft engines to obtain maximum pressure ratios per single stage while maintaining high efficiencies. High stage pressure ratios are important because make it possible to reduce the engine weight and size and, therefore, investment and operational costs. Performance of such machines has today reached a high level but engine manufacturers are oriented toward increasing it further. A small increment in efficiency, for instance, can result in huge savings in fuel costs and determine a key factor for product success. Another important target is the improvement of rotor stability toward near stall condition, resulting in a wider working range.

Today, the application of sweep and lean (in other words, the use of a curvilinear stacking line leading to a three-dimensional shaped blade) is considered one of the most promising technological evolutions to improve the performance of transonic compressor rotors. Many research efforts were spent in this direction and many hopeful results can be found in literature. However, the effects of sweep and lean on the aerodynamic behavior of transonic rotors were not completely understood and further studies are needed. This is mainly due to the complexity of the flow field inside these machines.

Effectively, the flow field that develops inside a transonic compressor rotor is extremely complex and presents many challenges to compressor designers, who have to deal with several and concurring phenomena such as shock waves, secondary flows, shock-boundary layer interaction etc. This complexity is accentuated if the blade is swept and/or leaned, due to a mutual interaction among the above phenomena.

The use of CFD (Computational Fluid Dynamics) can be of great help in giving insights on the flow structures and several examples of CFD calculations on transonic rotor blades can be found in literature. However, the reliability of numerical results has not always been proven and checked with the required considerations. This is true especially for commercial codes, which are today widespread among engine manufacturers, but the accuracy of which has not always been measured extensively and rigorously.

The purposes of this work are the following:

i. to explore the capability of a well-known commercial CFD code (ANSYS CFX) to compute the flow within a transonic rotor (this will be done carrying out various numerical models of a transonic compressor rotor, the NASA Rotor 37, and by accurately validating them against experimental data available in literature);

ii. to use the "best" models, resulting from validation, to study the aerodynamic impact of blade curvature on the performance of the original compressor blade of Rotor 37, by changing systematically its shape and by comparing the new performance with that of the original solution (this will be carried out by analysing in detail the computed flow within the blade passage of the original and the new blades and, in particular, the shock wave pattern and the shock interaction with the main flow as well as with wall boundary layers).

The thesis consists of following main chapters.

- Chapter 1 gives an overview on transonic compressor rotors. It deals with the fundamentals of flow field, showing the complex flow features which characterize these machines. Some of the most promising technological solutions recently studied to improve transonic compressor performance are also presented, including sweep and lean.

- Chapter 2 is concerned with the CFD code validation. A careful assessment of numerical consistency and accuracy of different models of Rotor 37 is presented. The chapter ends with the choice of the "best" numerical models among those evaluated.

- Chapter 3 describes the investigated blade curvatures and shows their impact on the overall performance of Rotor 37. A first understanding on the effects of sweep and lean on the flow field is also dealt with. In addition, a FEM (Finite Element Method) analysis is carried out to evaluate the impact of blade curvature from the structural point of view.

- In Chapter 4, the aerodynamic effects of some among the most interesting blade curvatures are analyzed in detail, with the aim to better understand the impact of sweep and lean on the flow features.

- Finally, in Conclusions the main results obtained in this work are summed up.

CHAPTER 1

Transonic compressor rotors

1.1 Introduction

In modern high-performance aircraft gas turbine engines, compressor stages must provide high values of both efficiency and total pressure ratio. High values of total pressure ratio are important to decrease the number of stages and, consequently, the compressor weight and size (the compressor section is still 50-60% of the engine length and 40-50% of the weight). Actually, the current trend is to increase the stage total pressure ratio by giving the rotor a higher tip speed. This leads to higher relative flow velocities at the outer span and, consequently, to a transonic flow field (supersonic at the outer span and subsonic at the inner span). Transonic compressor rotors are the direct consequence of this trend.

However, transonic compressor rotors have slightly lower efficiency and operating range than traditional subsonic solutions. This is mainly due to the presence of intense shock waves close to the blade tip and over part of span. At the outer span, the relative flow is supersonic and the deflection imposed by the blade pressure side wall gives rise to a shock wave, which starts from the blade leading edge and propagates into the blade passage (Figure 1.1(a)). As known, the shock is an irreversible process and induces entropy generation (i.e. aerodynamic losses in an adiabatic system without thermal sources), which negatively influences the overall rotor efficiency. Further, the interaction between the shock and secondary flows, such as tip clearance flows and wall boundary layers, has generally a negative impact on the local flow field, with detrimental effects on the overall rotor performance. The shock-tip clearance flows interaction is believed, for instance, to be one of the main stall-triggers in transonic compressor rotors.

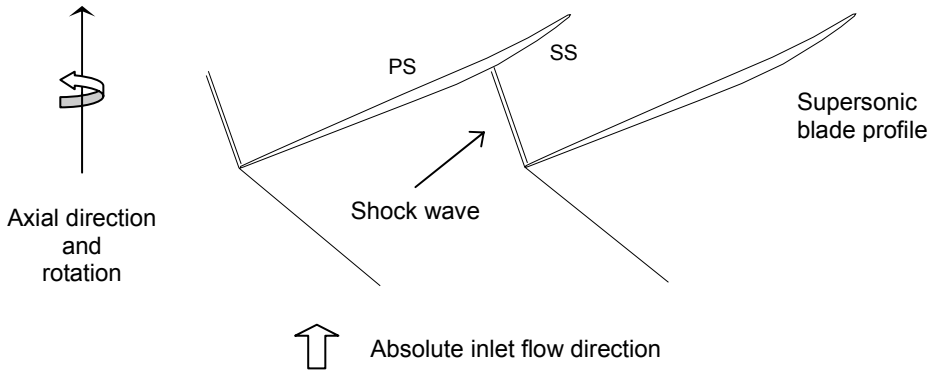

(a) Shock configuration – sketch.

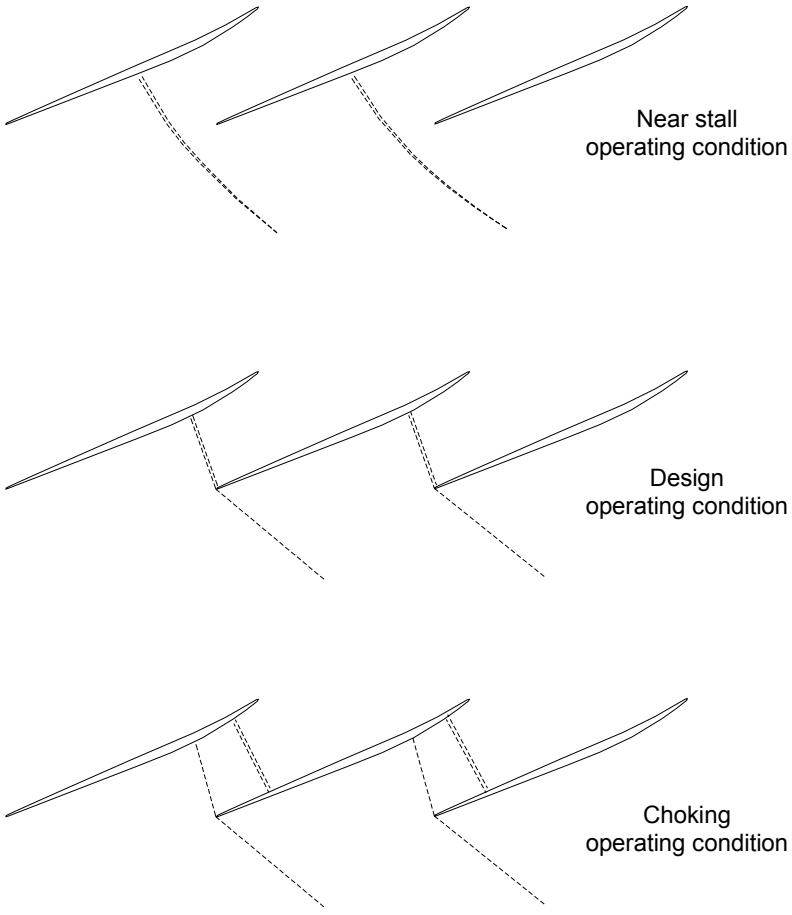

(b) Impact of operating condition (constant wheel speed).

Fig. 1.1 Shock wave configuration inside a transonic compressor rotor. (Blade-to-blade views)

Depending on rotor geometry and operating condition, the shock can develop in different ways. It can be more or less inclined to the incoming flow. It can bifurcate. Further shock waves can also develop more downstream inside the blade passage. Figure 1.1(b) shows, indicatively, the blade-to-blade shock configuration inside a generic transonic compressor rotor, moving from the choking condition to a near stall condition and maintaining a constant wheel speed. Generally, the shock shifts upstream and becomes normal to the incoming flow as the operating point moves toward lower mass flow operating conditions, as a consequence of the higher flow incidence due to the lower mass flow rate. This can also be observed in Figure 1.2, which shows some 3-D views of shock front at both peak efficiency and near stall conditions in a low hub-casing ratio transonic rotor.

The complexity of the flow field makes the aerodynamic optimization process of transonic compressor rotors very hard. Many theoretic, experimental and, in the last fifteen years, CFD analyses were carried out to better understand the aerodynamic behavior of these rotors, but many other research efforts are still needed. Some complex flow features are not still completely understood and, consequently, the optimization process remains hard.

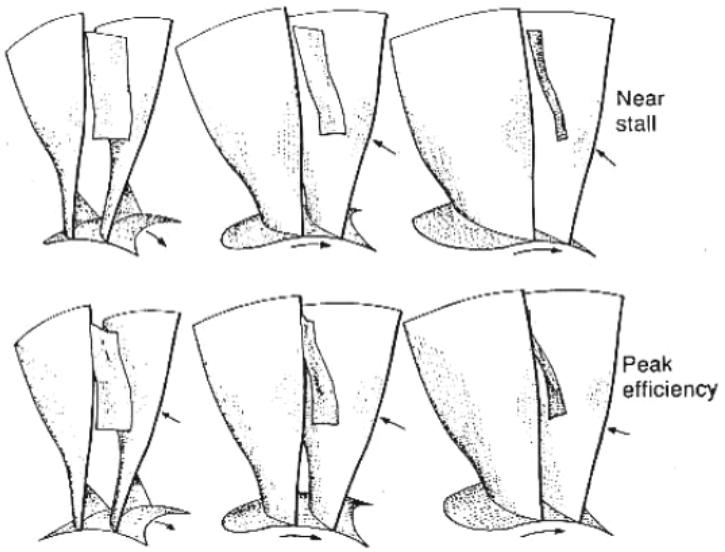

Fig. 1.2 Perspective views of shock in a transonic rotor (from Wood *et al.*, 1987). For each flow rate each of the three views is rotated by 20°.

1.2 The flow field

The knowledge of internal flow features is fundamental when trying to improve the aerodynamic behavior of a transonic compressor rotor. In particular, the impact of shock waves on the overall flow field must be understood clearly.

As said, transonic compressor rotors develop intense shock waves (generally normal or quasi-normal to the incoming flow), which are irreversible processes and hence source of entropy (the entropy creation occurs due to heat conduction and high viscous normal stresses within the shock). It is known, however, that the shock is a diffusion process and represents the most important diffusion system in these rotors (note that the profile camber and, consequently, the flow diffusion induced by the profile curvature are generally lower in transonic bladings than in subsonic ones).

Figure 1.3 shows the isoentropic (or adiabatic) efficiency η of the diffusion process associated with a normal shock in a one-dimensional flow through a duct with constant cross-sectional area. An ideal gas (constant specific heat capacities, k = 1.4) was considered. The parameter M_1 is the Mach number upstream the shock. Figure 1.3 was derived using the following equations (the subscript "1" indicates a section upstream the shock while the subscript "2" a section downstream):

$$\eta = \frac{\left(p_2 / p_1\right)^{\frac{k-1}{k}} - 1}{\left(t_2 / t_1\right) - 1} \tag{1.1}$$

$$\frac{p_2}{p_1} = \frac{2kM_1^{\,2} - \left(k-1\right)}{\left(k+1\right)} \tag{1.2}$$

$$\frac{t_2}{t_1} = \frac{\left(2 + \left(k-1\right)M_1^{\,2}\right)\left(2kM_1^{\,2} - \left(k-1\right)\right)}{\left(k+1\right)^2 M_1^{\,2}} \tag{1.3}$$

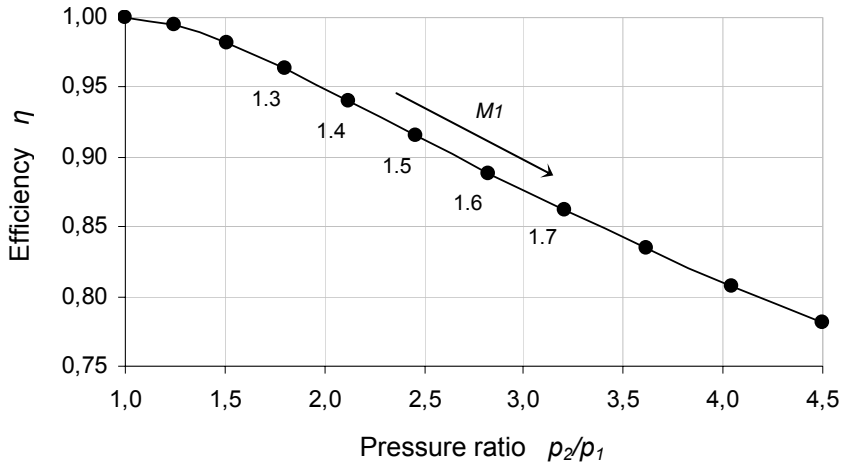

Fig. 1.3 Shock diffusion efficiency.

As shown, the diffusion efficiency decreases with the upstream Mach number, becoming unsatisfactory if the upstream Mach number is higher than 1.5. Generally, inlet relative Mach numbers in axial transonic compressor rotors exceeding about 1.4 are unusual and, at this condition, the shock can be considered a satisfactory diffusion mecha-

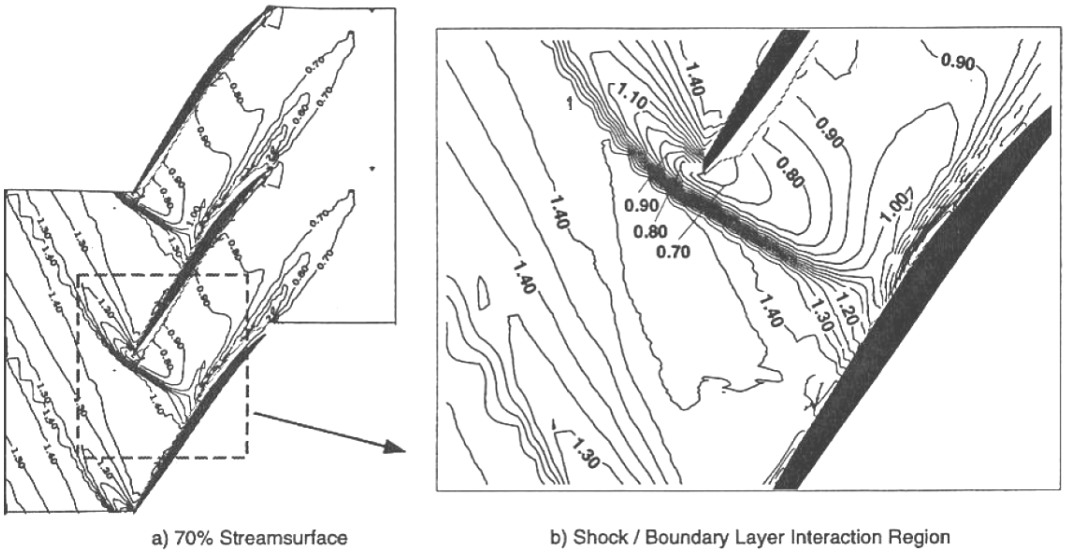

Fig. 1.4 Blade-to-blade view of measured relative Mach number (from Suder, 1998). (NASA Rotor 37 – design speed – low flow condition)

nism. Further, if the same pressure rise is accomplished by two oblique shock waves instead of by a single normal shock, the aerodynamic shock losses will be greatly reduced (further details on shock losses in turbomachines can be found in the 1993 International Gas Turbine Institute scholar lecture by Denton (1993)). Therefore, the shock can not be considered a problem in itself. The most serious aspects associated with the shock are due to its detrimental interactions with secondary flows, as remarked in the following.

At the outer half span region, the shock impacts strongly on the blade suction side and interacts negatively with the local boundary layer. Due to the adverse pressure gradient across the shock, a significant increment of boundary layer thickness is induced (Figure 1.4) and a separation bubble can occur. In case of separation, the boundary layer may reattach before the trailing edge or not. If not, larger and deeper blade wakes develop, leading to a considerable increment of aerodynamic losses.

Further, a strong outward radial fluid migration was generally observed inside the suction side boundary layer after the shock. This characteristic flow phenomenon is sketched in Figure 1.5. It induces an accumulation of low momentum fluid at the outer span region (which is considered to be detrimental for rotor stability) and causes a boundary layer thickening with a negative impact on the blade wake development. Further details on shock-boundary layer interaction, radial transport and wake development were provided by Hah and Reid (1992).

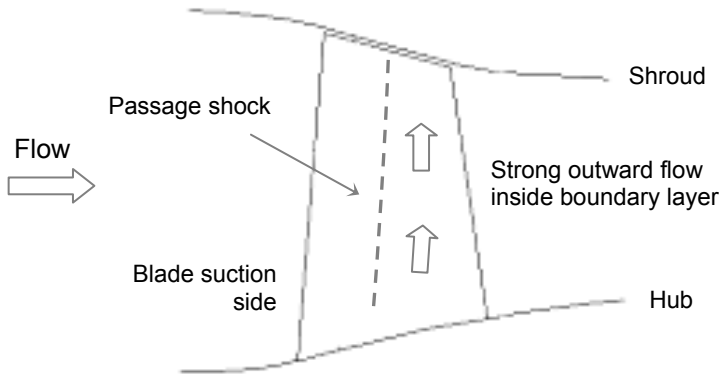

Fig. 1.5 Blade suction side boundary layer radial fluid flow – meridional view.

The most detrimental region in transonic compressor rotors is the tip endwall region. These rotors are typically unshrouded and the tip gap region develops intense secondary flows (Figure 1.6). The pressure difference between the suction side and pressure side drives the fluid through the blade tip gap, inducing a jet which propagates into the main flow. The interaction between the jet and the main flow gives rise to a vortex (known as "tip clearance vortex") which generally starts at the leading edge and develops into the passage. The complex flow structures arising from the interaction between these tip clearance flows, the casing boundary layer and the passage shock have detrimental effects on the overall rotor performance, since they induce aerodynamic losses (Fritsch *et al.*, 2000), blockage (Suder, 1998) and instabilities (Hofmann and Ballmann, 2002). The shock-tip clearance vortex interaction is believed, in particular, to have a key role on rotor instability. Interacting with the shock, the vortex is subject to a sudden and strong deceleration; at lower flow operating conditions, depending on the intensity of the interaction, vortex breakdown can occur inducing compressor stall (Figure 1.7).

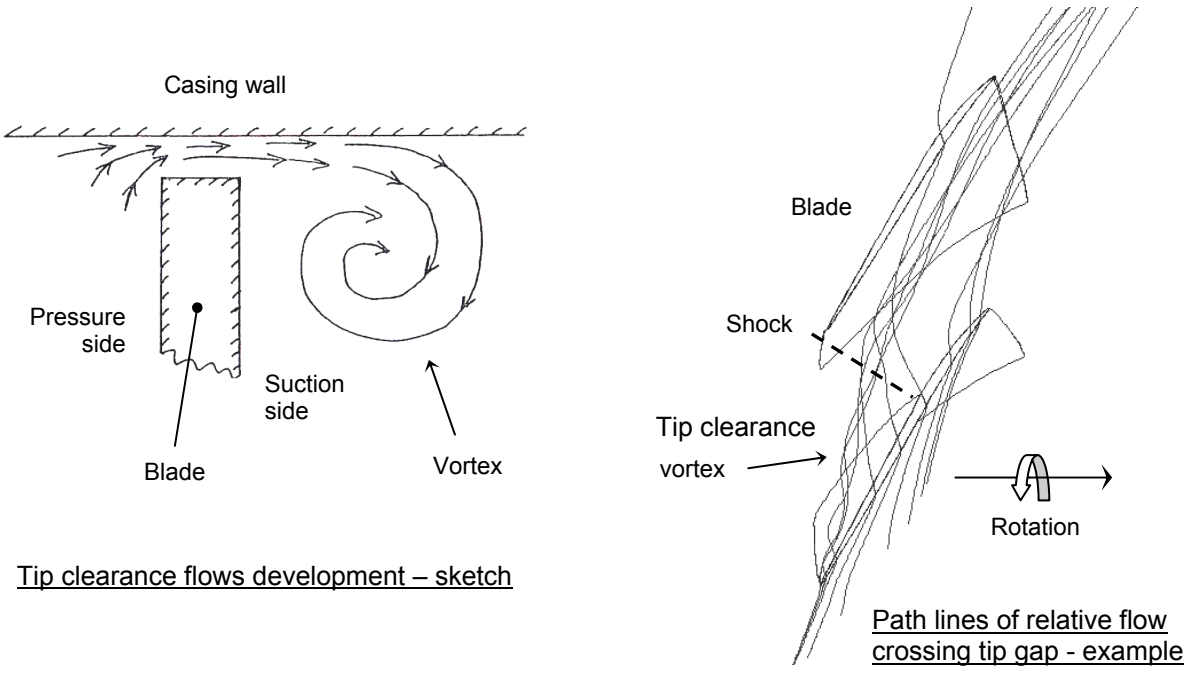

Fig. 1.6 Tip clearance gap secondary flows.

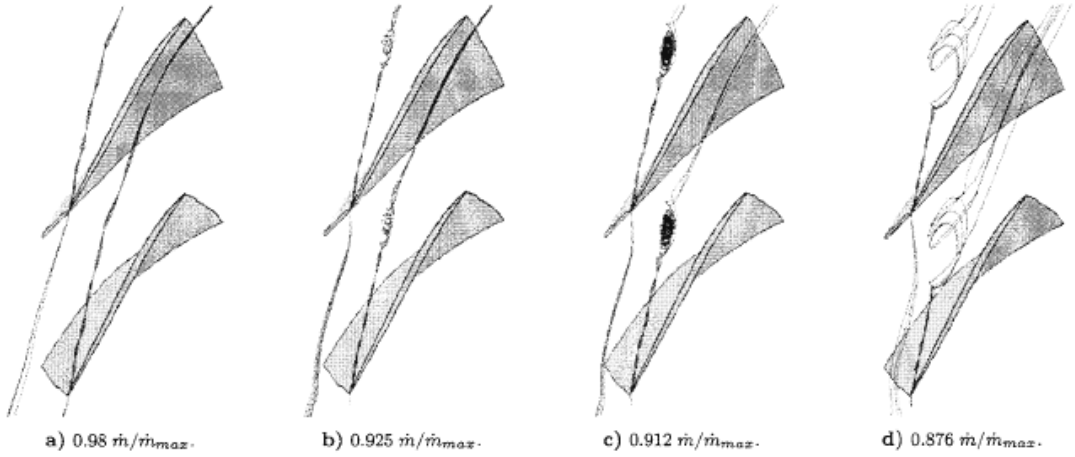

Fig. 1.7 Tip clearance vortex streamlines.
(From Hofmann and Ballmann, 2002)

1.3 Technological evolutions

Advanced technological solutions were developed to improve the aerodynamic behavior of transonic compressor rotors. Sweep and lean, casing treatment and tip injection can be considered the most important ones. They are briefly presented into the following.

Sweep and lean

Traditionally, rotor blades are radially-stacked. The application of sweep and/or lean leads to a curvilinear stacking line, i.e. to a three-dimensional shaped blade. Figure 1.8 gives the common definition of aerodynamic sweep and lean. As shown, sweep is defined as the movement of blade sections along the local chord direction, while lean the change in the perpendicular direction.

There are many aspects to be considered when trying to understand how sweep and lean influence the performance of a transonic blade row. The three-dimensional shock structure is one of the most important. As aforesaid, the shock starts from the blade leading edge and propagates into the blade passage. The application of sweep and/or lean modifies the spatial shape of the blade leading edge and, consequently, the spatial shape of the shock; an aft swept blade, for instance, develops an aft swept shock, at least far from the

tip (at the tip endwall region, the shock shape is influenced also by the presence of the casing, as explained below). It was also observed that the application of a 3-D blade curvature can induce the shock to change in two oblique shocks of lesser intensity (Benini, 2004; Jang *et al.*, 2006). In short, sweep and lean can lead to considerable changes in the overall shock configuration, influencing not only its shape and strength[1] but also its interactions with secondary flows.

The influence of sweep on shock structure and secondary flows has been widely analyzed in the literature and it seems to be of general agreement that forward sweep (i.e. upstream sweep) leads to significant benefits. Numerical and experimental analyses conducted by Hah *et al.* (1998) to evaluate the performance of a conventional unswept rotor, a

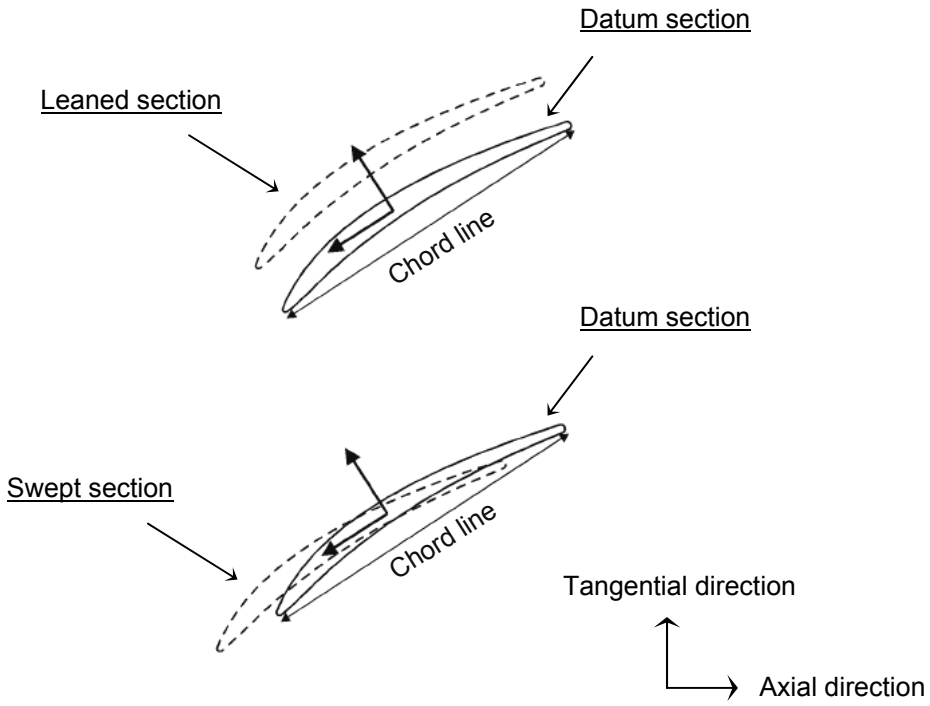

Fig. 1.8 Aerodynamic sweep and lean definition.

[1] The strength of a single shock front depends on both the upstream Mach number and the angle between the incoming flow direction and the shock front; for instance, a normal shock is stronger than an oblique one with the same upstream Mach number. At a higher strength corresponds higher aerodynamic losses.

forward swept rotor and an aft swept rotor showed that the forward swept rotor had a higher peak efficiency and a substantially larger stall margin than the baseline unswept rotor, and that the aft swept rotor had a similar peak efficiency with a significantly smaller stall margin. Similar results were obtained by Wadia *et al.* (1998) in a parallel investigation. On the other hand, however, Denton and Xu (2002) observed that the global effects of swept blades on transonic fan efficiency and total pressure ratio are not very remarkable, but confirmed the possibility to improve the compressor stability using forward sweep.

Near the casing, sweep impacts on shock structure in a particular way. As described by Hah *et al.* (1998), the shock must intersect the casing at right angles (a phenomenon

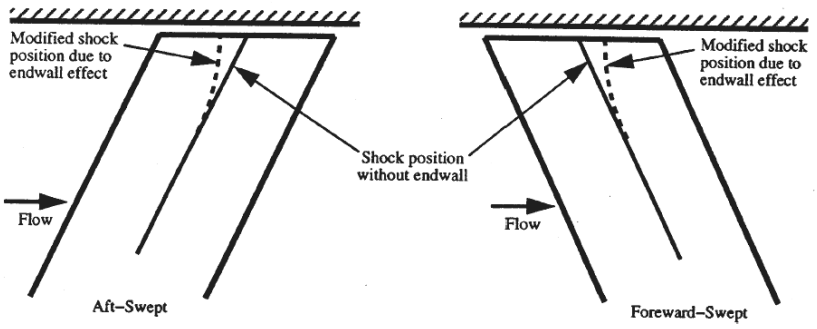

Fig. 1.9 Endwall effect on shock structure near the casing (from Hah *et al.*, 1998).

known as "endwall effect"). This fact induces the shock to move upstream in an aft swept rotor and downstream in a forward swept rotor (Figure 1.9). The high stability generally observed in forward swept rotors seems actually to be associated with the shock located more downstream near the casing.

In addition, sweep seems to have a considerable influence on the accumulation of low momentum fluid near the tip endwall region, a flow phenomenon described by Figure 1.5. Yamaguchi *et al.* (1991) found that in forward swept rotors this phenomenon is of lesser importance than in conventional radial rotor blades. The reason of that can be associated with a redistribution of pressure field around the blade, which contrasts the radial

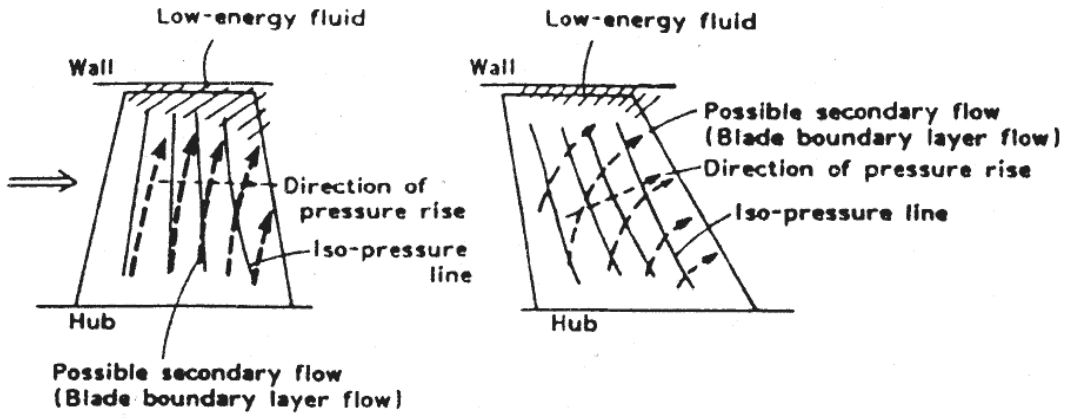

Fig. 1.10 Impact of sweep on radial migration of boundary layer fluid particles. (From Yamaguchi *et al.*, 1991)

migration of boundary layer fluid particles, as schematically shown in Figure 1.10 for a subsonic compressor rotor.

Moreover, as observed by Denton and Xu (1999), sweep influences the loading on the blade near the walls; in particular, forward sweep can reduce the blade loading in the front area of the tip region, where the loading rapidly falls down to zero (no blade) as one

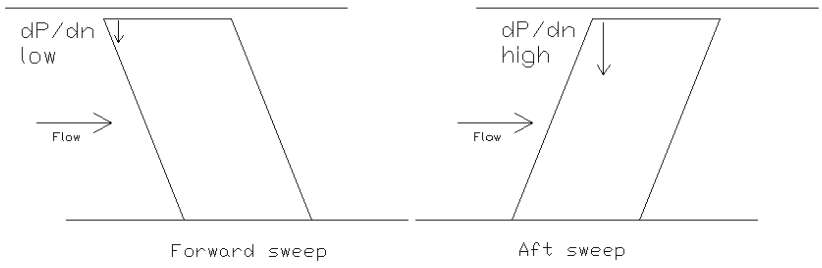

Fig. 1.11 Impact of sweep on blade loading in the front area near the casing.

moves radially from the tip to a lower span (Figure 1.11). This helps to reduce the sensitivity to changes in incidence and the intensity of the tip leakage flows in this area.

The influence of lean in transonic compressor rotors is not extensively described in literature. However, some researches were carried out to investigate the use of a blade

curved in the tangential direction. Bergner *et al.* (2002) observed that the use of a stacking line curved in the tangential plane can induce a significant change in the shock pattern within the blade passage. Ahn and Kim (2002) used an optimization technique for the well-known NASA Rotor 37 and showed the possibility to increase the overall rotor efficiency by skewing the blade toward the direction of rotor rotation. Benini (2004) performed a multi-objective design optimization on the same rotor and obtained similar results. The positive impact of this kind of blade curvature was confirmed recently also by Jang *et al.* (2006) and Yi *et al.* (2006). It seems that the better performance induced by such a curvature of stacking line is associated with a favorable modification of the three-dimensional shock structure; however, in general, the induced flow fields were not studied in depth and detailed information about the flow mechanisms that lead to the aerodynamic improvements were not provided.

Casing treatment

Hollow structures in the casing that aim to improve the tip endwall flow field of axial-flow compressors are commonly referred to as "casing treatments". Figure 1.12 shows some examples of casing treatments investigated in the 1970's. The interaction of the main flow with the flow circulating in these cavities seems to have a positive impact on the rotor stability. However, early studies did not reach a detailed understanding of the phenomenon, since experimental investigations were too expensive and only few configurations could be tested (Cumpsty, 1989). Only in the past ten years numerical simulations made it possible to investigate a larger number of casing treatments and their effects on different compressors. Many researches were carried out on transonic compressor rotors (Thompson *et al.*, 1997; Qing *et al.*, 2002; Rabe and Hah, 2002) and the potential of this kind of passive devices was revealed: a proper treatment can not only widen the stable working range of a transonic compressor rotor, but also improve its efficiency.

Recently, for instance, Beheshti *et al.* (2004) conducted a numerical parametric study of tip clearance coupled with casing treatment for the transonic axial-flow compressor NASA Rotor 37. Figure 1.13(a) shows the configuration of the solution adopted (circumferential groove) and Figure 1.13(b) depicts the position of the casing treatment with re-

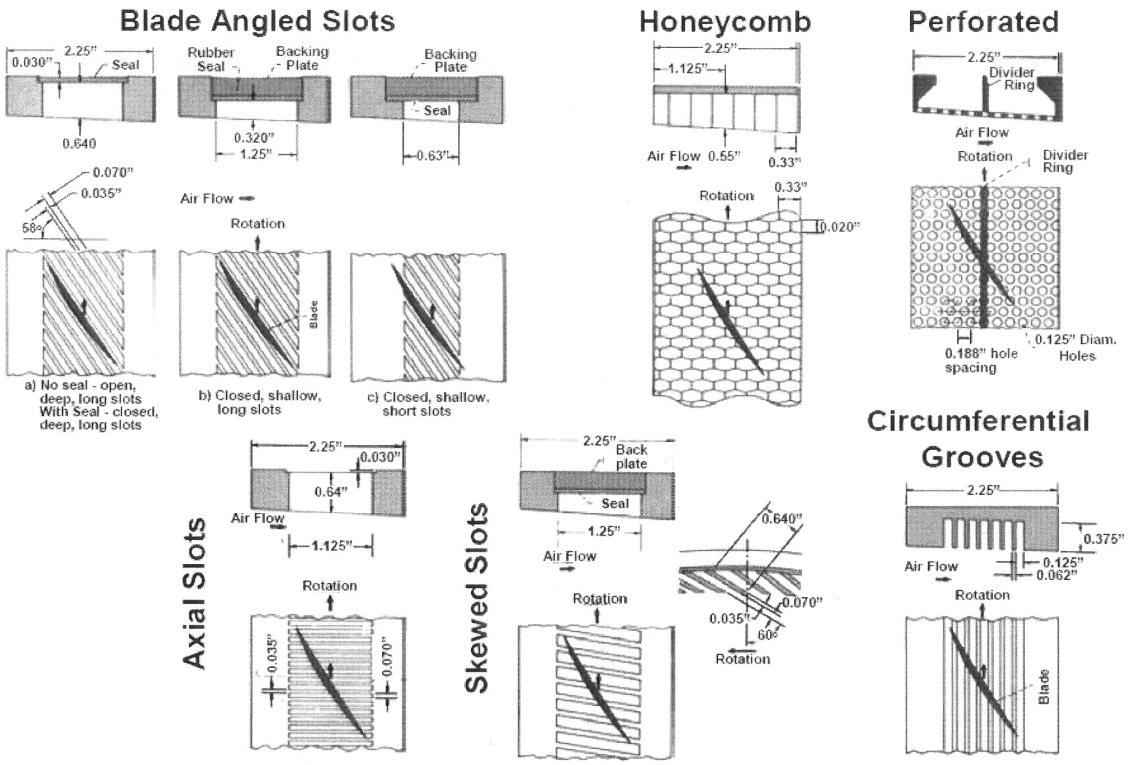

Fig. 1.12 Examples of various casing treatments investigated in the 1970's. (From the open literature)

spect to one of the compressor rotor blade. It seems that such a casing treatment provides a means for fluid to exit the flow path where the blade loading is severe, migrate circumferentially, and re-enter the flow path at a location where the pressure is more moderate. This can lead to stability improvement since the flow relocation helps to relieve the locally severe blade loading. Using this device, the authors showed the possibility to improve both the efficiency and the stall margin.

On the other side, Wilke and Kau (2004) analyzed the impact of axial slots on the flow field of a transonic rotor blade row. Figure 1.14 shows a representation of the casing treatments tested. They consist of four identical axial slots per blade passage and have an open area of 50% in the circumferential direction. The slots are parallel to the rotation axis of the rotor and are inclined by 45° against a meridional plane in the direction of blade rotation. The slot shape is designed as a semi-circle. In configuration 1, the position of the

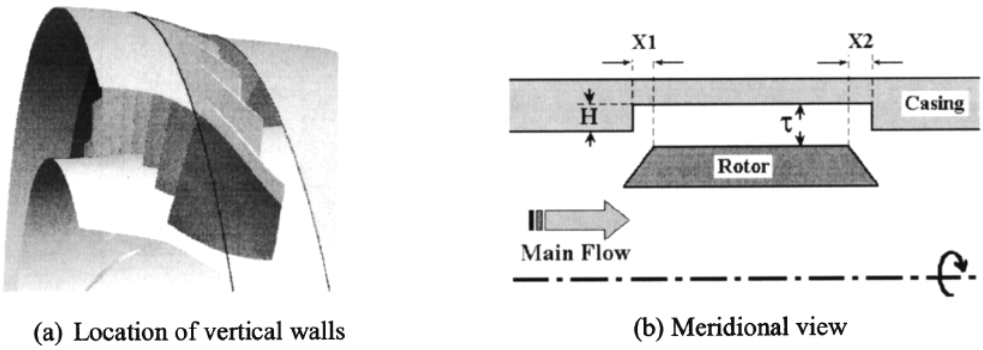

Fig. 1.13 Casing treatments (from Beheshti *et al.*, 2004).

slots is centered above the rotor blade tip reaching from 7.5% to 92.5% of the chord length. In configuration 2, the slots are moved upstream so that only 25% of the blade chord length remains covered by the casing treatment. The study was numerically carried out.

For both configurations, the simulations showed a significant increment in flow stability near surge compared to the solid wall. It was observed that the stabilizing effects are based on the positive impact of casing treatments on the tip leakage flow and its resulting vortex. Configuration 1 leads to a massive destruction of the tip leakage vortex, whereas configuration 2 weakens the rolling-up of the tip leakage flow. Configuration 2, gave also a positive impact on the overall efficiency.

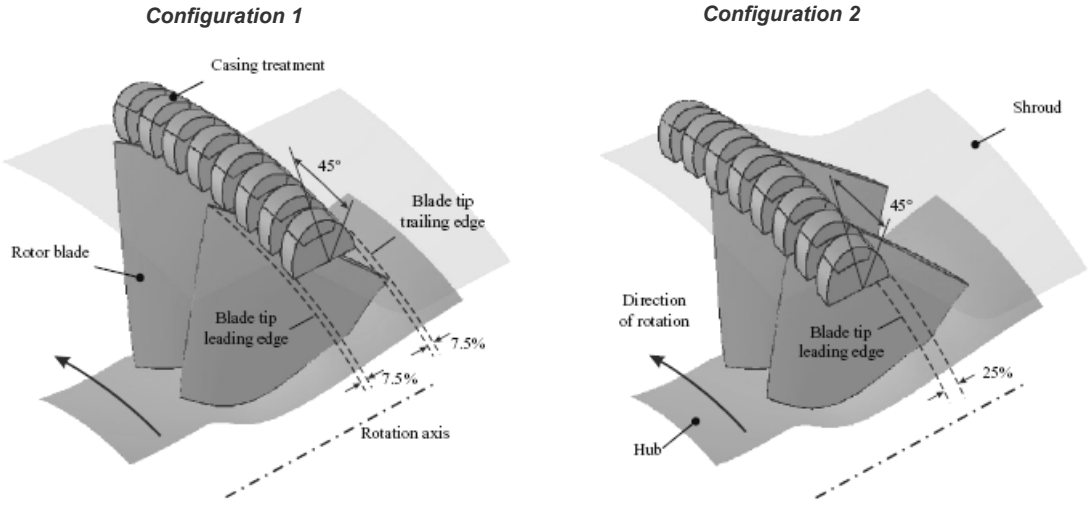

Fig. 1.14 Casing treatments (from Wilke and Kau, 2004).

Tip injection

Mass flow injection at the tip endwall region of a high-speed axial compressor rotor is a stability enhancement approach which can be effective in suppressing stall in tip-critical rotors.

Numerical simulations and experimental measurements conducted by Suder *et al.* (2001) showed that the range extension can be achieved by injecting air through discrete wall jets upstream of the tip region in a transonic rotor operating in isolation (Fig. 1.15). The analysis was conducted for a range of injection rates and distributions of injectors around the annulus. It was observed that tip injection can help to decrease incidence and blade loading at the tip, allowing increased loading at lower blade spans before the blade stalls. With tip injection present, the blade stalls when the loading at the tip reaches the level equal to that for which the blade stalls with no injection.

Beheshti *et al.* (2006) presented a state of the art design for the blade tip injection. The design includes the means to inject high pressure air jet directly into a circumferential groove formed in the casing over the blade tip (Fig. 1.16). Different injection mass flow rates and injection angles were considered in order to explore the key role parameters for

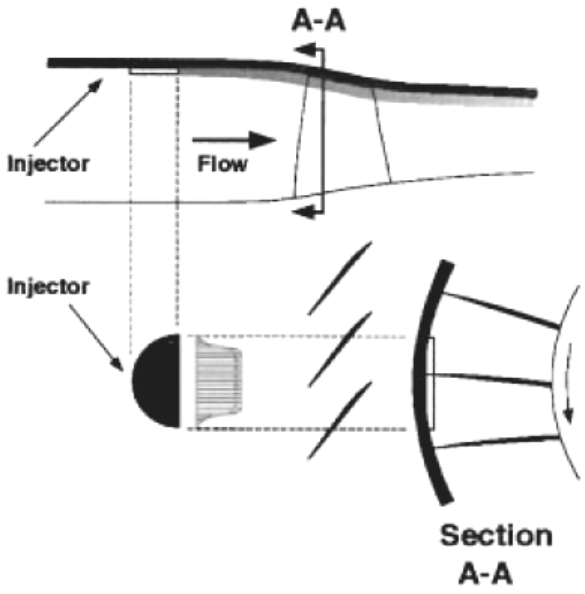

Fig. 1.15 Casing-mounted injector (from Suder *et al.*, 2001).

an optimum design. Compared to classical designs for casing-mounted injectors (Fig. 1.15), this design can lead to more advantageous effects on the compressor stability, thanks to the direct injection of flow over the rotor tip. It was observed that the air injected can beneficially affect the stall margin by energizing the decelerated flow which arises downstream the shock-vortex interaction point at low flow operating conditions (a detrimental flow feature associated with the flow phenomenon illustrated in Fig. 1.7). It was also observed that for a constant injection mass flow rate the stall margin enhancement is the highest when the injected air in the rotating frame is set aligned with the camber line at the blade leading edge.

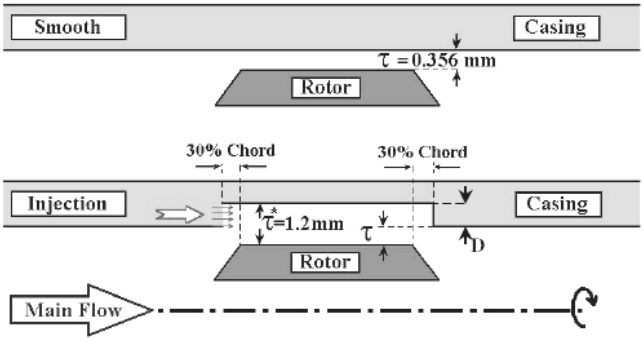

Fig. 1.16 Tip injection design (from Beheshti *et al.*, 2006).

A natural and intended follow on to the development of tip injection technology is to couple the injectors to a high pressure bled source within the compression system rather than providing injection by an external air source (as supposed in previous examples). This solution is commonly referred to as "endwall recirculation". The idea of endwall recirculation is certainly not new and is schematically presented in Fig. 1.17. Both rotor recirculation (confined to the rotor tip region) and stage recirculation (which can encompass one or multiple stages) were investigated by Strazisar *et al.* (2004) and Hathaway (2000, 2002).

These two endwall recirculation concepts present some advantages and disadvantages in terms of design trades. Compared to the rotor recirculation, some advantages of the stage recirculation are the higher pressure and the reduced swirl of the bled fluid flow

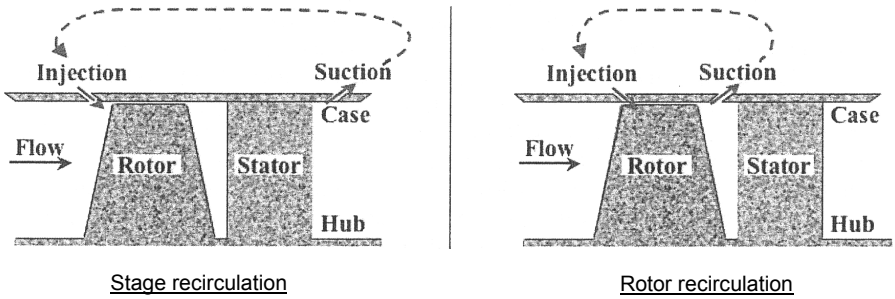

Fig. 1.17 Endwall recirculation.

downstream the stator. A disadvantage of stage recirculation is finding an appropriate re-circulation path to circumvent the casing hardware. On the other hand, the main advantage of the rotor recirculation is that it can be more easily integrated with the case, while its biggest disadvantages are that the injector supply pressure is limited by the rotor tip pressure rise and that the high rotor exit swirl must be removed in an efficient compact flow path. In both cases, the air can be injected upstream of the rotor tip (thereby reducing the rotor tip incidence) or it can be directly targeted at the rotor tip leakage flow (or other flow feature considered detrimental for rotor stability).

An important characteristic of endwall recirculation concept is that it removes fluid from the power stream, thereby preventing it from passing through the combustor and turbine where it would otherwise produce thrust. It is therefore evermore important to reduce the mass flow rate of the recirculated air as it can adversely impact on aircraft gas turbine performance.

CHAPTER 2

NASA Rotor 37: numerical modeling and validation

2.1 NASA Rotor 37

The Rotor 37 is a well-known test case designed by the NASA Lewis Research Center and representative of complex three-dimensional viscous flow structures in transonic axial-flow compressor bladings. Figure 2.1 shows the meridional view of Rotor 37. It had 36 Multiple-Circular-Arc (MCA) blades with an inlet hub-tip diameter ratio of 0.7, a blade aspect ratio of 1.19 and a tip solidity of 1.29. The running tip clearance gap was 0.0356 cm (0.45% of blade span). The design pressure ratio and isoentropic efficiency were respectively 2.106 and 0.877, with a mass flow of 20.19 kg/s. The design wheel speed was

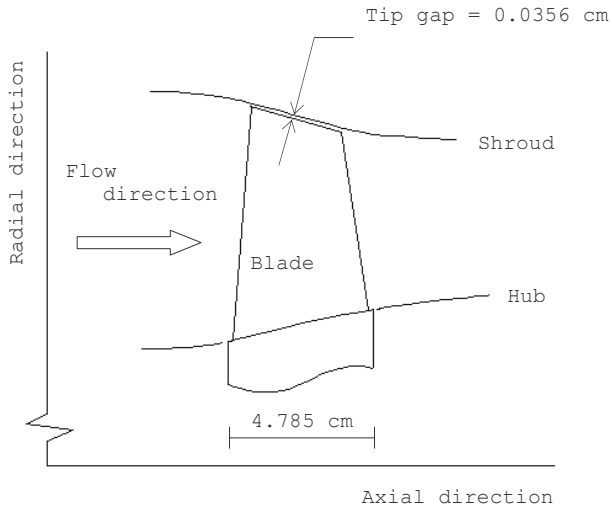

Fig 2.1 Meridional view of NASA Rotor 37.

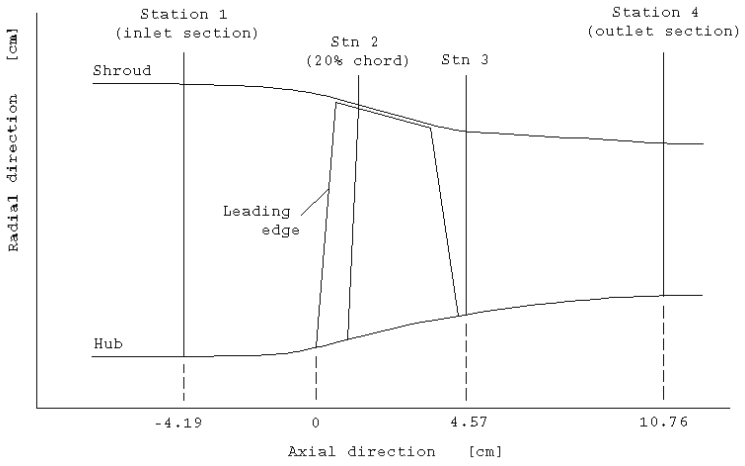

Fig. 2.2 Axial location of measurement stations.

17,188.7 rpm (1800 rad/s), with a nominal tip speed of 454 m/s.

The Rotor 37 was designed and initially tested in the 1970's as part of a research programme involving four axial-flow compressor stages; one of them, the Stage 37, involved actually the Rotor 37. These stages were intended to cover a range of design parameters typical of aircraft turbine engine high-pressure (core) compressor inlet stages. Some design information and overall performance of Stage 37 came from Reid and Moore (1978). More detailed measurement data were successively provided by Moore and Reid (1980).

Next to the tests of Moore and Reid (1980), the rotor (the Rotor 37) of Stage 37 was tested again as an isolated component. A brief description of the related test facility was given by Suder *et al.* (1995), and Suder and Celestina (1996). Figure 2.2 shows the axial location of some measurement stations. Measurement results are available in many published research works and were used here to validate a three-dimensional RANS (Reynolds-averaged Navier-Stokes) model for the Rotor 37 and, more in general, for transonic compressor rotors.

Figure 2.3 shows the Rotor 37 measured speed line at the design wheel speed in the form of total pressure ratio P_4/P_{ref} and adiabatic efficiency, against the normalized mass flow rate. The adiabatic efficiency was calculated as follows:

$$\eta = \frac{\left(\frac{P_4}{P_1}\right)^{\frac{k-1}{k}} - 1}{\frac{T_4}{T_1} - 1} \tag{2.1}$$

The subscripts "1" and "4" indicate the measurement sections (Figure 2.2), while the subscript "ref" indicates the corresponding sea-level standard atmosphere value (P_{ref} = 101325 Pa). The mass flow rates were normalized using the mass flow rate at the choking condition. Measurements provided a choking mass flow of 20.93 ± 0.14 kg/s.

Figure 2.4 shows the spanwise distributions of pitchwise mass-averaged performance at Station 4 for 98% of choking mass flow (T_{ref} = 288.15 K). It is possible to observe a severe reduction of isoentropic efficiency over the 80% span, associated with a considerable

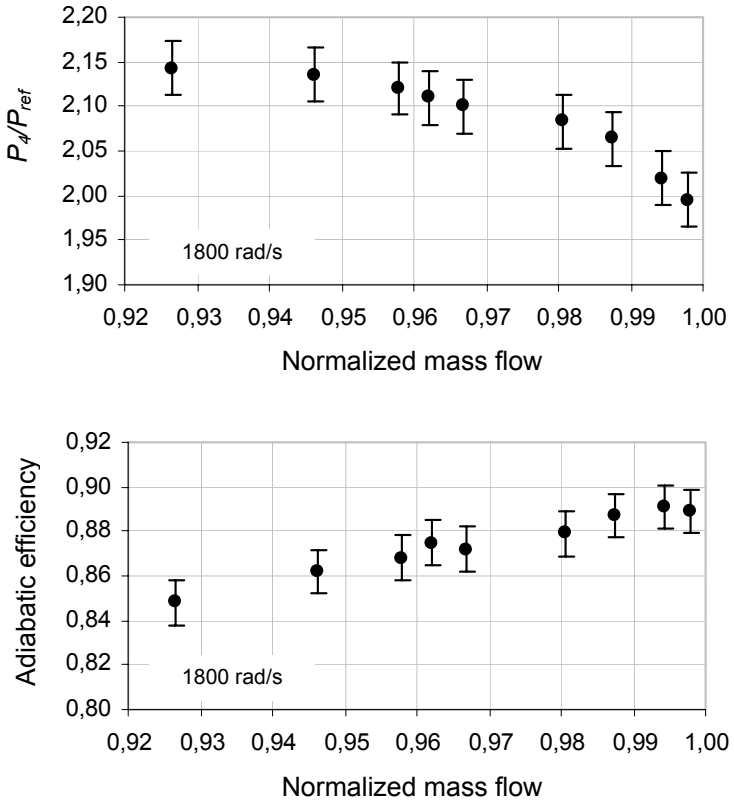

Fig. 2.3 Measured speed line of Rotor 37 (data from AGARD (1998)).

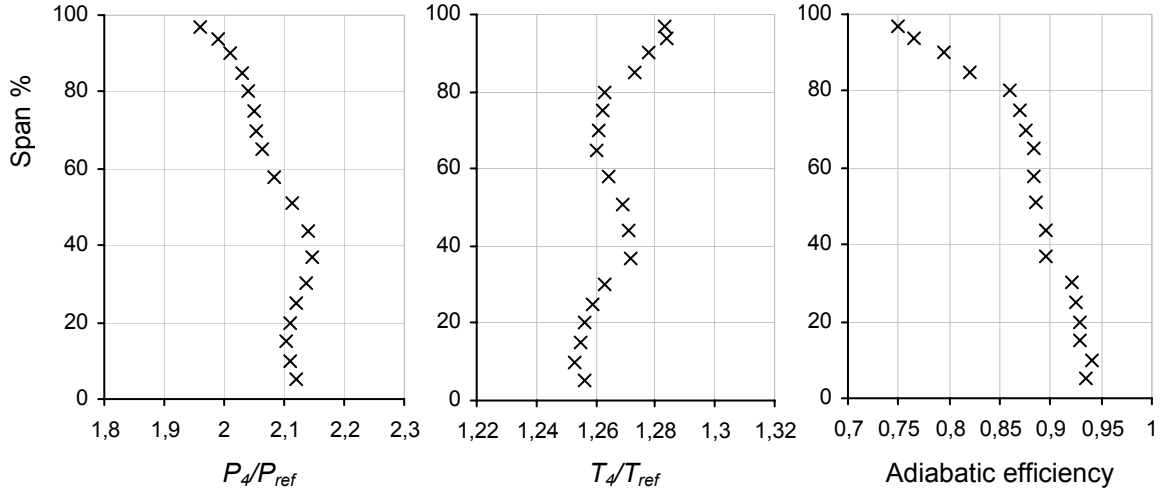

Fig. 2.4 Spanwise performance profiles at Station 4 – 98% of choking mass flow – 1800 rad/s (data from AGARD (1998)).

increment of total temperature ratio. This is a typical negative feature in transonic axial-flow compressor rotors, as a result of the irreversibilities that occur at the tip endwall region; as introduced in Chapter 1, these irreversibilities are mainly due to the presence of strong shock waves, intense tip clearance flows and casing boundary layer, as well as to their detrimental interaction.

2.2 Numerical modeling

The commercial CFD code CFX (ANSYS, PA, USA) was used to develop a numerical model able to predict accurately the aerodynamic behavior of transonic compressor rotors. A 3-D RANS model was implemented. The three-dimensional Reynolds-averaged Navier-Stokes equations were solved by means of the finite volume technique. An Algebraic Multigrid method, based on the Additive Correction Multigrid strategy (Hutchinson and Raithby, 1986), was utilized automatically by the code to improve the convergence rates.

In order for the numerical model to be well defined, an investigation on the impact of model features (discretization scheme, grid topology, grid density and turbulence model)

on the accuracy of predictions was carried out. This was done simulating the flow field of Rotor 37 using five different models (see Table 2.1) and comparing predictions with experimental data available in literature. Comparisons were made in terms of both rotor performance (performance maps and downstream radial profiles) and internal flow features (Mach number distributions, tip clearance flows, blade wakes etc.).

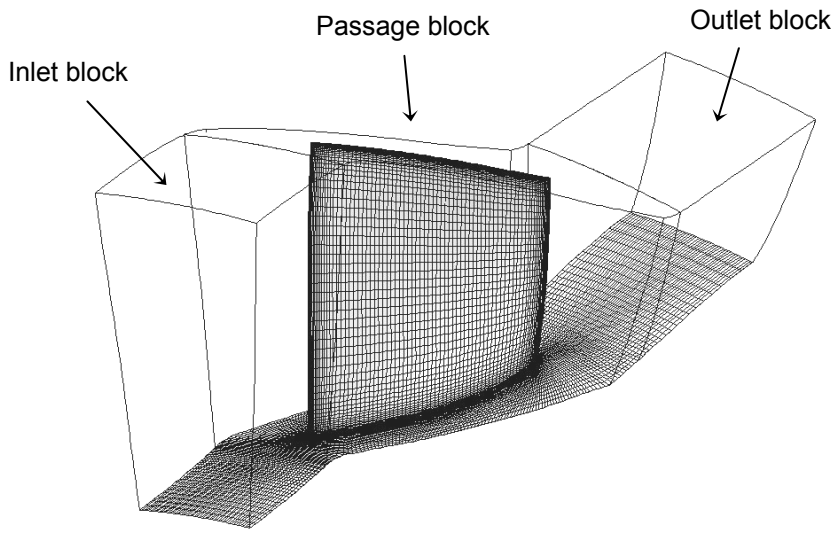

Fig. 2.5 Computational domain (Model 3) – TurboGrid (ANSYS, PA, USA).

For each model, a multi-block structured grid was used to discretize the computational domain (Figure 2.5). The computational domain regards a single blade passage (periodic boundary conditions were applied on the lateral faces). Inlet and outlet boundaries correspond to Station 1 and Station 4 of Figure 2.2 respectively. The total pressure, total temperature, and absolute flow angle of the incoming flow were fixed at the inlet boundary, while the average static pressure of the delivered flow was imposed at the outlet (the boundary pressure profile is a result of the computation). In order to reproduce the boundary conditions of the above mentioned Rotor 37 test facility (Suder *et al.*, 1995; Suder and Celestina, 1996), which provided the experimental data used here, the inlet total pressure and total temperature were fixed at P_1 = 101325 Pa and T_1 = 288.15 K. The tip clearance

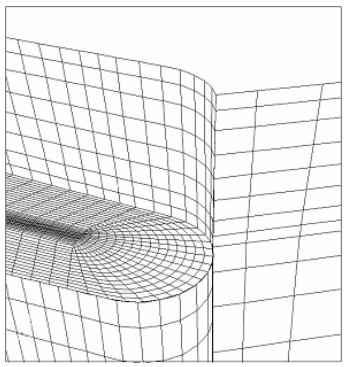

Fig. 2.6 Tip gap grid near the leading edge (Model 1).

gap was modeled (Figure 2.6) including the relative motion between the rotor and the casing. The walls were treated as smooth and adiabatic. An angular velocity corresponding to the nominal rotational speed of Rotor 37 was applied. For each simulation, the convergence criterion was established when normalized RMS (root mean square) residuals were less than 10^{-6}.

Tab. 2.1 Models tested.

Model No.	Discretiz. scheme	Passage grid topology	Cells number	Turbul. model
1	UDS+PAC	H/O grid	500,000 ca.	k-ε
2	LPS+PAC	H/O grid	500,000 ca.	k-ε
3	LPS+PAC	J/O grid	500,000 ca.	k-ε
4	LPS+PAC	J/O grid	1,000,000 ca.	k-ε
5	LPS+PAC	J/O grid	1,200,000 ca.	SST k-ω

Table 2.1 gives the main features of the five models tested. As shown, two different discretization schemes, among those implemented in the code, were considered: the conventional Upwind Differencing Scheme (UDS) in Model 1 and the more accurate Modified

Linear Profile Scheme (LPS) in Model 2, both along with Physical Advection Correction (PAC) terms. More details on such discretization schemes can be found in CFX-TASCflow Theory Documentation (2000). After that, the impact of a different passage grid topology was examined in Model 3 (Figure 2.7). In Model 4 the sensitivity of the solver on the grid density was evaluated. As far as the turbulence model, the standard k-ε turbulence model (Launder and Spalding, 1974) along with scalable wall-functions was adopted in all the models except in Model 5, where the more advanced Shear Stress Transport (SST) k-ω model (Menter, 1994) was tested. Steady-state simulations were conducted for the validation process. All simulations were run on an Intel Pentium IV PC, 3.4 GHz, 2 GB RAM.

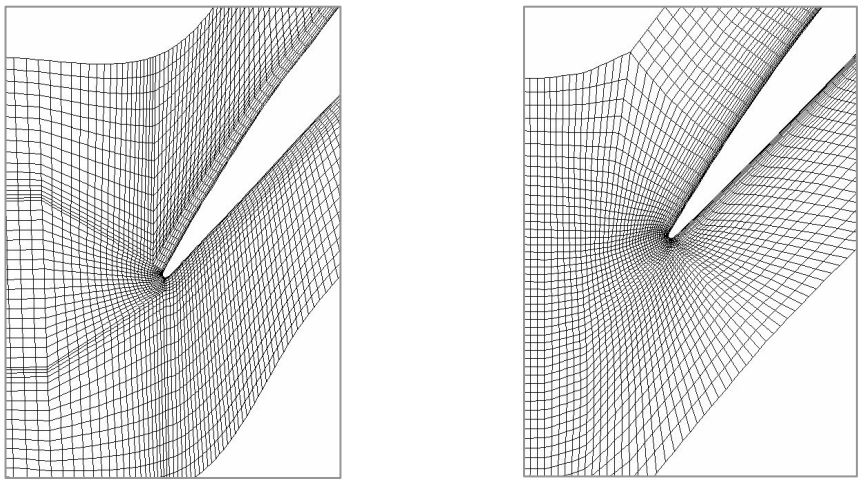

Fig. 2.7 Passage grid topology – hub view.

2.2.1 Validation

Model 1 was developed in accordance with the guidelines supplied by a well-known report of AGARD (1998), which sums up a famous "CFD code test" organized by the Turbomachinery Technical Committee during the 1994 ASME/IGTI Turbo Expo. In that

event, both CFD users and developers were invited to submit numerical solutions for a "blind test case" to the organizers; the test case was actually the Rotor 37.

Model 1 provided satisfactory predictions of overall rotor performance. The grid had about 500,000 hexahedral cells clustered near the walls, giving a y^{+}[1] at the walls ranging from 20 to 300. The blade tip gap region was model using 8 cells in the spanwise direction (Figure 2.6). Calculations gave a choking mass flow rate of 20.64 kg/s, against the measured value of 20.93 ± 0.14 kg/s. The choking operating condition was run by imposing a low back pressure. Figure 2.8 compares the calculated and measured performance down-

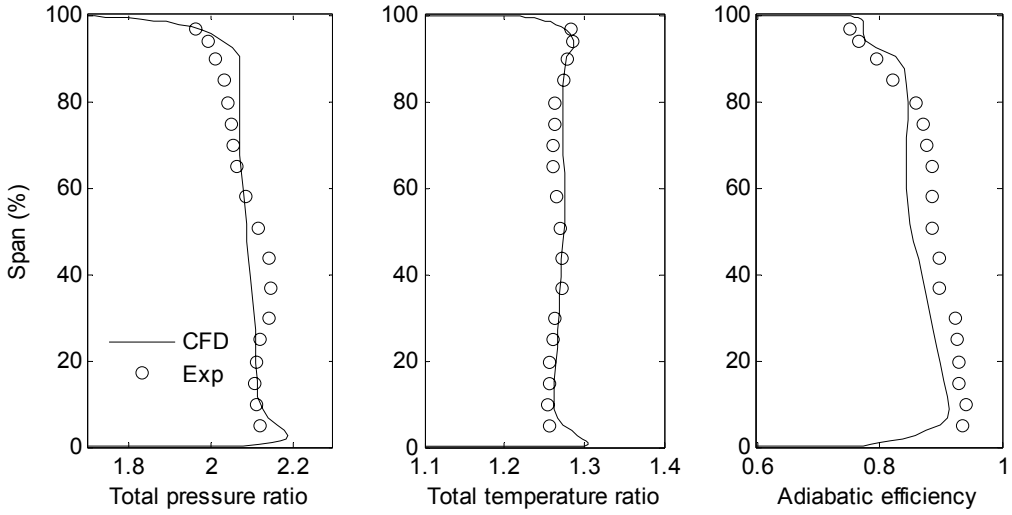

Fig. 2.8 Performance radial profiles at Station 4.
(98% choking mass flow – Model 1)

stream profiles at 98% normalized mass flow (that is, 98% of choking mass flow). In this work, the calculated mass flows were normalized using the choking mass flow rate predicted by the respective model, as well as the experimental mass flows were normalized

[1] Yplus (y^{+}) is the dimensionless distance from the wall. It is used to check the location of the first node away from a wall. This was more important when standard wall-functions were used, as one had to avoid y^{+} values smaller than approximately 20. With the scalable wall-functions, these values are only provided for information on the near-wall resolution.

using the choking mass flow rate provided by measurements. Both numerical and experimental spanwise data are pitchwise mass-averaged. As shown, predictions matched fairly well the overall integrated level of property distributions but failed to match the shape at all. In particular, the model failed to predict the total pressure stagnation suggested by measurements around 20% span. As observed by Hah and Loellbach (1999), that dip of total pressure may be due to the presence of the so-called "hub corner stall", a flow phenomenon which occurs near the blade suction side corner and seems to be partially due to the glancing side wall shock wave interaction with the hub boundary layer, as postulated by Povinelli (1997). Most of the code used in the above mentioned CFD code test were not able to predict that phenomenon.

In Figure 2.9, the computed relative Mach number (relative to the rotating reference frame) at 70% span and 98% of choking mass flow is compared with corresponding measured contours. The model predicted fairly well the shock position and resolution even if, as in many solutions published by AGARD (1998), the Mach number after the shock is too low. This could be induced by a too thin post-shock predicted boundary layer on the blade suction side (Denton, 1996); this is because the subsonic Mach number after the shock is reduced if the flow blockage diminishes. However, experimental data were not found to

Computed results (Model 1)

Exp. data
(extracted from Suder *et al.*, 1995)

Fig. 2.9 Relative Mach number distribution.
(70% span – 98% of choking mass flow)

confirm this hypothesis.

Model 1 required about 600 iterations to reach the convergence criterion, taking about 10 hours and using about 0.7 GB RAM.

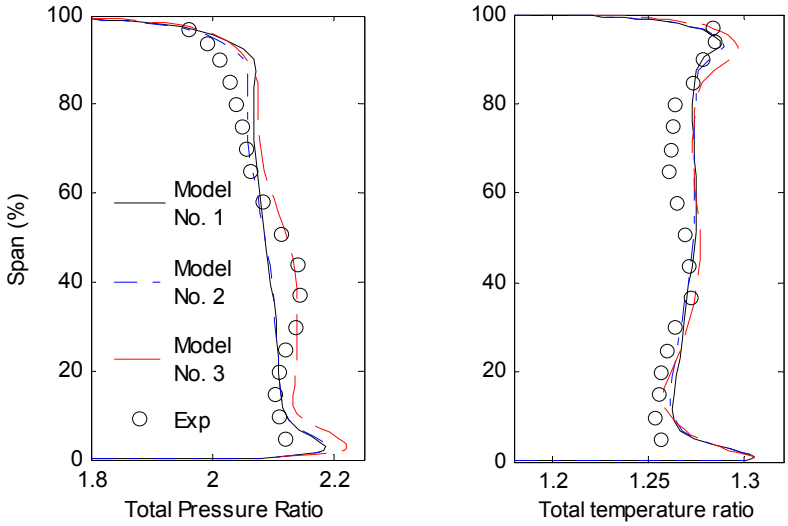

Fig. 2.10 Performance radial profiles at Station 4 (98% of choking mass flow).

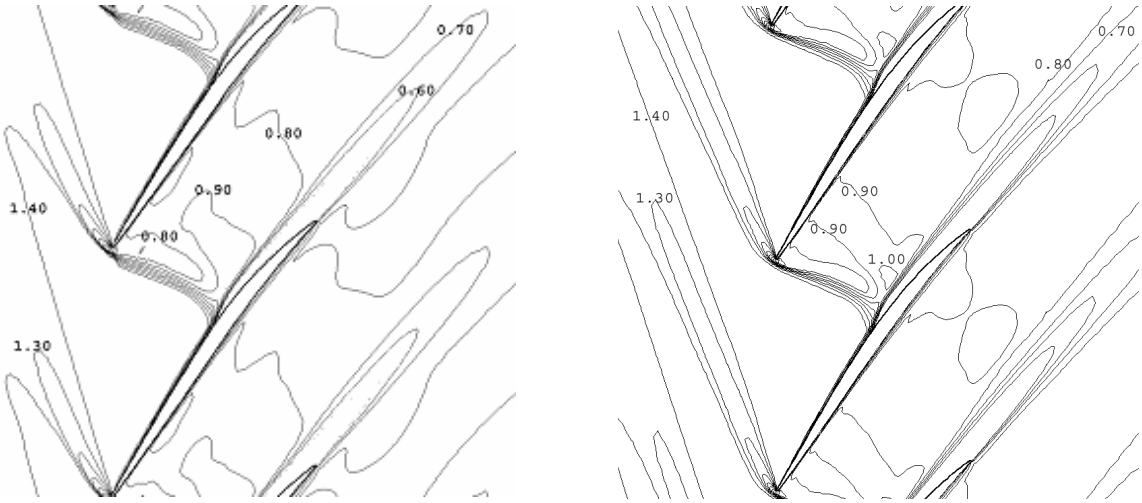

Model 2 – H/O-grid

Model 3 – J/O-grid

Fig. 2.11 Influence of grid topology.
(CFD relative Mach number contours – 98% of choking mass flow – 70% span)

The use of a more accurate discretization scheme (adopted in Model 2) did not provide substantial improvements in predictions. Performance downstream profiles (Figure 2.10) and interblade relative Mach number distribution (Figure 2.11 left) are very similar to the corresponding ones of Model 1. However, it is possible to note a slightly less smeared and better defined shock front (cf. Figures 2.9 left and 2.11 left).

With respect to Model 2, Model 3 is characterized by a more regular and less skewed passage grid. This led to better predictions. As shown in Figure 2.10, the computed spanwise profile of total pressure ratio matches rather well the experimental data. In addition, with respect to the two previous models, a better agreement with measured Mach number contours was obtained (cf. Figures 2.9 right and 2.11 right). This model predicted a choking mass flow rate of 20.96 kg/s against the experimental value of 20.93 kg/s.

Compared to Model 3, Model 4 is characterized by a finer grid of about 1,000,000 cells, while all the other features were kept constant. Model 4 computed the same choking mass flow of Model 3. As shown in Figure 2.12, changes in the calculated performance profiles due to the grid refinement are negligible. The predicted Mach number distribution is also similar to that of Model 3 (cf. Figures 2.11 right and 2.13 left). This does not mean that grid density is not important for the accuracy of a CFD solution, but only that a finer

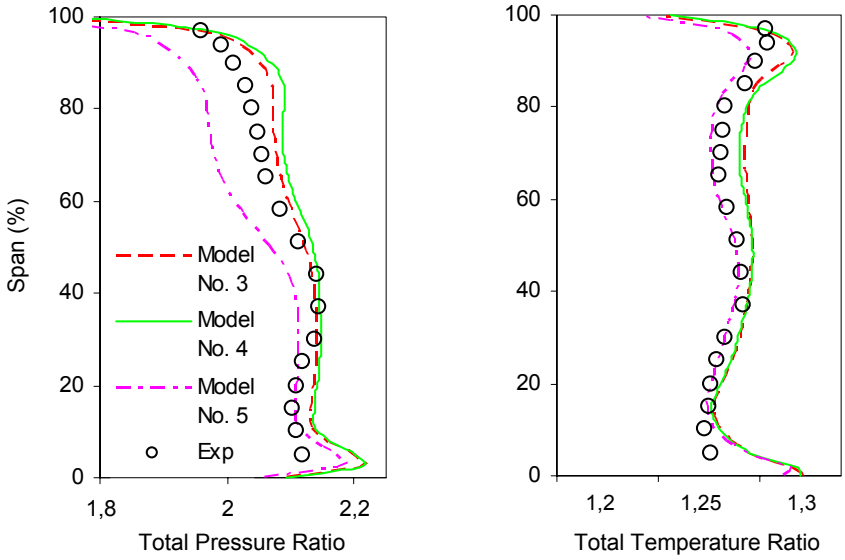

Fig. 2.12 Performance radial profiles at Station 4 (98% of choking mass flow).

grid is not necessary in Model 3, at least for a preliminary prediction of overall rotor behavior.

Finally, the Shear Stress Transport k-ω turbulence model, designed to give highly accurate predictions of the onset and the amount of flow separation under adverse pressure gradients, was adopted and tested in Model 5. A grid similar to that of Model 4 was used, but refined at the walls to have a near-wall grid resolution of at least $y^+ < 1$, needed to guarantee a strict low-Reynolds number model implementation. Automatic near-wall treatment, which switches from low-Reynolds near-wall formulation to scalable wall-functions as the mesh is not sufficiently refined, was also adopted. Model 5 provided correctly the choking flow rate but underestimated the total pressure ratio at 98% of choking mass flow, as shown in Figure 2.12. The relative Mach number distribution was instead well predicted. Figure 2.13 (right) shows a good agreement with measurement data (Figure 2.9 right), especially after the shock, where previous models failed. This model took about 24 hours to reach the convergence criterion, using about 1.7 GB RAM.

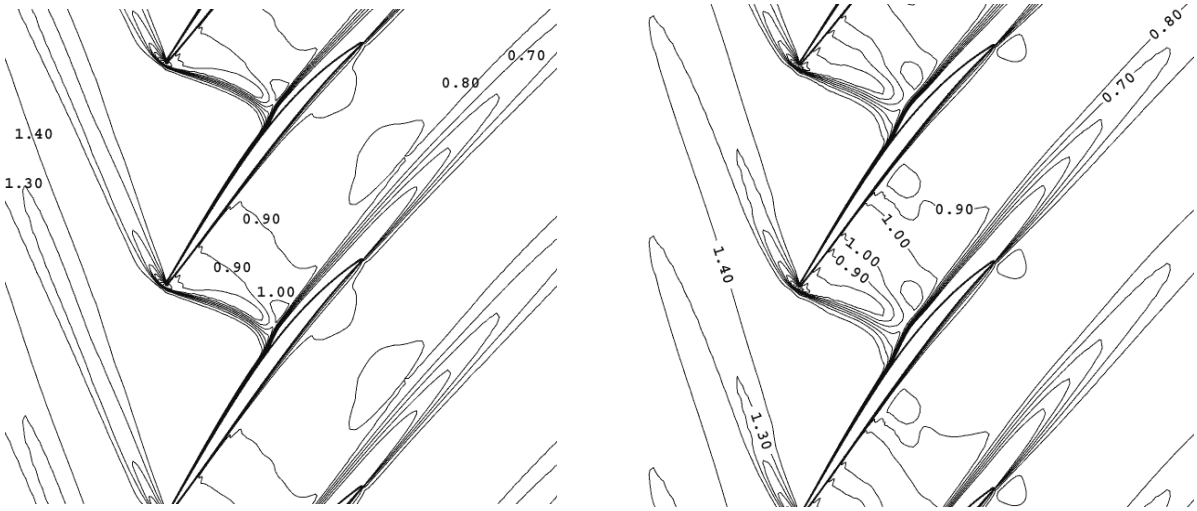

Model 4 (k-ε) Model 5 (SST k-ω)

Fig. 2.13 Influence of turbulence model.
(CFD relative Mach number contours – 98% of choking mass flow – 70% span)

Among the five models evaluated, Model 3 and Model 5 can be considered the most interesting ones. The first one showed fairly good predictions of overall rotor behavior, requiring no excessive computing resources; it can be used for a preliminary prevision of overall performance. The second one seems to predict more accurately the internal flow features of a transonic flow field and could be used for detailed flow analyses. Model 3 and Model 5 were validated more in detail in the following.

Measured and calculated maps of adiabatic efficiency are shown in Figure 2.14. The calculated operating points were obtained by varying the back pressure. The lower mass flow operating point in the predicted speed lines corresponds to the last point for which the steady-state model implemented was able to converge (a further increment of about 500 Pa in the back pressure boundary condition leads to a not converging solution). As shown, Model 5 underestimated the overall efficiency along the entire operating range, while Model 3 only around the peak efficiency condition. At 98% normalized mass flow, Model 5 and Model 3 gave an efficiency of 0.858 and 0.866 respectively, against the experimental value of 0.879. The working range was slightly overestimated by both models.

Figure 2.15 compares the computed and experimental relative Mach number distributions at the 70% span for a low flow operating condition (about 93% normalized mass flow). Model 3 provided slightly low values of Mach number after the shock; Model 5 gave a very realistic prediction.

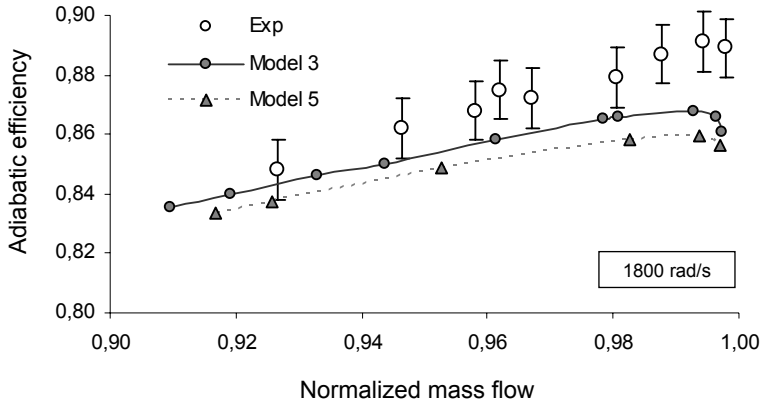

Fig. 2.14 Calculated and measured adiabatic efficiency (Rotor 37).

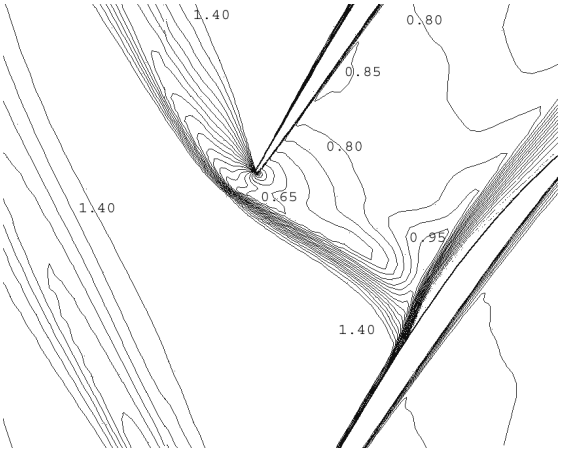

Model 3 calculations

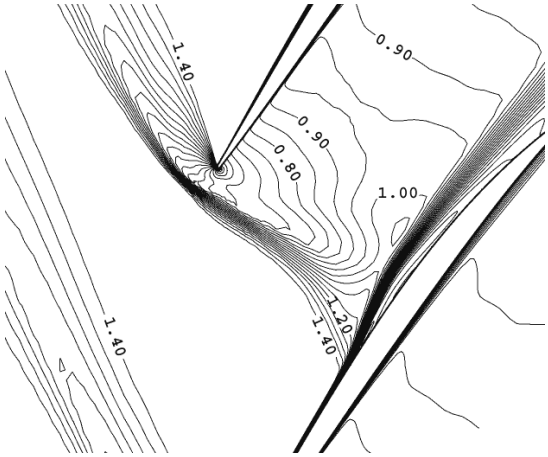

Model 5 calculations

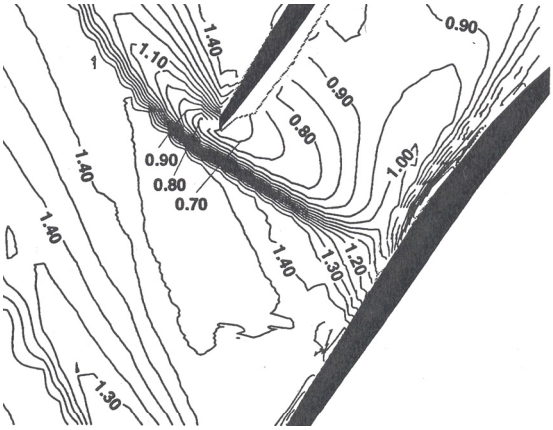

Experimental data (from Suder, 1998).

Fig. 2.15 Contours of relative Mach number at 70% span. Low flow operating condition.

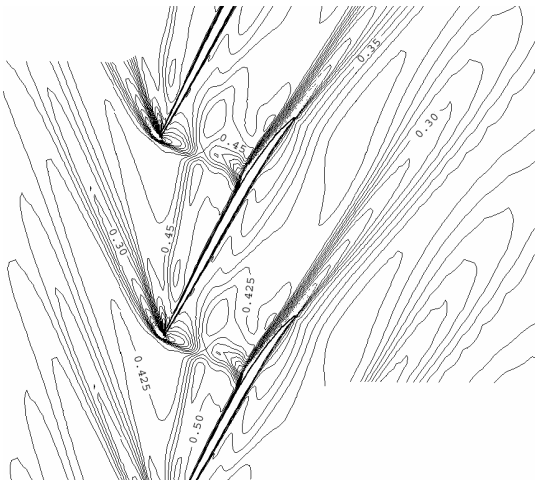

Model 3 calculations

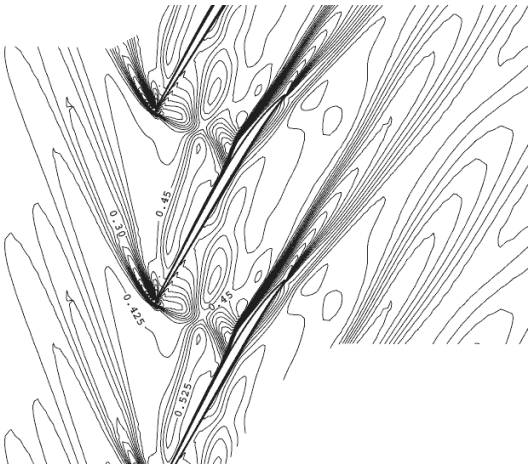

Model 5 calculations

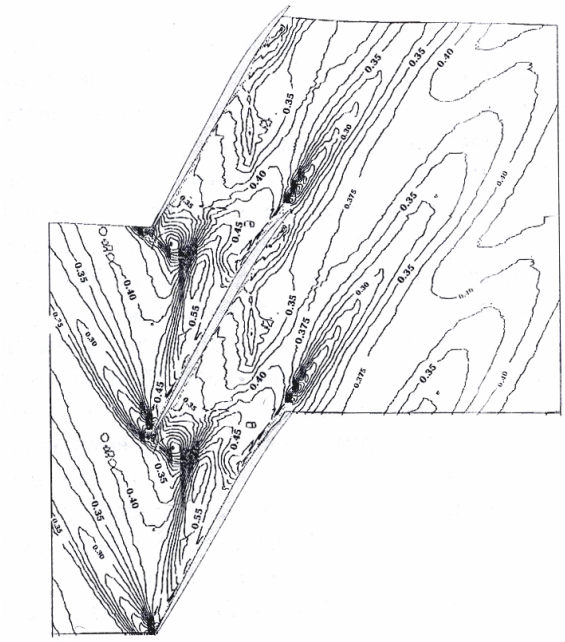

Experimental data (from Chima, 1998)

Fig. 2.16 Normalized axial velocity (95% span – 98% of choking mass flow).

Figure 2.16 shows the calculated and measured contours of normalized axial velocity (normalized using blade tip velocity) at 95% span for the 98% of choking mass flow. The agreement with experimental results is quite good for both Model 3 and Model 5.

Figure 2.17 compares the computed and experimental relative Mach number at 95% span, Station 2 (located at 20% of profile chord from leading edge) and 98% normalized mass flow. Some disagreements in the profile shape and shock location can be observed between numerical and experimental data. As underlined by Chima (1998), at 95% span the fluid is well within the casing boundary layer and computations are, probably, strongly influenced by approximations due to current turbulence modeling in RANS computations.

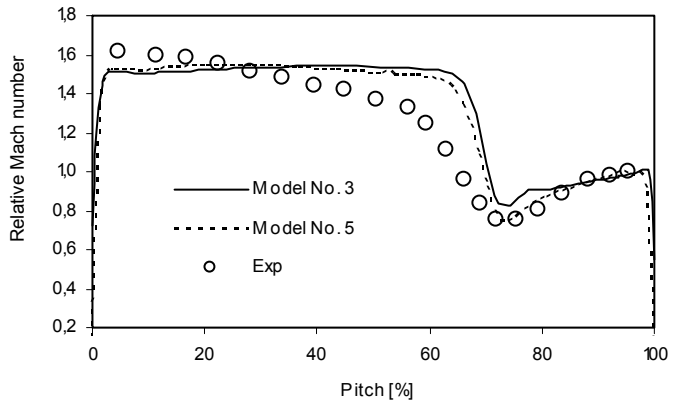

Fig. 2.17 Blade-to-blade relative Mach number (exp data extracted from Chima (1998)). (98% choking flow rate – 95% span – Station 2)

CHAPTER 3

Aerodynamic sweep and lean: overall impact

3.1 Introduction

As introduced in Chapter 1 (Section 1.3), the application of a three-dimensional curvature to the blade stacking line (in other words, sweep and lean) can have considerable effects on the overall performance of a transonic compressor rotor. In this chapter, a systematic numerical investigation was conducted to better understand the impact of sweep and lean on the aerodynamic behavior of these rotors, with particular regard to the overall efficiency. That being stated, the following specification is now needed. As shown in Section 1.3 (see Figure 1.8), a common choice in compressor community is to define sweep the movement of blade sections along the local chord direction and lean the change in the perpendicular direction. In the present work, instead, sweep and lean were defined relative to the axial and tangential directions respectively (Figure 3.1). In this way, the effects induced by the use of a stacking line curved in the meridional plane and/or in the circumferential plane were analyzed, leading to the definition of another point of view on the study of the influence of blade shape in transonic compressor rotors. Clearly, following results can not be directly compared with those obtained starting from the common definition of sweep and lean.

3.2 Investigated rotor geometries

New swept and leaned rotors were modeled starting from the baseline radially-stacked Rotor 37 (see Chapter 2), by changing the curvature of the original stacking line in the meridional and circumferential plane respectively. As schematically shown in Figure

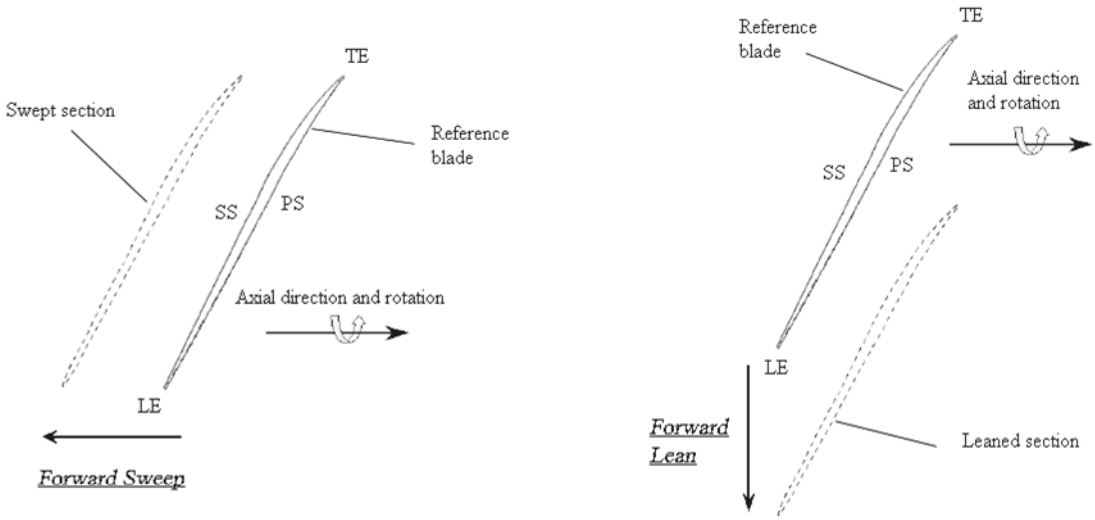

Fig. 3.1 Sweep and lean definition used in this work.

3.2, the radial stacking line of Rotor 37 (the solid vertical line) was systematically modified by moving three control points (located on 33%, 67% and 100% span from the hub, signed as black circles) on predefined positions (the x-marked locations)[1]. All possible combinations were considered (26 for sweep and 26 for lean). Dashed lines represent some of all the new stacking lines so obtained. Figures 3.3(a) and 3.3(b) show, for instance, the blades obtained using the stacking lines signed as "A" and "B" in Figure 3.2 respectively.

Being the radial position of casing line not constant along the axial direction and the tip endwall region characterized by very complex flow structures, it was preferred not to change the meridional position of the tip blade profile, with the aim to avoid any other variables of influence. Therefore, the curvature of the new swept stacking lines was applied to the blade starting always from the tip section instead from the hub section, as shown in Figure 3.4 for the swept stacking line "C" of Figure 3.2.

As shown in Figure 3.1, the adjective of "forward" was given to lean when the blade is skewed toward the direction of rotation and to sweep when the blade is curved upstream.

[1] The positions where to move the control points (the x-marked locations in Figure 3.2) were chosen with the aim to give the blade a reasonable curvature, that is a curvature not excessively pronounced but able to impact noticeably on the flow field.

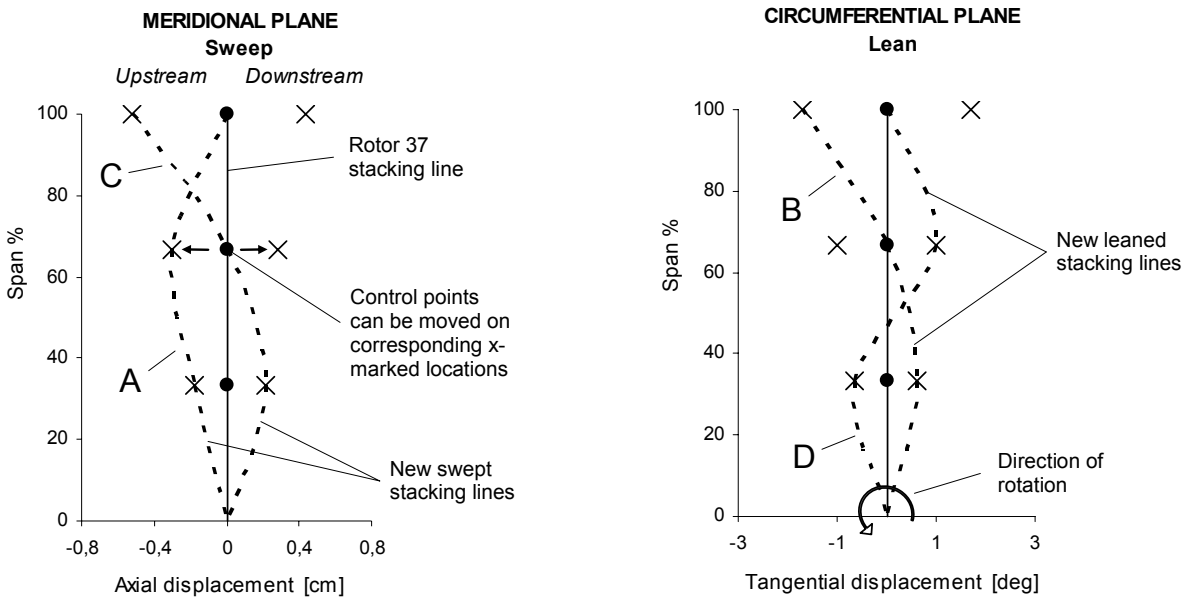

Fig. 3.2 Swept and leaned stacking line definition.

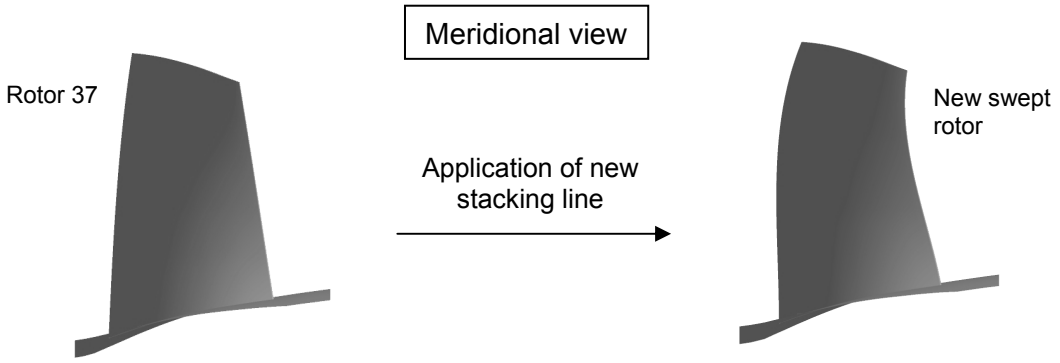

Fig. 3.3(a) Application of swept stacking line "A" of Figure 3.2.

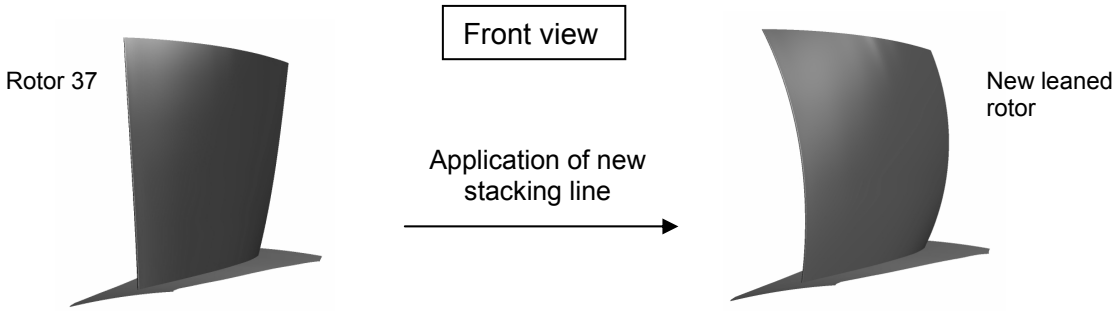

Fig. 3.3(b) Application of leaned stacking line "B" of Figure 3.2.

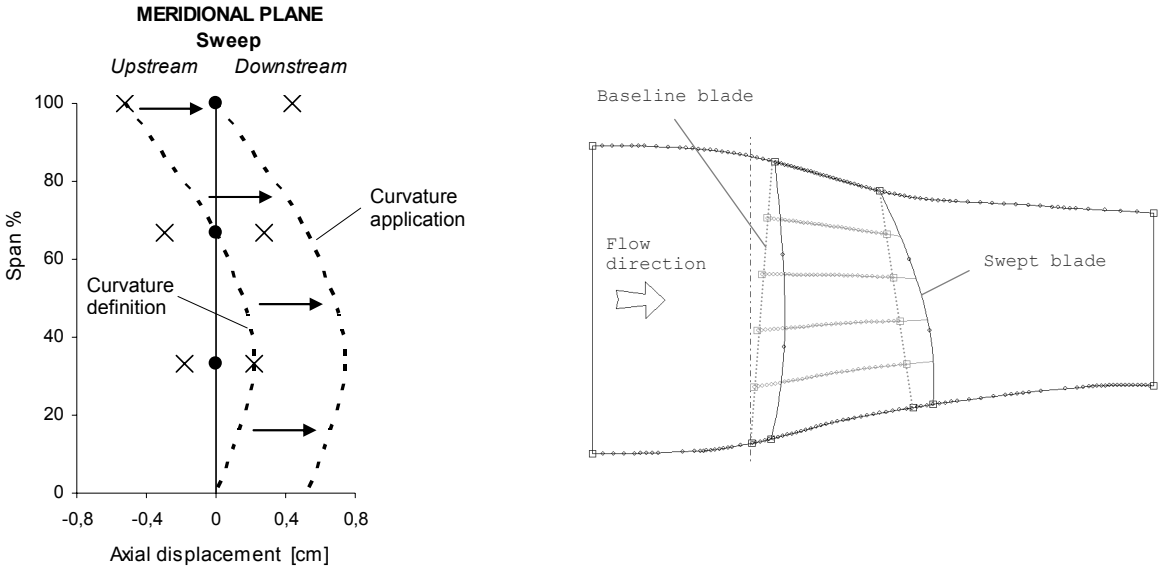

Fig. 3.4 The curvature of new swept stacking lines was applied to the original blade maintaining the axial position of tip profile.

3.3 Aerodynamic impact

All the modeled rotors were simulated using the numerical model identified as "Model 3" in Chapter 2 (see Table 2.1). As shown in Chapter 2, the model was successfully validated.

Steady-state simulations were conducted imposing the same static pressure (129000 Pa) at the outlet boundary of each modeled rotor. Even if this is not the appropriate boundary condition for consistently comparing the performance of different designs (each rotor can be at a different aerodynamic loading level), this approach makes it possible a direct comparison with the baseline rotor performance (Figure 3.6).

Figure 3.6 compares the predicted efficiency of each new rotor to the computed one of Rotor 37 at the same normalized mass flow. For each rotor, the mass flow was normalized using the corresponding computed choking mass flow rate. For completeness, Figure 3.7 shows the predicted choking mass flow rate of different designs. The rotors named as "others" in Figures 3.6 and 3.7 correspond to those modeled rotors which can not simply

classified as “forward or backward curved”, such as the rotor derived from the application of stacking line “D” in Figure 3.2.

An observation is important at this point about sweep application. When swept rotors were modeled, no attempt was made to redesign the blade profiles at each stack option to retain the cascade area ratios of Rotor 37 in terms of throat margin (ratio of the throat area to the upstream inlet area, see Figure 3.5), internal contraction (ratio of the throat area to the mouth area) and effective camber (ratio of the throat area to the discharge area). Each cascade area of Figure 3.5 is to be considered as a quasi-three-dimensional flow area, that is the product of the two-dimensional passage width times a streamtube lamina thickness determined from an axisymmetric flow calculation. The cascade area ratios above mentioned can have a considerable influence on transonic airfoil performance (Wadia and Copenhaver, 1996) and can be significantly altered by sweep application. The idea is to obtain a first overview of performance of modeled swept rotors and adjust, if it is worthwhile doing it, the most promising of them later, according to the procedure suggested by Wadia and Copenhaver (1996). Therefore, while the results in Figure 3.6(b) can be considered a direct consequence of the stacking line shape (no changes in cascade area ratios are induced by the application of lean), the perceived performance changes with the swept rotors (Figure 3.6(a)) could not be an effect of blade curvature only.

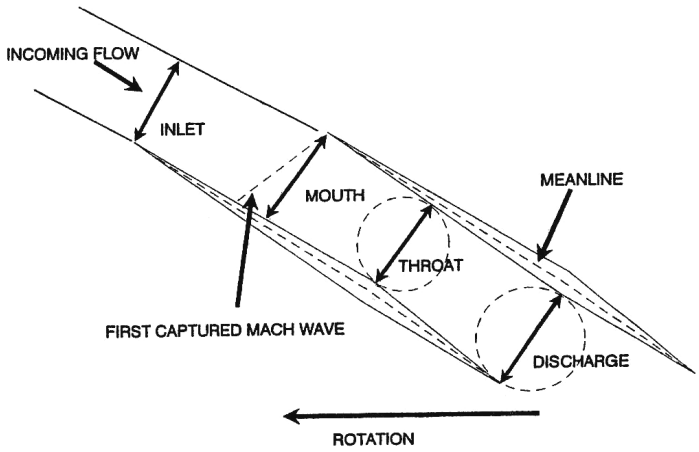

Fig. 3.5 Definition of cascade areas (from Wadia and Copenhawer, 1996).

In Figure 3.6(a), all the rotors with a blade regularly curved downstream (aft swept) are marked with red triangles, while blue rhombuses indicate all the rotors with a blade significantly turned upstream (forward swept). Among swept rotors, the highest efficiencies were obtained by the aft swept rotors, which showed an efficiency of about 0.5-0.6% higher than that of Rotor 37 considering the same working condition. They gave also the highest choking mass flows, up to 4% higher compared to that of baseline rotor. Similar results were obtained by Abdelhamid *et al.* (1998). The application of forward sweep, instead, did not provide substantial improvements in the overall efficiency, inducing also a significant reduction of choking mass flow.

Forward leaned rotor blades (light blue square in Figure 3.6(b)) showed the most promising results. Some of them gave an efficiency increment of 1.2% with respect to the baseline blade. Backward leaned curvature, instead, was detrimental in most cases (pink rhombuses). All the leaned rotors produced a choking mass flow very similar to that of Rotor 37 (see Figure 3.7).

The aerodynamic behavior of the most interesting rotors (including the most promising rotors) was then simulated imposing different values of back pressure. Figure 3.8 shows some of the efficiency maps so obtained. For each map, the lower mass flow operating point corresponds to the last point for which the steady-state model implemented was able to converge. Note the impact of sweep and lean on the operating range. The possibility to widen the operating range using blade curvature will be argued in Chapter 4 (Section 4.2). As far as the overall efficiency, Figure 3.8 confirms observations made about Figure 3.6. Note the efficiency improvements induced using forward lean. Note also the disappointing performance shown by the selected forward swept rotor. In general, all the forward swept rotors did not show promising results. This seems to be in opposition with the general opinion that forward sweep can improve transonic compressor rotor performance (Wadia *et al.*, 1998; Hah *et al.*, 1998; Denton and Xu, 2002). Really, this is due to the different definition of “sweep” used here. As underlined in the introduction of this chapter (Section 3.1), here sweep was defined relative to the axial direction while compressor community generally defines it relative to the local chord direction. Therefore, a direct comparison is not possible.

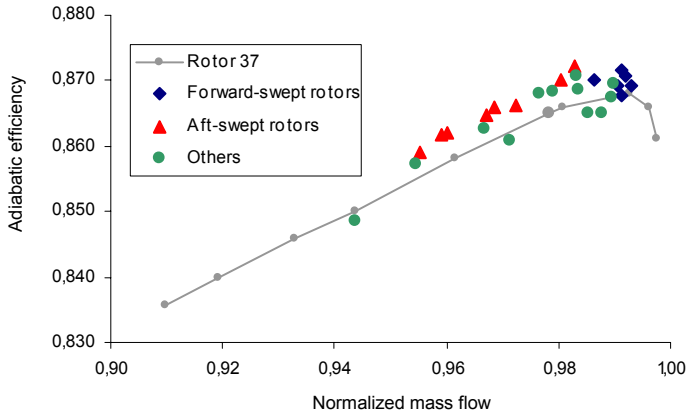

(a) Swept rotors.

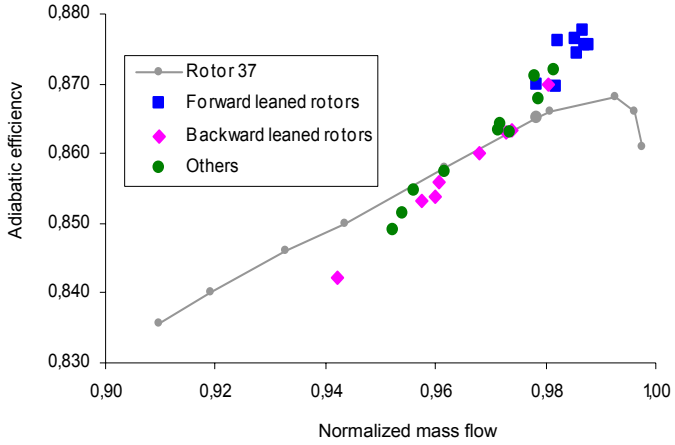

(b) Leaned rotors.

Fig. 3.6 Computed adiabatic efficiency (1800 rad/s).

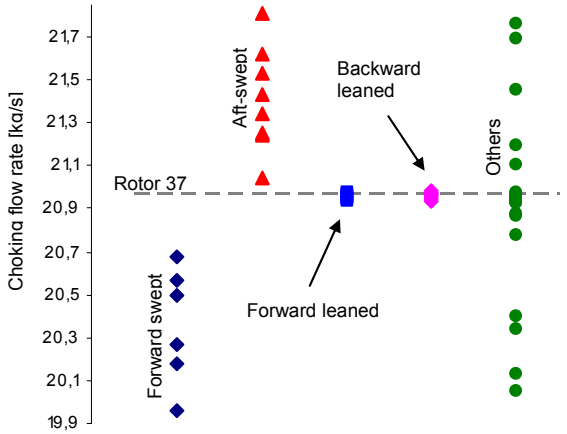

Fig. 3.7 Computed choking mass flows of new designs (1800 rad/s).

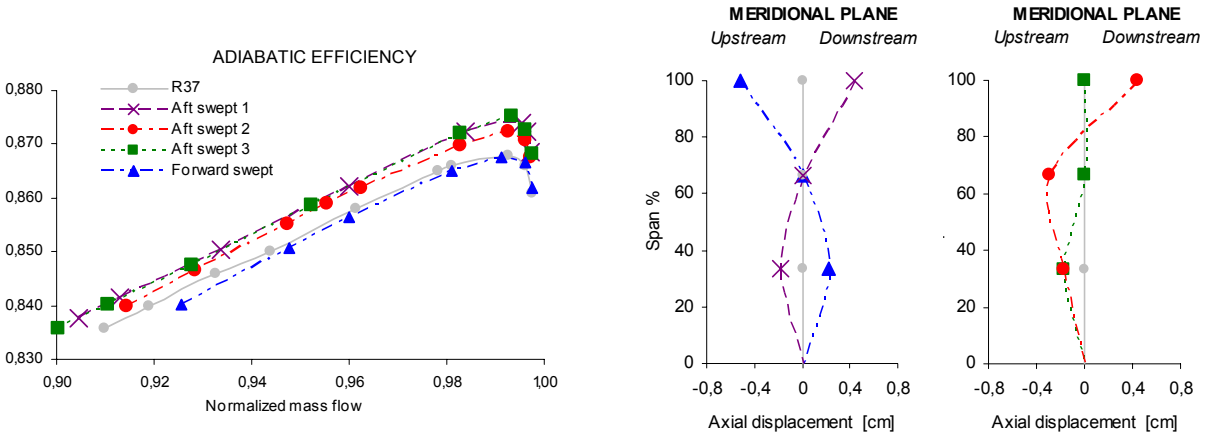

(a) Swept rotors.

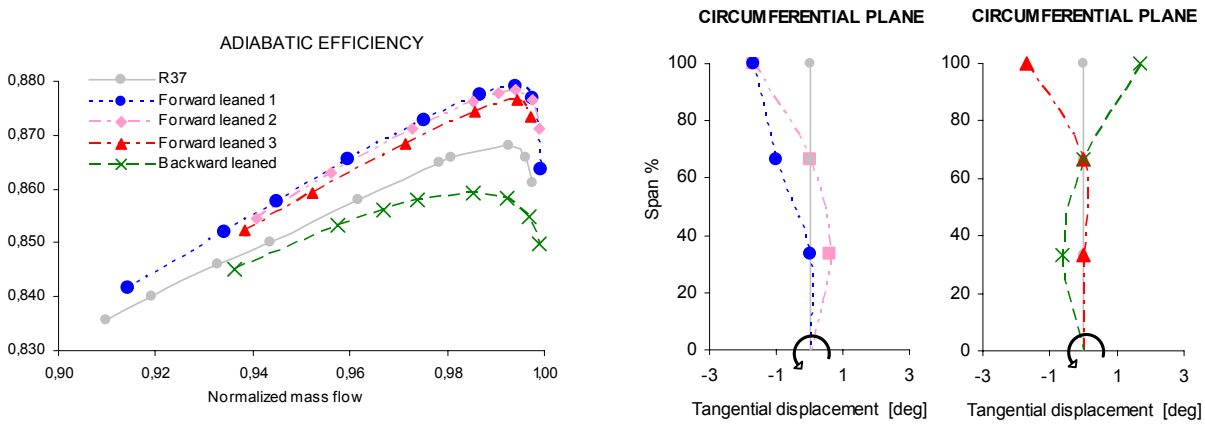

(b) Leaned rotors.

Fig. 3.8 Computed adiabatic efficiency maps.

Figures 3.9(a), 3.9(b), 3.9(c), 3.9(d) and 3.9(e) show the impact of blade stacking line shape on Mach number distribution (94% span and meridional mid plane, 98% normalized mass flow). In those figures, a representative sample of modeled rotors was analyzed and compared to the baseline configuration. The aim is a first understanding on how the blade curvature can impact on the flow field of a transonic compressor rotor. In all those figures, both the Mach number range and the number of contours were kept constant. The Mach number ranges from 0.0 to 1.8 and the interval between contour lines is 0.5.

The impact of blade curvature on the three-dimensional shock structure is clearly visible. As far as the swept rotors (Figures 3.9(b) and 3.9(c)), the applied blade curvatures impacted considerably on the meridional shape of shock front, which clearly tends to follow the meridional blade leading edge curvature. This shows the possibility to influence the inclination of shock front to the incoming flow in the meridional plane and, consequently, to act on the shock strength (which depends on both the upstream Mach number and the angle between the impacting flow direction and the local shock front surface). No significant changes were instead induced by sweep on the blade-to-blade shock structure inside the blade passage. It is interesting, however, to underline the impact on the shock bow departing from the blade leading edge and moving upstream. With respect to the baseline configuration, its strength is lower when the blade is locally curved upstream (cases (*i*) and (*ii*) of Figure 3.9(b), case (*ii*) of Figure 3.9(c)) and slightly higher when the blade is locally curved downstream (case (*iii*) of Figure 3.9(b), cases (*i*) and (*iii*) of Figure 3.9(c)).

As well as the swept rotors, also the leaned rotors (Figures 3.9(d) and 3.9(e)) showed a meridional shock front considerably influenced by the applied blade curvatures. In the case of lean, however, this is not due to a change in the meridional blade leading edge

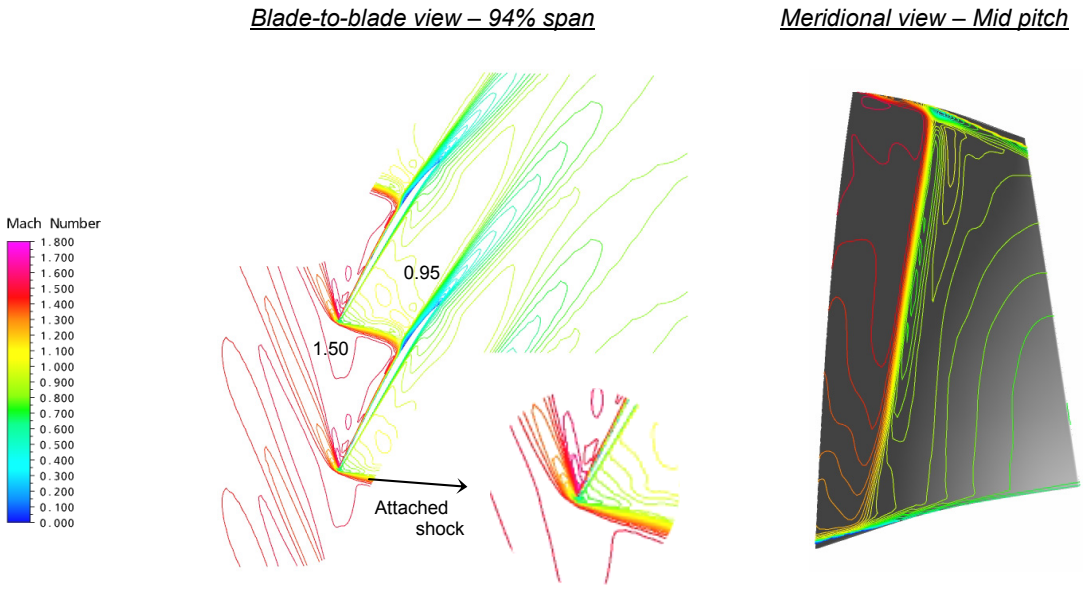

Fig. 3.9(a) Relative Mach number contours – Rotor 37 (98% ch. mass flow).

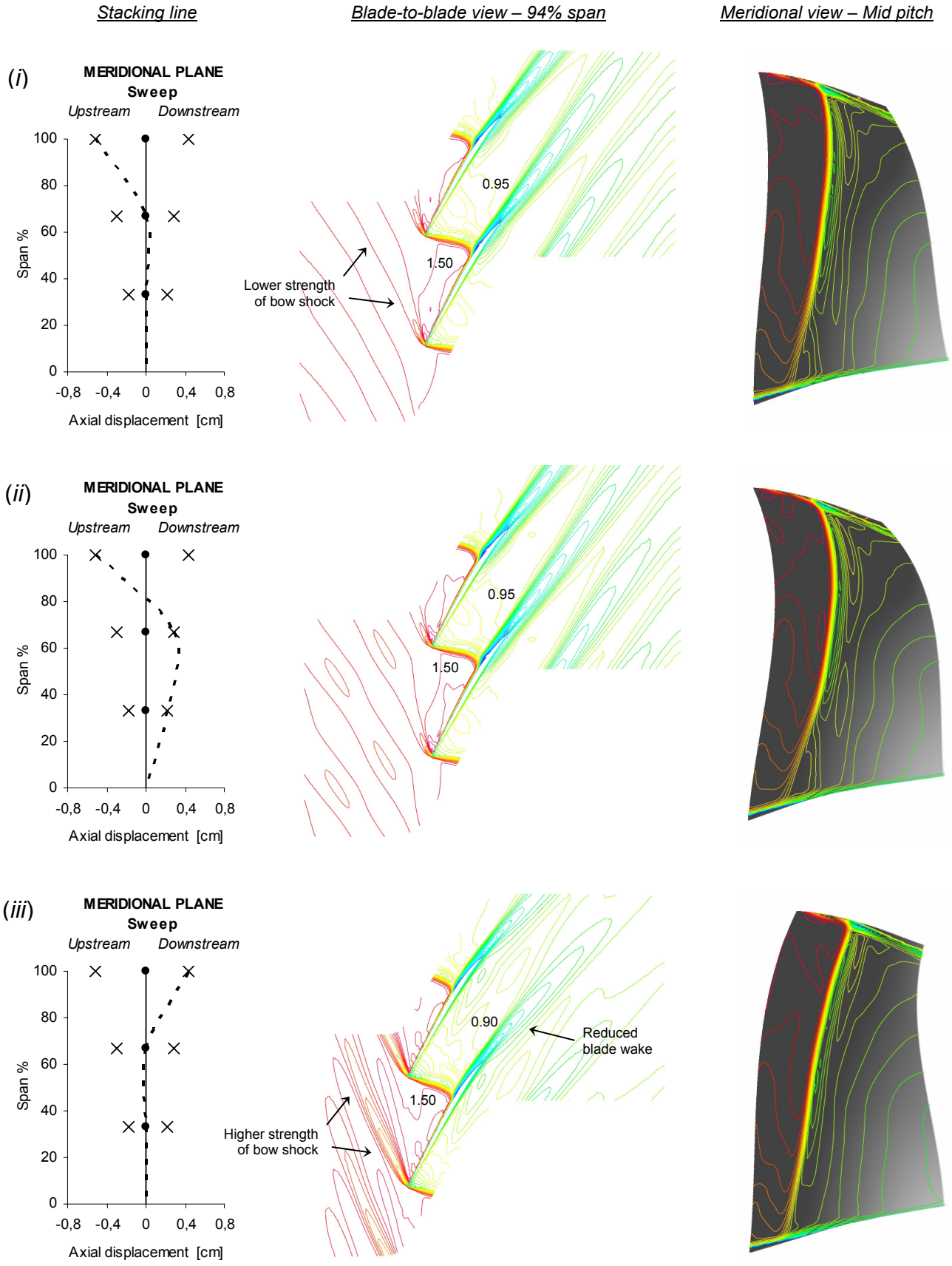

Fig. 3.9(b) Swept rotors.

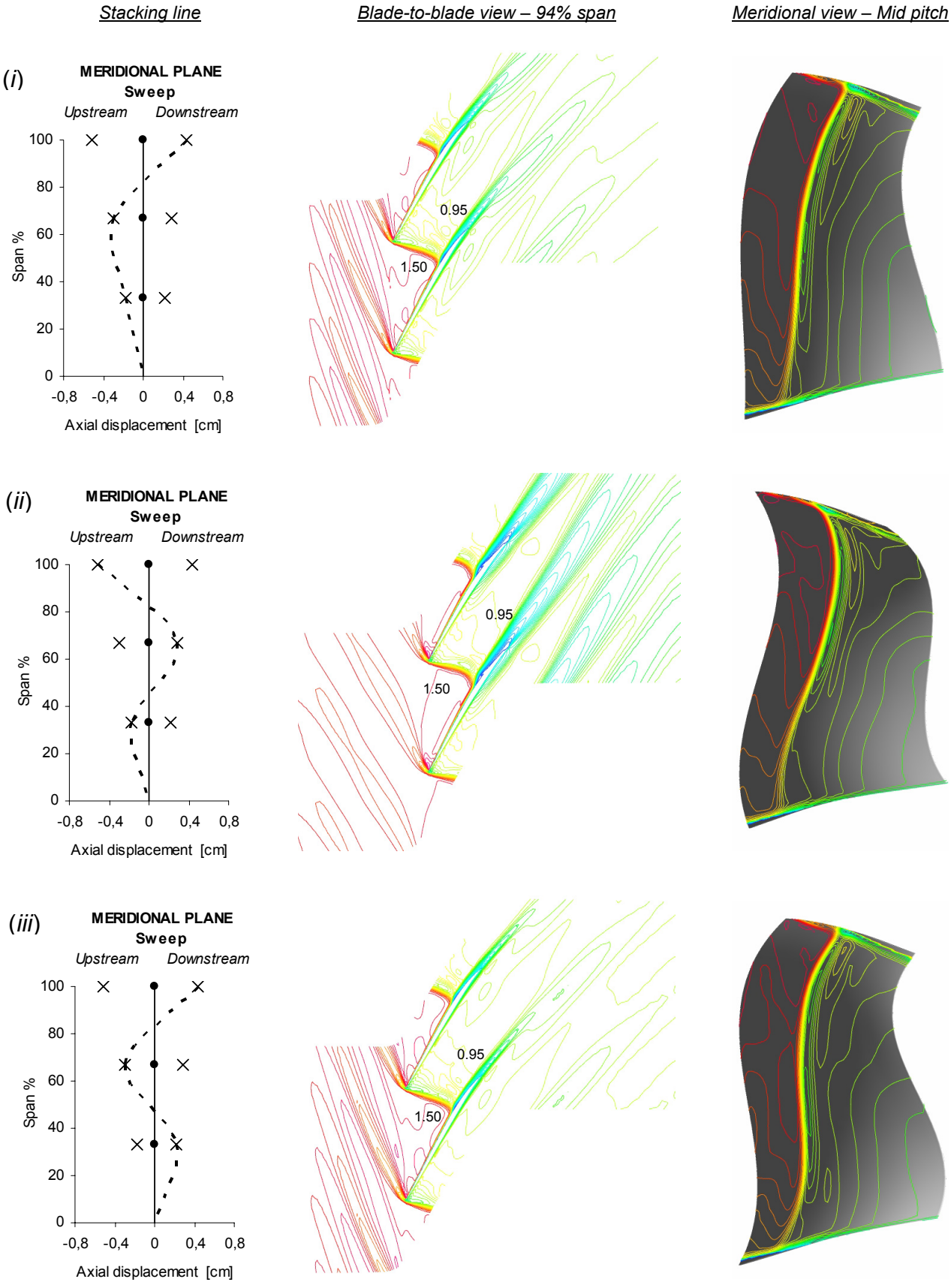

Fig. 3.9(c) Swept rotors.

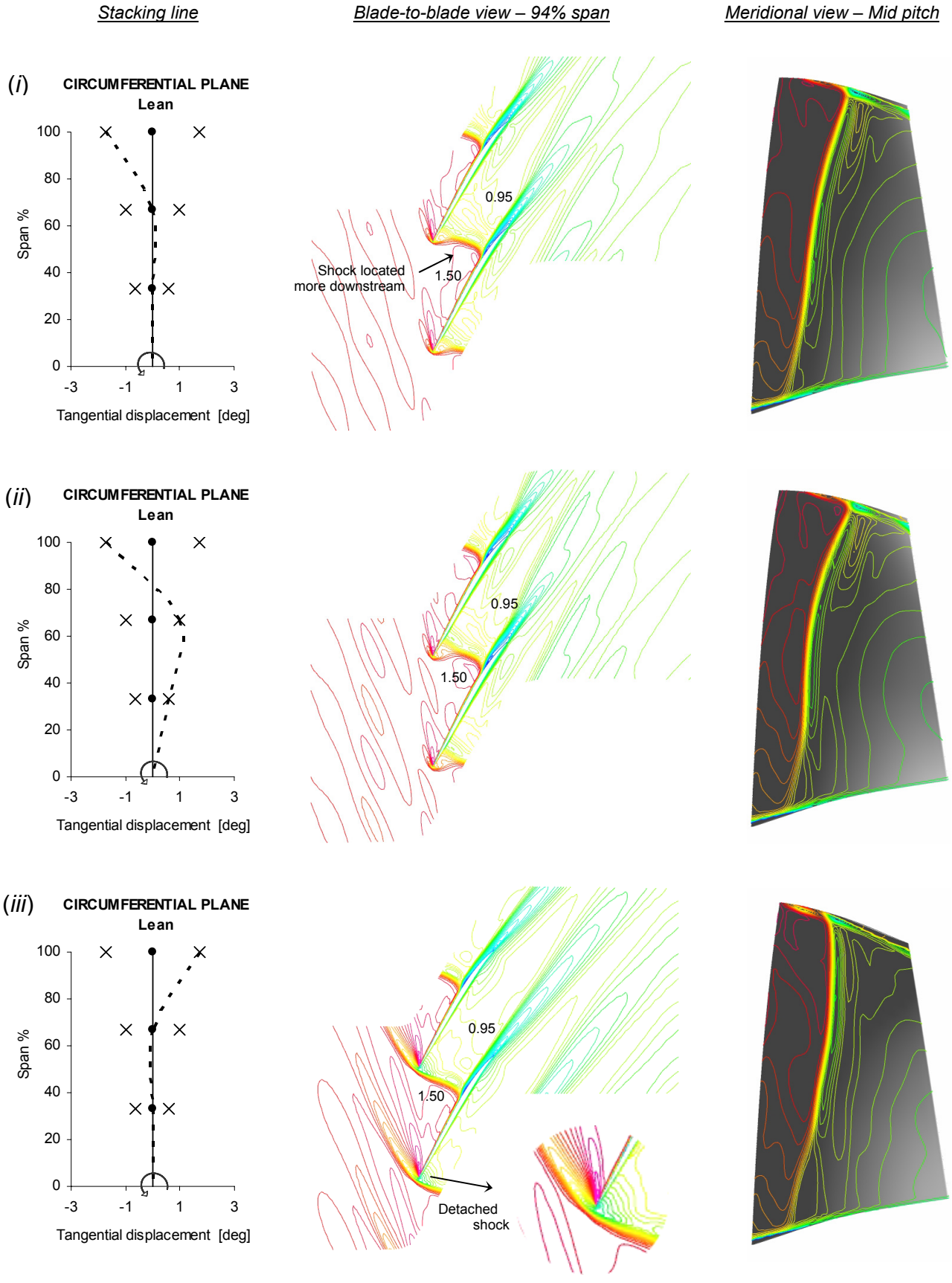

Fig. 3.9(d) Leaned rotors.

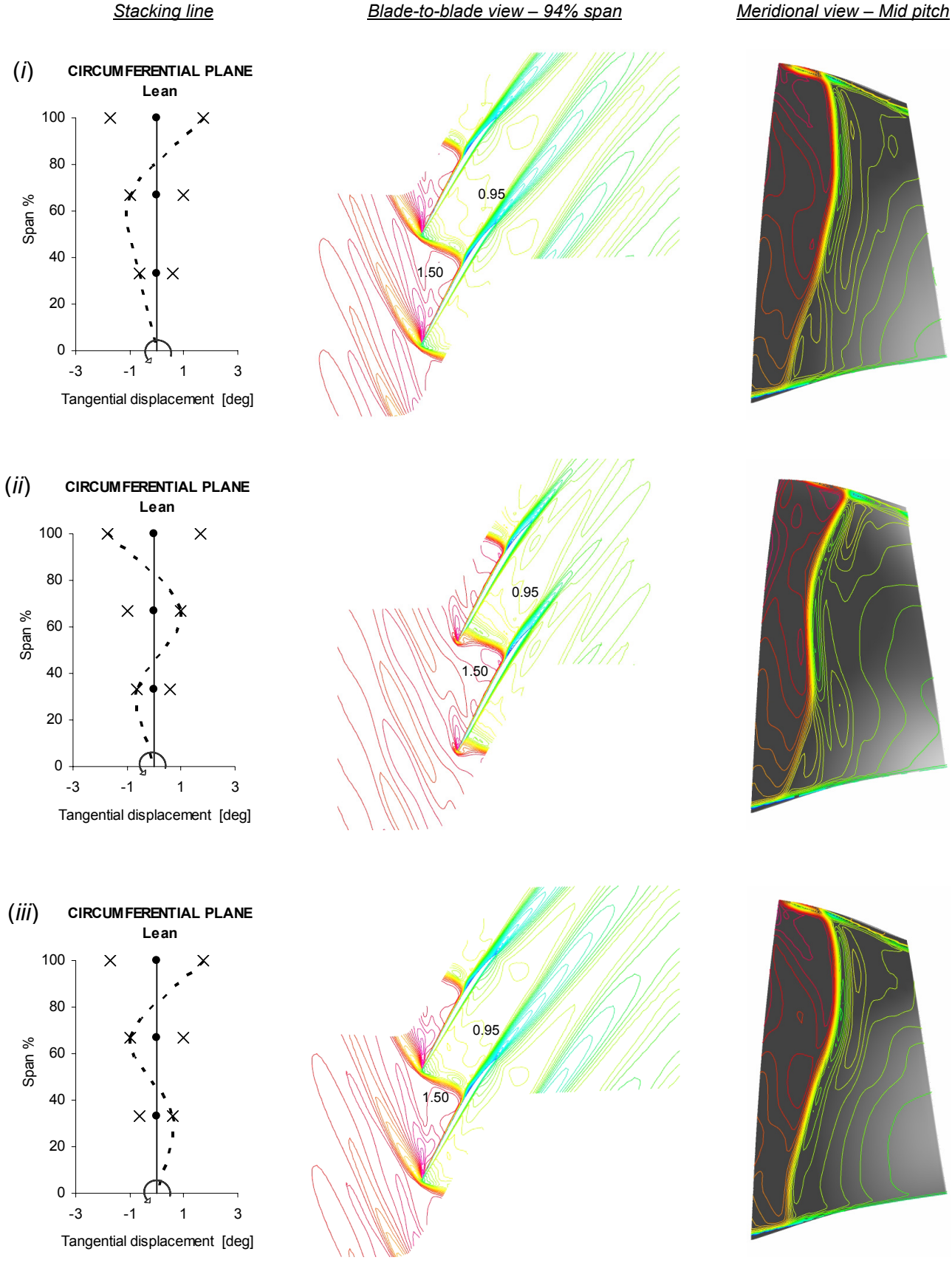

Fig. 3.9(e) Leaned rotors.

shape (which is equal to that of baseline configuration), but is a direct consequence of a considerable modification of blade-to-blade shock structure. In fact, when the blade is locally curved toward the direction of rotor rotation (see cases (*i*) and (*ii*) of Figure 3.9(d), case (*ii*) of Figure 3.9(e)) the shock undergoes a turning toward a more oblique pattern on the blade-to-blade view and then turns again, becoming orthogonal to the suction surface of the adjacent profile. Instead, when the blade is contrarily curved (case (*iii*) of Figure 3.9(d), cases (*i*) and (*iii*) of Figure 3.9(e)) the blade-to-blade shock front moves slightly upstream, detaching from the blade leading edge. All this impacts on the blade-to-blade shock location and, consequently, on the meridional shock shape. Note also the impact of lean on the shock bow that develops outside the vanes. It does not appear when the blade is curved toward the direction of rotor rotation, while becomes stronger when the blade is contrarily curved.

A strong impact of blade stacking line curvature on blade wakes was also observed. At 94% span, for instance, a significant reduction of wideness and deepness of blade wake was observed in locally aft swept rotors (case (*iii*) of Figure 3.9(b) and cases (*i*) and (*iii*) of Figure 3.9(c)) and locally forward leaned rotors (cases (*i*) and (*ii*) of Figure 3.9(d), case (*ii*) of Figure 3.9(e)).

In short, the applied blade curvatures showed a significant impact on the flow field of Rotor 37. As described above, the three-dimensional shock structure was considerably influenced and a significant impact on blade wakes was also observed. Both shock and blade wakes are source of entropy and induce aerodynamic losses, therefore changes in their structure can have a great influence on rotor performance. Effectively, a noticeable impact on overall efficiency was observed. Forward lean and aft sweep, in particular, allowed to obtain significant increments in the rotor efficiency, up to 1.2 percentage points at the design working condition.

In the first part of Chapter 4 (Section 4.1), the aerodynamic behavior of some swept and leaned blades will be analyzed in detail with the aim to understand the relationships between the induced changes in the flow field and the calculated overall efficiency, as well as to investigate the aerodynamic reasons for the induced flow changes.

3.4 Structural impact

Sweep and lean were investigated also from the structural point of view. The structural behavior of two among the most promising rotor blades (a leaned one and a swept one which showed good aerodynamic performance) was numerically calculated. Figure 3.10 shows the geometry of the selected blades.

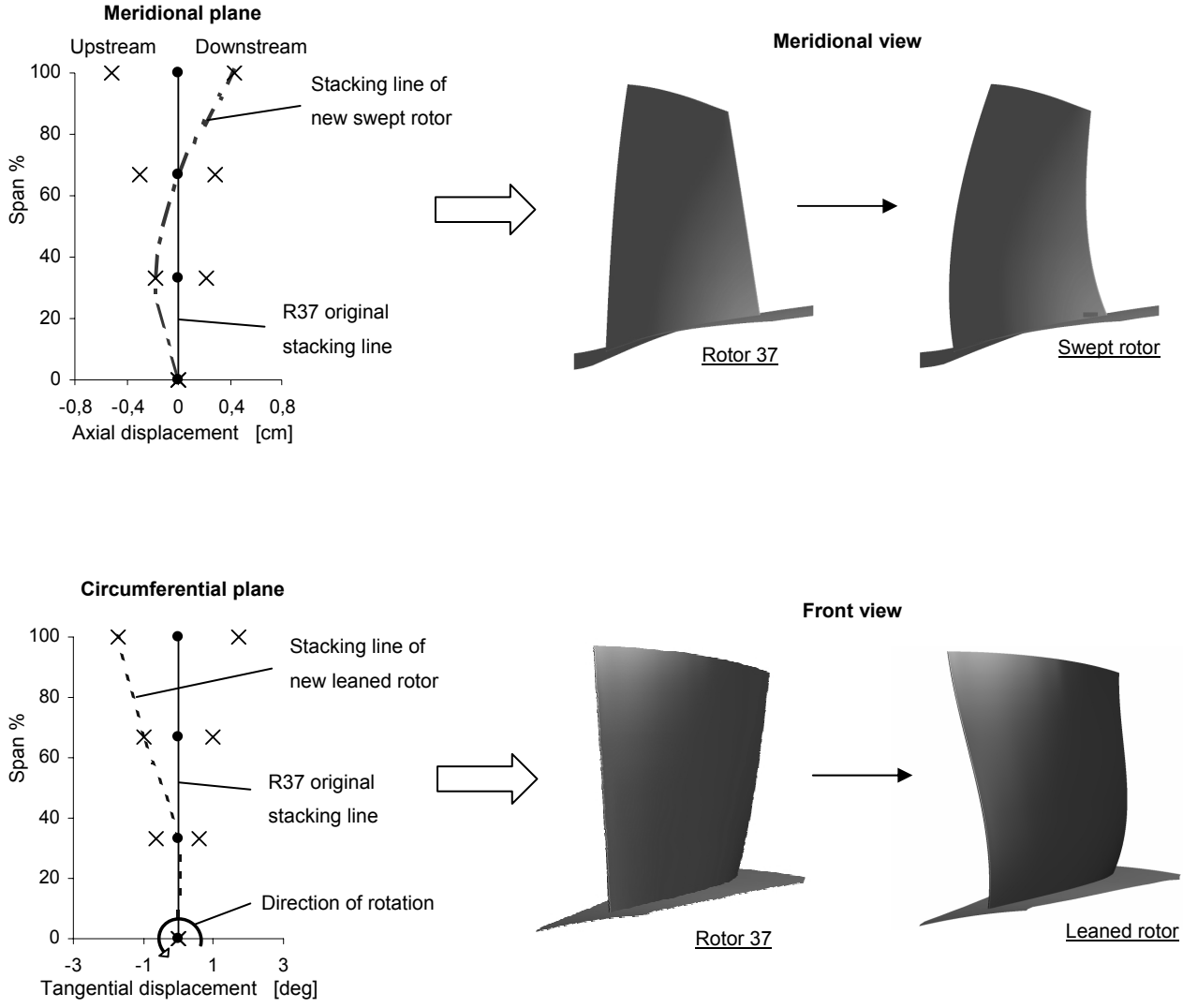

Fig. 3.10 Swept (top) and leaned (bottom) selected blades for FEM analysis.

The structural behavior of the selected blades was compared to that of baseline configuration at the design operating condition (98% normalized mass flow, 1800 rad/s). The FEM package "ANSYS Structural" was used. Both static and modal responses were evaluated. A mapped mesh with hexahedral-shaped (brick) elements was utilized (Figure 3.11). Both aerodynamic and centrifugal loads were considered in the analysis. No displacements were permitted at the hub section.

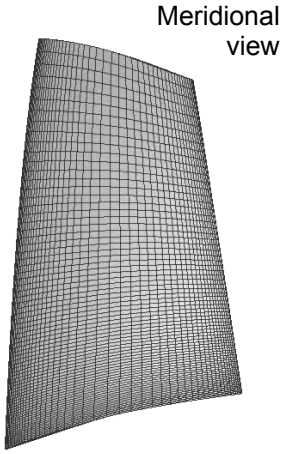

Fig. 3.11 Blade FEM mesh (Rotor 37).

A predefined unidirectional "ANSYS CFX" to "ANSYS Structural" load transfer method was utilized to transfer the static pressure distribution around the blade (calculated

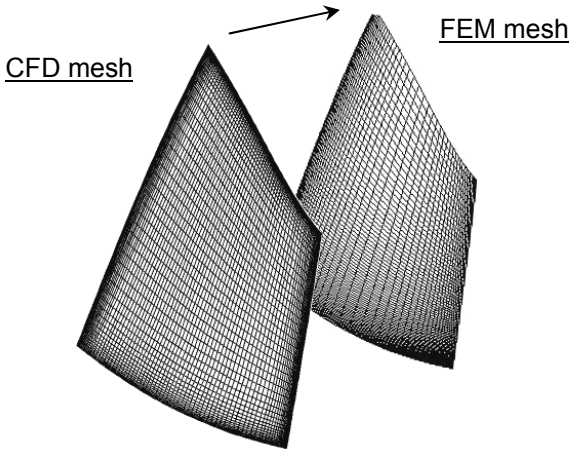

Fig. 3.12 One-way fluid-structure interface.

using Model 3 of Table 2.1) from the CFD mesh to the FEM mesh of the structural model (Figure 3.12).

First of all, the computed modal response of selected blades was compared to that of baseline blade. The analysis did not show significant changes due to the applied blade curvatures in the vibration natural frequencies (Table 3.1) or in vibration mode shapes (not reported here for brevity).

Table 3.1 – Computed natural frequencies (Hz).

Mode number	Baseline blade	Swept blade	Leaned blade
1	827	784	774
2	2320	2047	2131
3	2962	2829	2907

A considerable impact of blade curvature on the structural behavior was instead observed in terms of static response. Differently from the baseline blade, both the swept blade and the leaned blade showed a central region characterized by high values of Von Mises stress. This is shown in Figures 3.13 and 3.14.

It was observed that the blade curvature has not a significant impact on the static response if the pressure load is the only load applied. Therefore, the structural behavior shown by new blades in Figures 3.13 and 3.14 is due fundamentally to the action of centrifugal load. The phenomenon can be simply explained as follows. If the blade is radially-stacked, such as the baseline blade, the centrifugal load gives rise to a tensile stress only; but if the blade is curved, such as the new blades analyzed, the centrifugal load gives rise to both a tensile stress and a bending stress (Figure 3.15). In transonic compressor rotors the centrifugal load is very strong (due to the high blade tip velocity) and considerable bending stresses can arise, leading to the static structural response shown in Figures 3.13

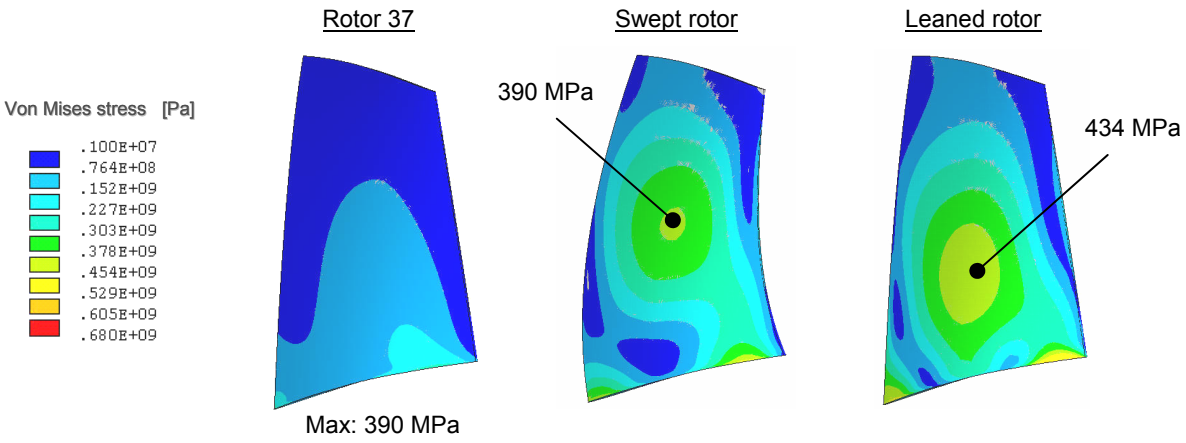

Fig. 3.13 Computed Von Mises stress contours – Suction surface.

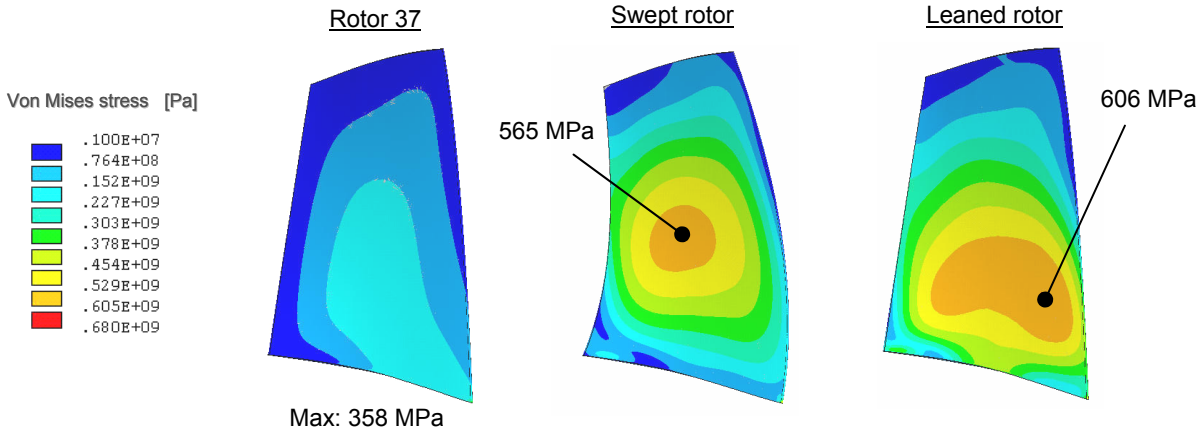

Fig. 3.14 Computed Von Mises stress contours – Pressure surface.

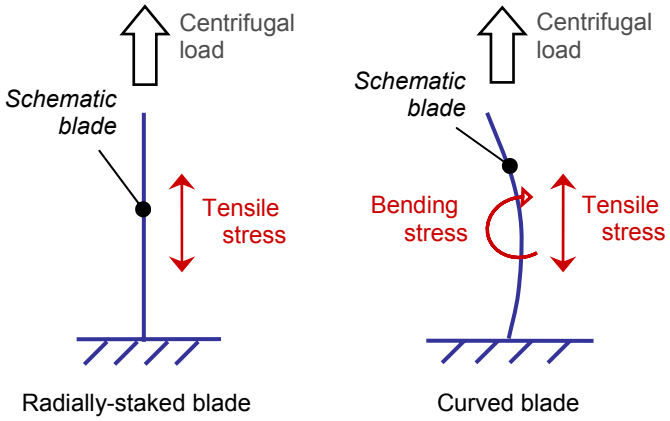

Fig. 3.15 Blade structural behavior.

and 3.14. This does not mean that the concepts of sweep and lean can not be used in transonic rotors, but that the aerodynamic design of a swept and/or leaned transonic rotor blade must be developed also from the structural point of view.

CHAPTER 4

Aerodynamic sweep and lean: detailed analyses

4.1 On the efficiency improvements induced by aft sweep and forward lean

In Chapter 3 the impact of blade stacking line curvature on the overall efficiency of Rotor 37 was systematically investigated. Starting from the Rotor 37, a quite large number of new axially swept and tangentially leaned rotors were modeled and numerically simulated. The forward leaned rotors and the aft swept rotors gave a substantially higher efficiency compared to the baseline radially-stacked Rotor 37, showing considerable changes in the three-dimensional shock structure as well as in the development of blade wakes. In following sections, some of such promising rotors will be analyzed in details with the aim to understand the relationships between the induced changes in the flow field and the calculated overall efficiency, as well as to investigate the aerodynamic reasons for the induced flow changes. When not specified, Model 3 of Table 2.1 was used for computations. Steady-state simulations were carried out.

4.1.1 The most promising aft swept and forward leaned rotors

Figure 4.1 shows the blade stacking line of the two rotors analyzed in this section: the most promising swept rotor and the most promising leaned rotor among those presented in Chapter 3 (see Section 3.2). Figure 4.2 shows the calculated performance maps. Compared to the baseline rotor, both the new rotors gave substantial improvements in the overall efficiency along the entire operating range (the leaned rotor, in particular,

gave an efficiency increment of about 1.3 percentage points at 99% of choking mass flow). In addition, a slightly higher total pressure ratio was achieved.

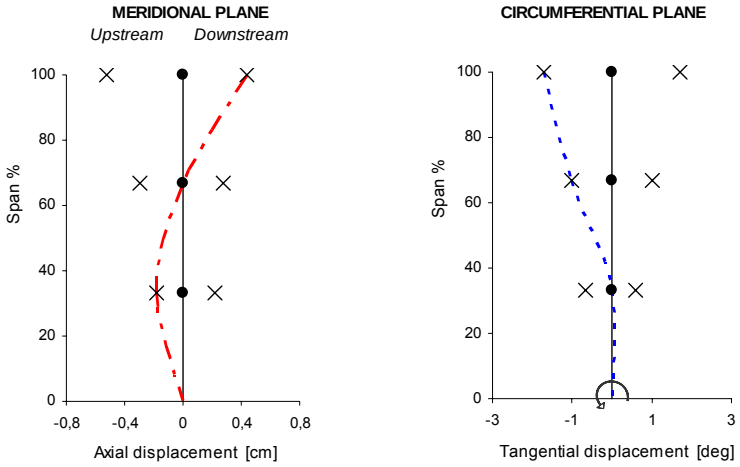

(a) Swept **(b) Leaned**

Fig. 4.1 Blade stacking lines.

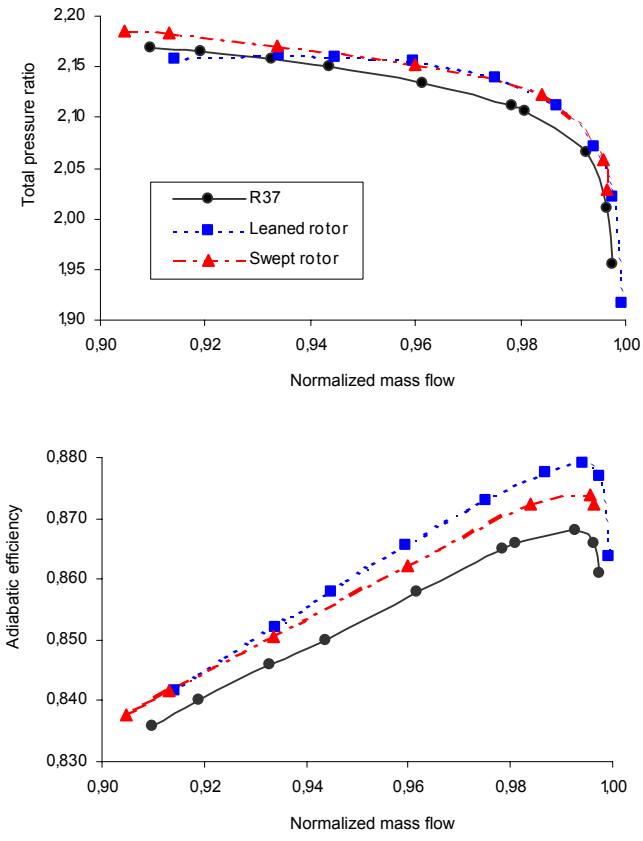

Fig. 4.2 Computed performance maps.

Figure 4.3 shows the distribution of the relative Mach number inside the blade passage at the peak efficiency condition (close to the 99% of choking mass flow). As shown, changes in shock structure are in a great agreement with observations made in Chapter 3 (Section 3.3). At the upper half of the span height, the leaned rotor showed a shock front considerably curved downstream in the blade-to-blade view (Figures 4.3(b) and 4.3(c)); in consequence, a slightly aft swept inclination was induced in the meridional plane (Figure 4.3(a)). The swept rotor showed a more oblique shock pattern from hub to tip compared to the unswept rotor (Figure 4.3(a)), due to the meridional blade leading edge curvature; no significant changes are instead noticeable in the blade-to-blade views with respect to the Rotor 37. In short, both rotors developed a shock structure somehow more inclined to the incoming relative flow than in the baseline rotor, making it possible a reduction of shock strength.

Figure 4.4 compares the computed downstream radial distributions of performance quantities at peak efficiency condition. Compared to the baseline rotor, the swept rotor showed a higher efficiency in the spanwise region far from the walls, while the leaned rotor from 40% to 80% span (especially around 60-70% span).

Figure 4.5 shows the entropy distribution downstream the rotor (circumferential view). In an adiabatic flow, as modeled here, the entropy creation is due exclusively to the aerodynamic irreversibilities; therefore, Figure 4.5 can be used to identify the regions which are sources of aerodynamic losses. As shown, compared to the baseline rotor, the new rotors gave a reduction of entropy creation (i.e. a reduction of aerodynamic losses) both in the main flow and in blade wakes. In particular, a drop of entropy distribution can be observed in the main flow of the leaned rotor at the outer span, while a reduction of blade wake entropy generation characterizes the swept rotor in the spanwise region ranging from 20% to 80% span.

In short, the higher efficiency shown by the forward leaned blade can be mainly associated with a more efficient flow diffusion at the outer half span region, due to a more favorable three-dimensional shock structure. In fact, toward the peripheral region the shock is considerably inclined to the incoming flow (both in the blade-to-blade and meridional views), leading to a local reduction of aerodynamic shock losses and entropy generation.

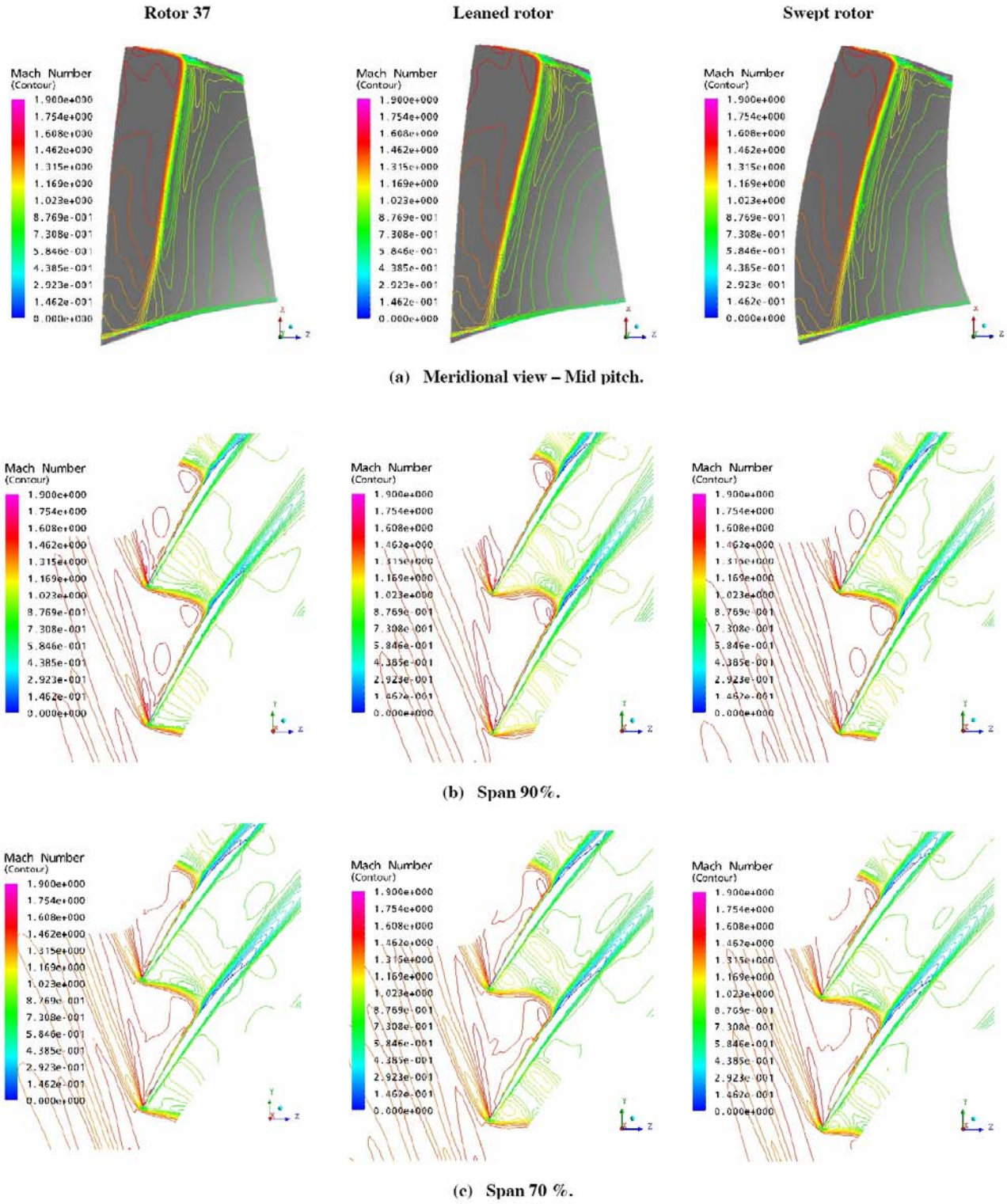

Fig. 4.3 Comparison of relative Mach number distributions – peak efficiency.

Instead, the increment in efficiency given by the aft swept rotor is largely due to a less detrimental blade wake development. Blade wakes are a great source of entropy and aerodynamic losses, and a reduction in their magnitude has a positive impact on the overall rotor efficiency.

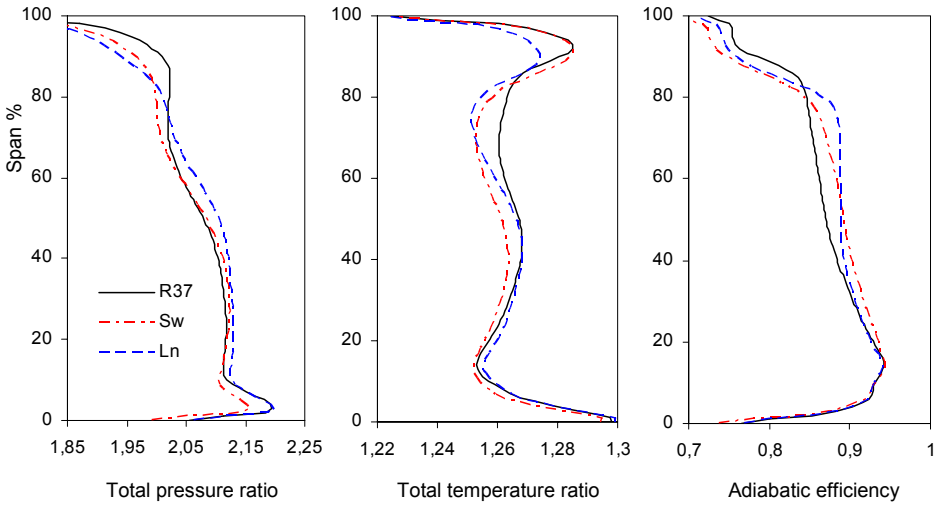

Fig. 4.4 Radial plots at outlet – peak efficiency.

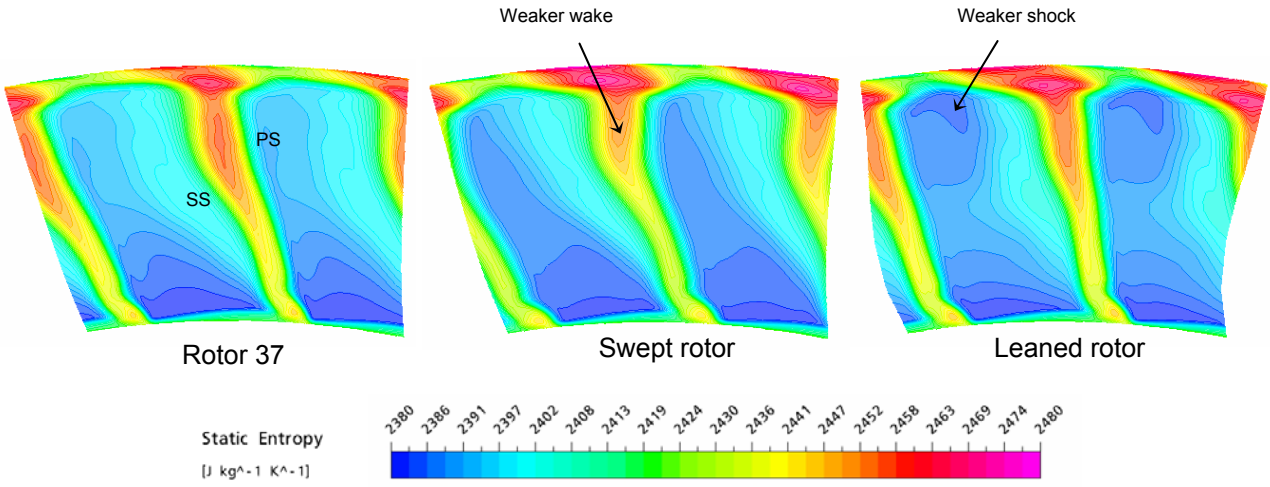

Fig. 4.5 Static entropy distribution after the trailing edge – peak efficiency.

4.1.2 A promising locally swept rotor

In this section, the swept rotor shown in Figure 4.6 was analyzed. The given stacking line led to a blade slightly swept downstream above the 30-35% span. Contrary to all expectations, this rotor showed interesting aerodynamic performance (Fig. 3.8(a)), giving an efficiency of about 0.5-0.8% higher than that of baseline configuration along the entire operating range. It gave also slightly higher values of both total pressure ratio and choking mass flow.

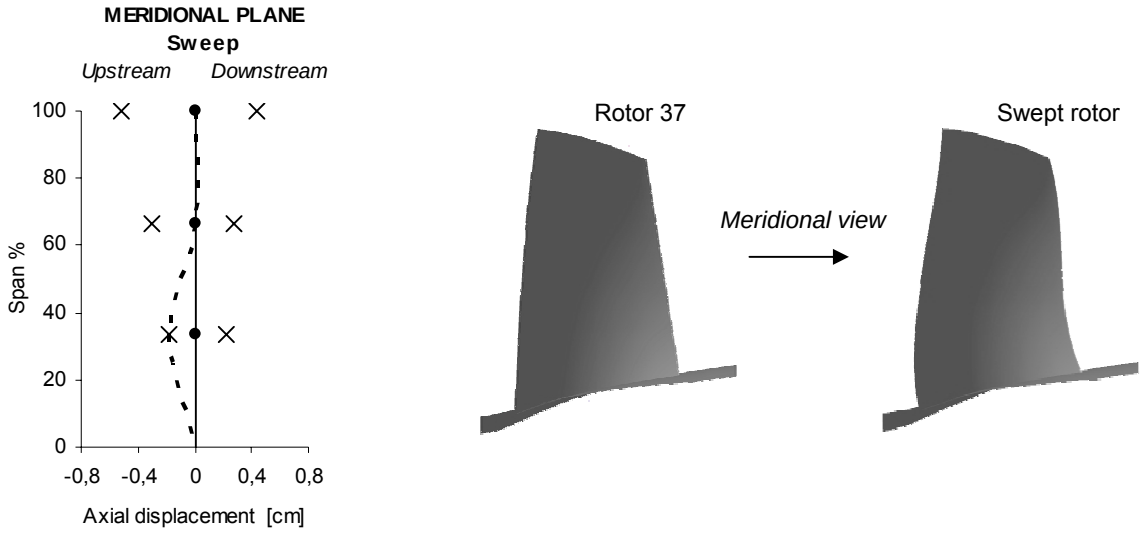

Fig. 4.6 Baseline and redesigned blade geometry.

As mentioned in Chapter 3 (Section 3.3), the swept blade profiles of modeled swept rotors (including the swept one considered here) were not recambered to retain the cascade area ratios of baseline configuration, in terms of throat margin, internal contraction and effective camber. This can have introduced other variables of influence in addition to the applied blade curvature. Here, in order to isolate the aerodynamic impact of the applied blade curvature, the swept blade was redesigned at 33% span in according to the procedure suggested by Wadia and Copenhaver (1996). The result is shown in Figure 4.7. In this way, the new swept rotor (the recambered rotor) achieved the aerodynamic similarity (in terms of cascade area ratios) with Rotor 37.

Figure 4.8 shows the calculated speed line of the recambered rotor and compares it to that of both not recambered and baseline versions. As shown, recambering did not impact significantly on the overall efficiency (a slightly increment was induced), but reduced the total pressure ratio to the corresponding values of Rotor 37. It reduced also the choking mass flow rate to that of Rotor 37. All this showed the possibility to increase the overall efficiency of a radially-stacked transonic compressor rotor using such a swept blade curvature and maintain the design requirements, especially in terms of choking mass flow rate (differently from lean, sweep showed a considerable impact on the mass flow at choking condition, as can be observed in Figure 3.7).

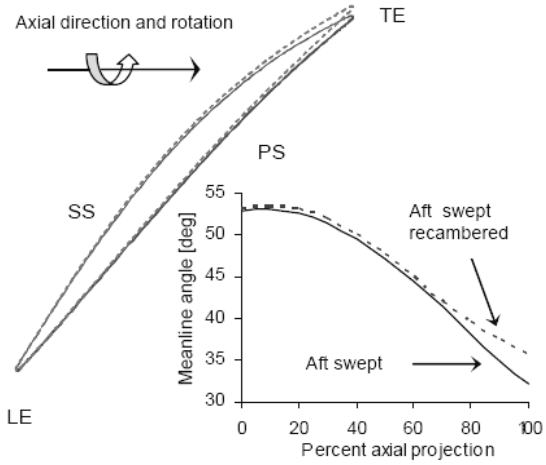

Fig. 4.7 Swept rotor recambering – 33% span section.

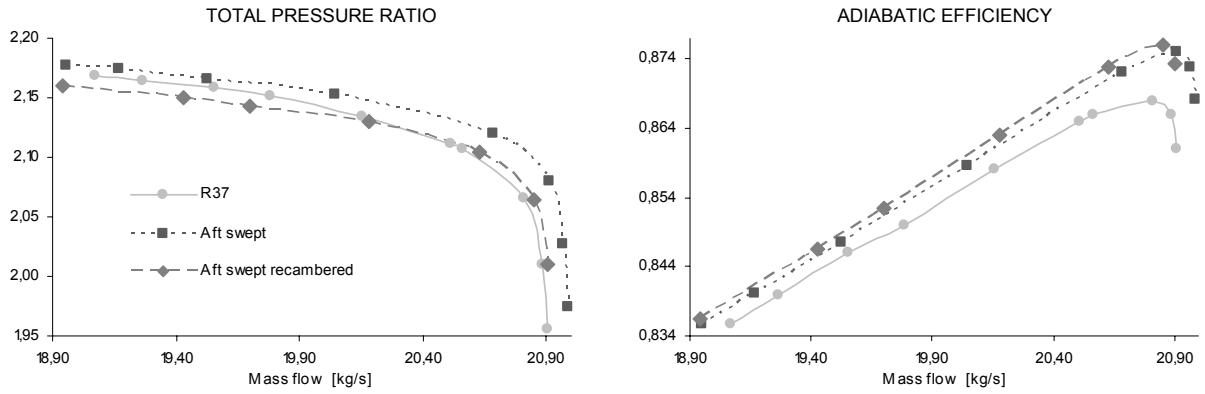

Fig. 4.8 Total pressure ratio and adiabatic efficiency speed lines (1800 rad/s).

After that, the internal flow features of recambered swept rotor were analyzed in detail and compared to that of Rotor 37. Figure 4.9 shows the performance spanwise profiles calculated at the outlet section of the computational domain (peak efficiency condition). Similarly to the swept rotor of Section 4.1.1, the higher overall efficiency is due to a better aerodynamic behavior in the spanwise region ranging from 20% and 80% span, thanks to a less detrimental blade wake development (Figure 4.10).

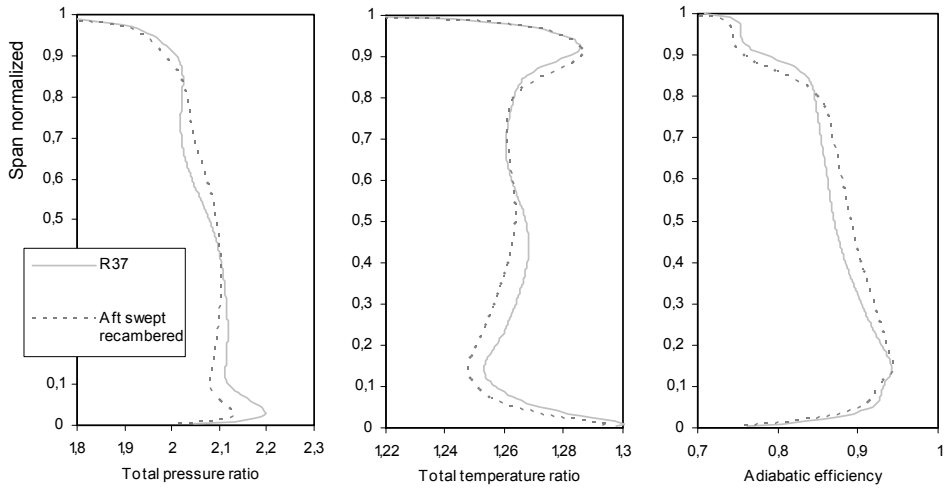

Fig. 4.9 Performance spanwise profiles at outlet – peak efficiency condition.

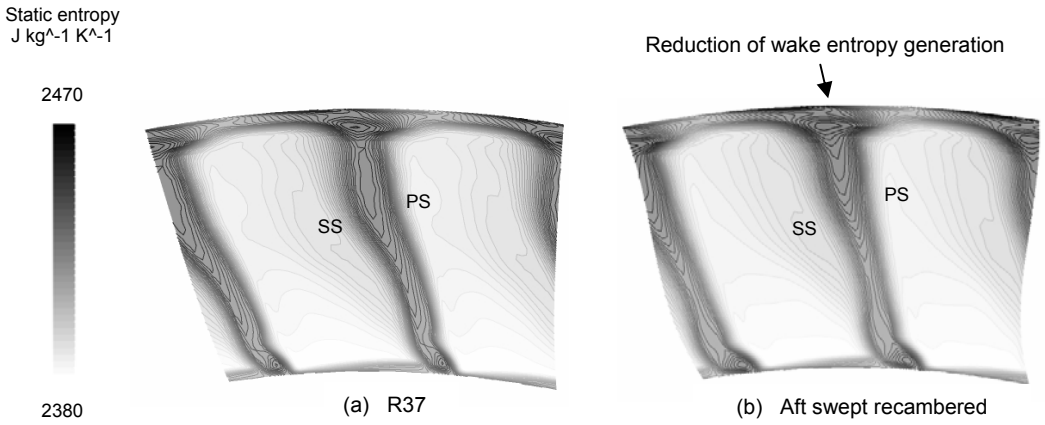

Fig. 4.10 Static entropy distribution after the trailing edge – peak eff.

It is particularly evident that the blade wake developed inside the swept rotor is less wide than that of baseline rotor. Around 33% span, this is mainly due to the recambering of blade profile, which led to a lower camber angle than in the baseline configuration (see Figure 4.7 for details). Instead, at span locations where the blade profile was not changed (at 67% span for instance) the improvements in blade wake development must be associated with other aerodynamic reasons.

Figure 4.11 suggests that, around 67% span, the blade wake inside the swept rotor is less wide than in the Rotor 37 thanks to a reduction of the blade suction side boundary layer thickness. This was attributed to a weaker outward radial flow of fluid particle inside the boundary layer. As outlined in Chapter 1 (Section 1.2), transonic compressor rotors are characterized by a strong radial fluid migration inside the blade suction side boundary layer after the shock. The flow phenomenon is well visible in Figure 4.12, which shows the relative Mach number distribution near the suction surface at peak efficiency condition, along with some streamlines inside the boundary layer released at the leading edge. This flow feature is detrimental because obstructs the boundary layer flow in the streamwise direction, inducing a boundary layer thickening. Figure 4.12 shows that the radial fluid migration is slightly less pronounced in the swept rotor than in the Rotor 37. This allows a higher streamwise velocity component inside the boundary layer (Figure 4.13), with a positive impact on the boundary layer thickness and wake development.

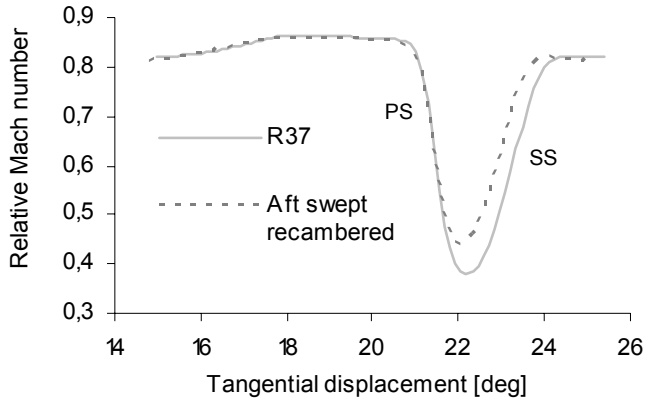

Fig. 4.11 Pitchwise distribution of relative Mach number after the TE. (67% span – peak efficiency condition)

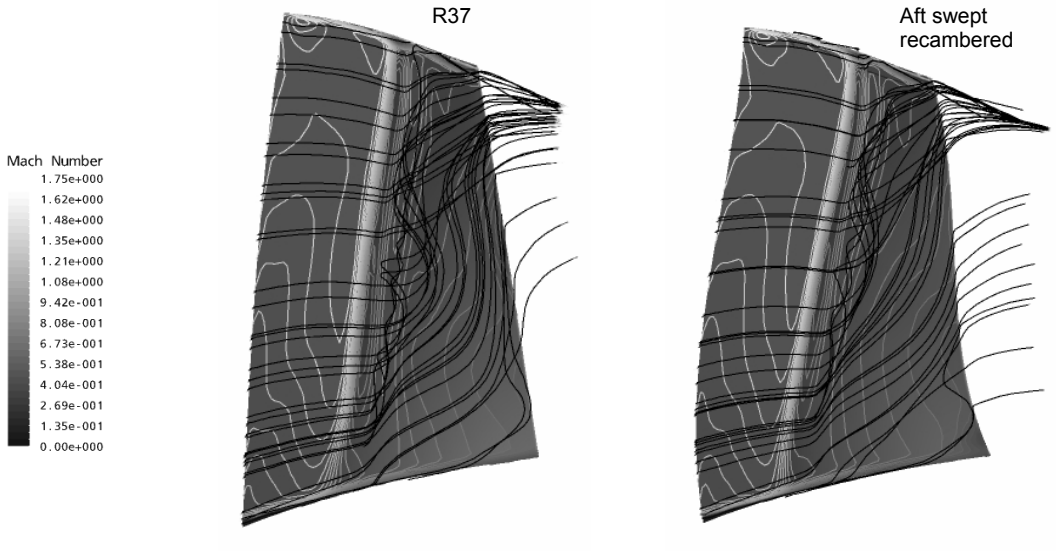

Fig. 4.12 Relative Mach number contours near suction surface and streamlines inside boundary layer – peak efficiency condition.

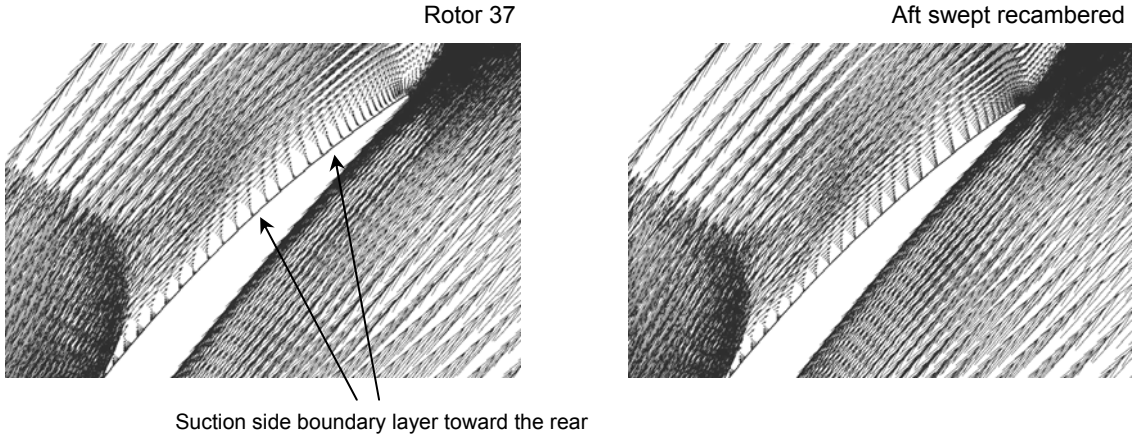

Fig. 4.13 Comparison of relative velocity vectors – blade-to-blade view. (Peak efficiency – 67% span)

The reasons why the radial outward fluid migration is stronger in the baseline configuration than in the swept rotor were not completely understood. The shock-blade boundary layer interaction is clearly the origin of that characteristic flow phenomenon and a change in the shock structure can have a considerable impact on it. However, that flow phenomenon seems to be mainly influenced by the blade curvature in itself. It seems, in

particular, that the blade curvature impacts considerably on its development after the action of the shock, as can be observed in Figures 4.14 (a), 4.14(b) and 4.14(c). Such figures show clearly that, when the blade is curved upstream the radial fluid flow migration is stronger than when the blade is curved downstream. This was observed both when the blade is regularly curved upstream or downstream (cases (*ii*) and (*iii*) of Figure 4.14(c), for instance) and when the blade is only locally curved upstream or downstream (cases (*i*) and (*ii*) of Figure 4.14(b)). It seems that the downstream curvature helps the fluid particles inside the suction side boundary layer to leave the blade, giving them a higher streamwise velocity component. Instead, the upstream curvature seems to act contrarily.

Figures 4.14 (a), 4.14(b) and 4.14(c) remark also the impact of the radial fluid flow on the blade wake. In general, as can be observed, a strong radial fluid flow is very detrimental to the blade wake development. Cases *i* and *ii* of Figure 4.14(b) point out that at spanwise region where the radial fluid migration is stronger the circumferential blade wake thickness is higher, while where the radial fluid migration is less strong the circumferential blade wake thickness is lower. The other cases of Figures 4.14 (a), 4.14(b) and 4.14(c) confirm these observations.

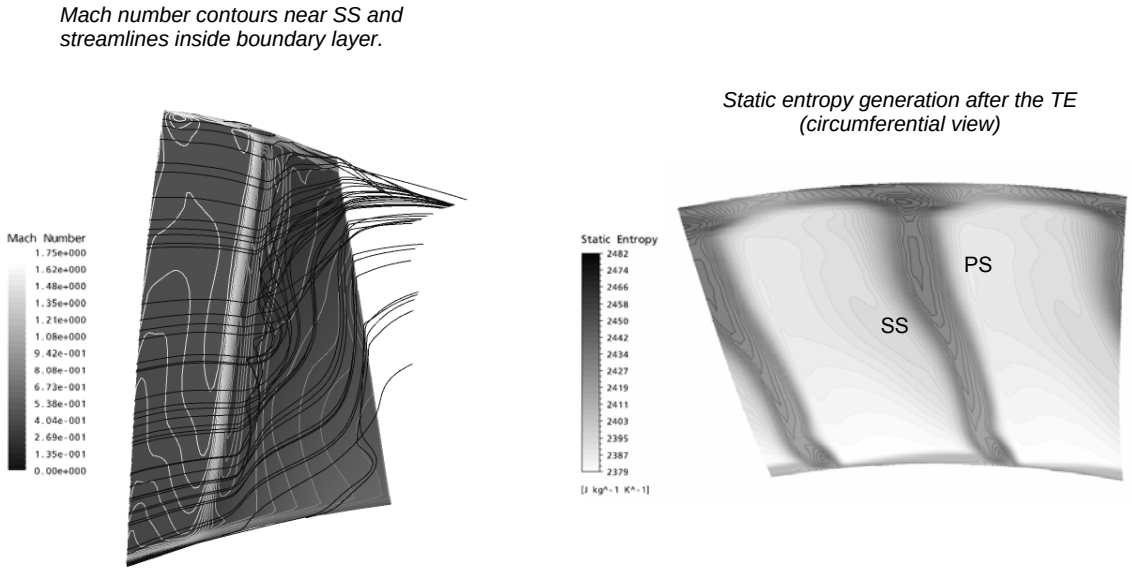

Fig. 4.14(a) Rotor 37 – about 98% choking mass flow.

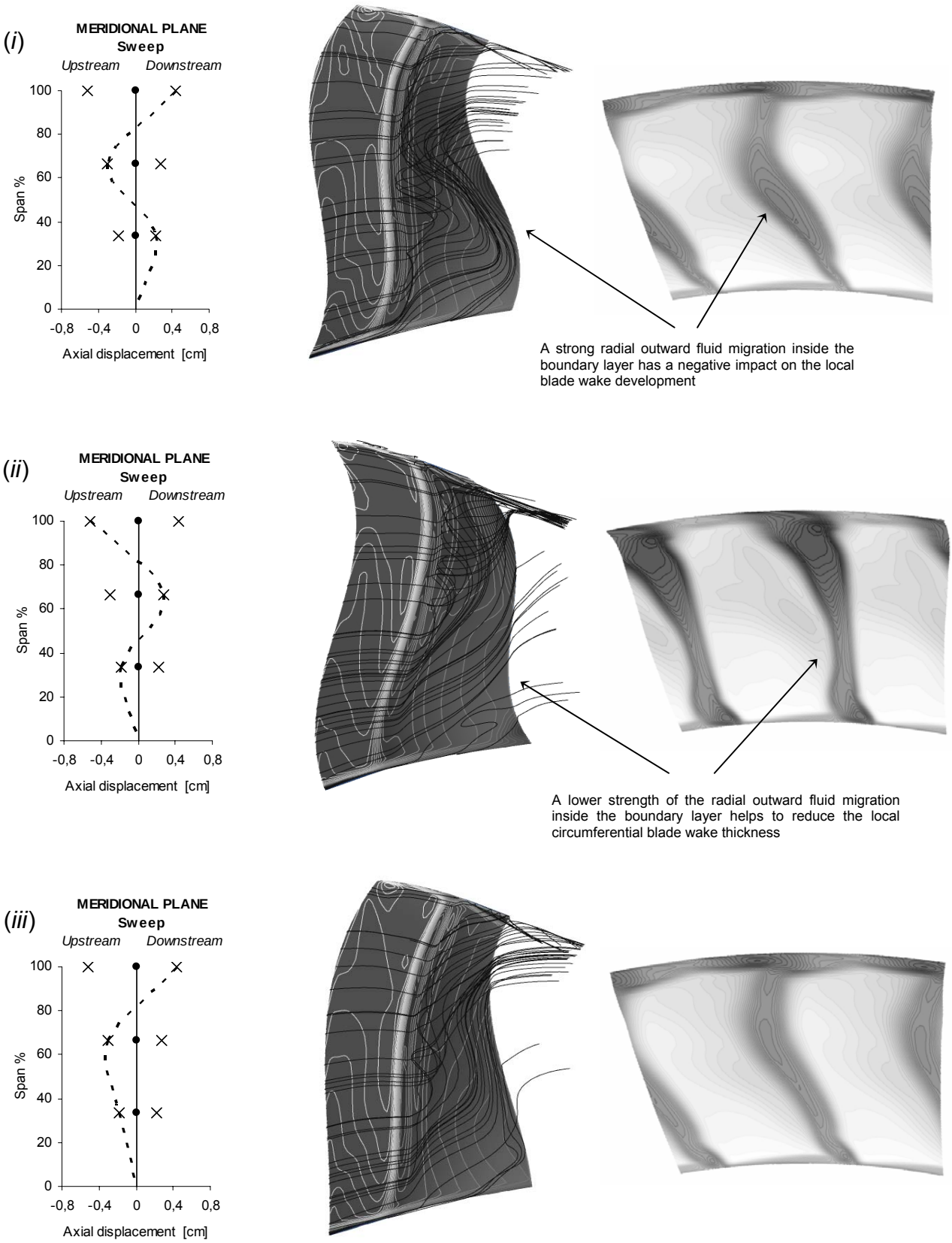

Fig. 4.14(b) Swept rotors – about 98% choking mass flow.

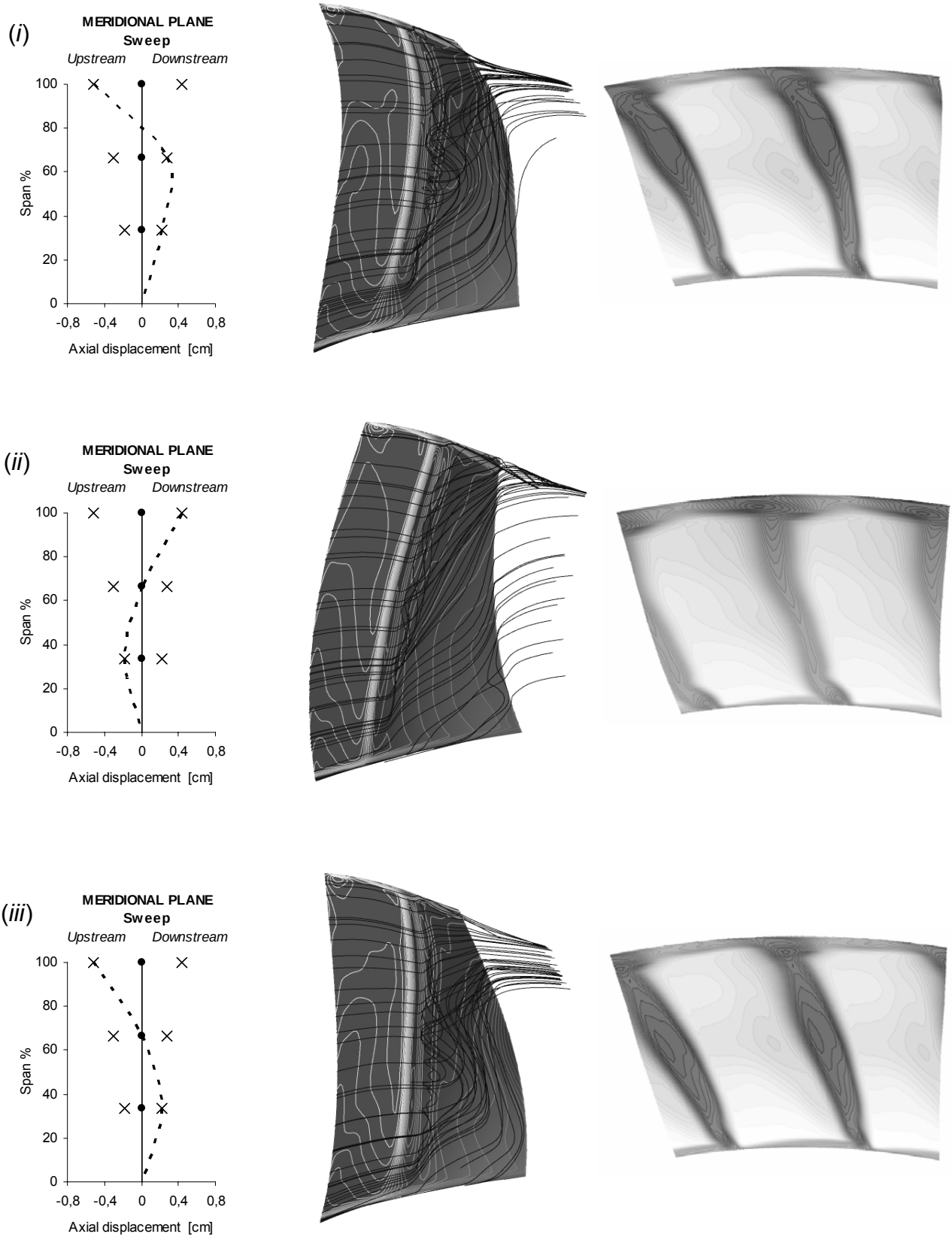

Fig. 4.14(c) Swept rotors – about 98% choking mass flow.

4.1.3 A promising locally leaned rotor

In this section the aerodynamic behavior of the leaned rotor shown in Figure 4.15 was investigated in detail. It gave a higher overall efficiency compared to the baseline rotor, with a maximum increment of about one percentage point around the peak efficiency condition (Figure 4.16). On the other hand, it gave a lower operating range, similarly to some other modeled forward leaned rotors (see Figure 3.8(b)). This aspect will be investigated in detail in Section 4.2.

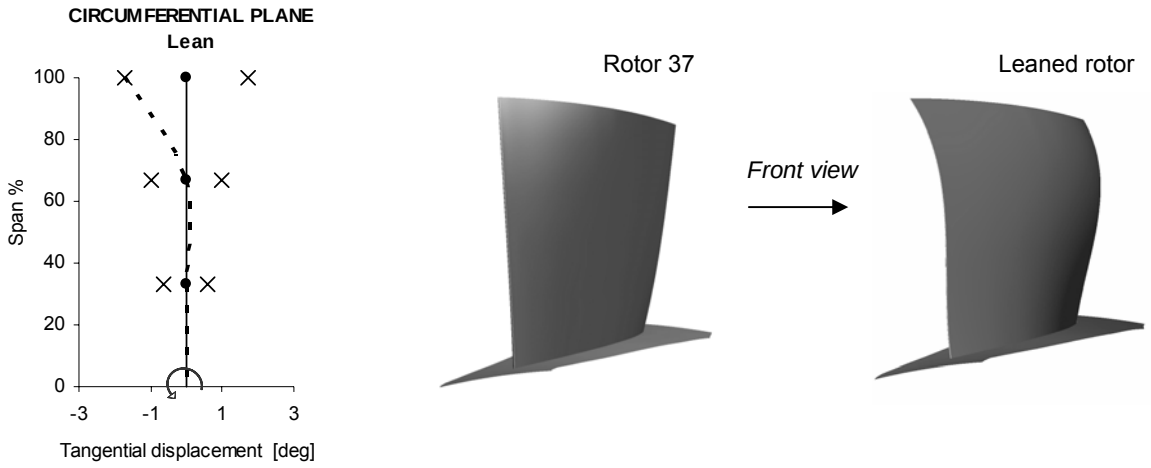

Fig. 4.15 Baseline and redesigned blade geometry.

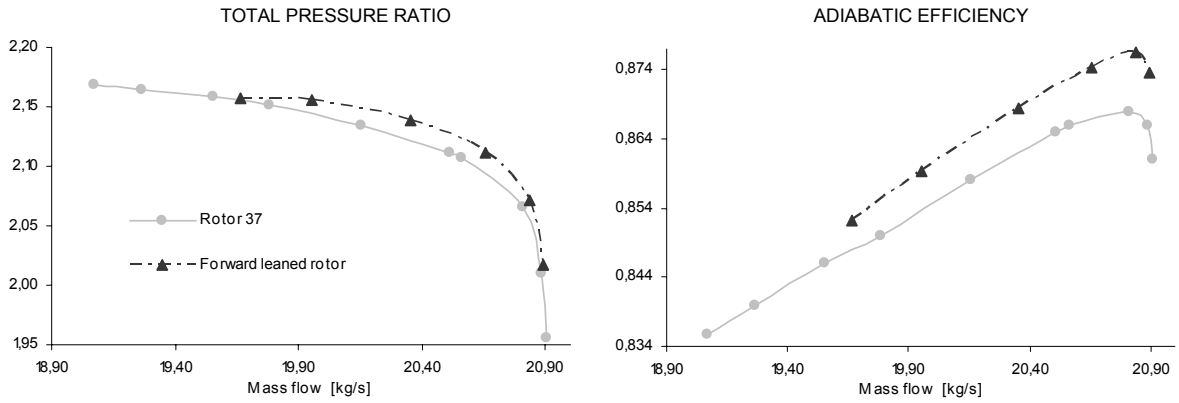

Fig. 4.16 Total pressure ratio and adiabatic efficiency speed lines (1800 rad/s).

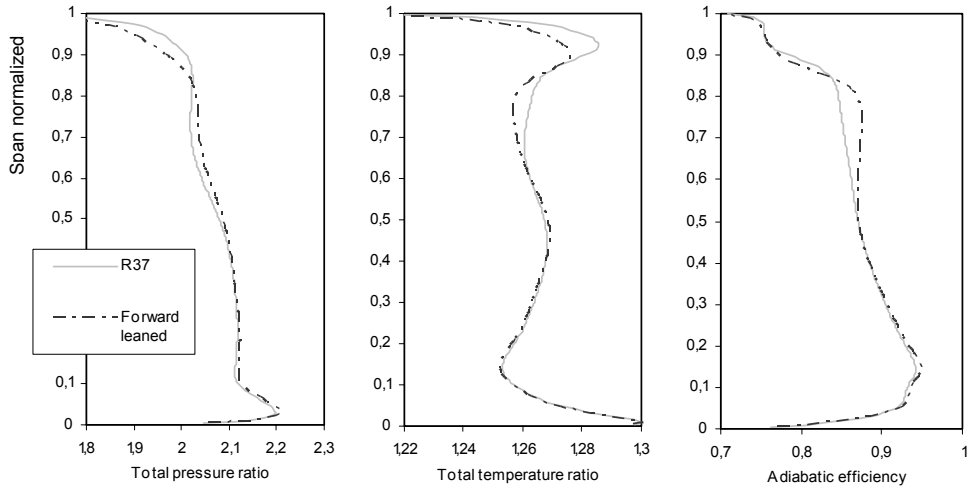

Fig. 4.17 Performance spanwise profiles at outlet – peak efficiency condition.

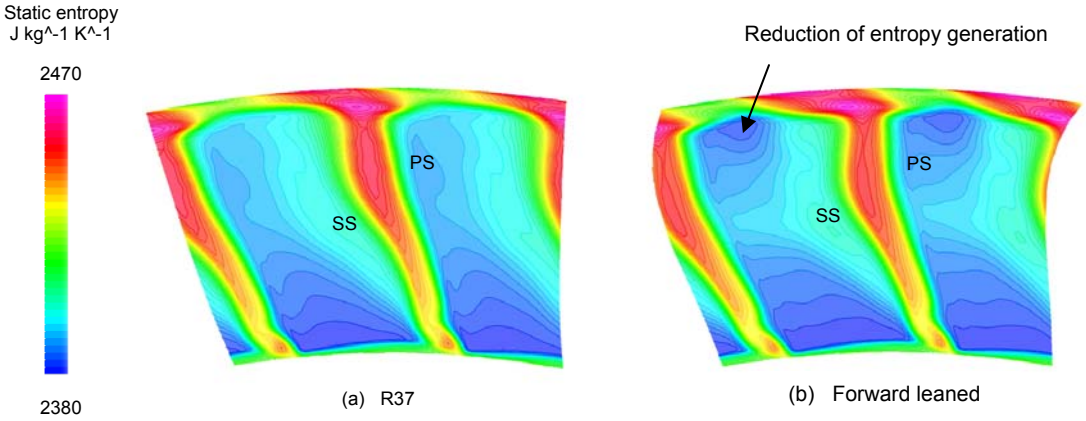

Fig. 4.18 Static entropy distribution after the trailing edge – peak eff.

Similarly to the forward leaned rotor investigated in Section 4.1.1, the leaned rotor analyzed here showed a significant improvement in the adiabatic efficiency around 70-80% span (Figure 4.17). Around this spanwise region, an evident drop of entropy distribution was observed downstream the rotor toward the pressure side (Figure 4.18). This is the direct consequence of the dramatic change in the blade-to-blade relative Mach number distribution induced by the applied blade curvature, as shown in Figure 4.19 (left).

Differently from the baseline rotor, in the leaned rotor the shock front moves downstream and bifurcates in two weaker shocks near the pressure side, laying the bases for a more efficient local flow diffusion.

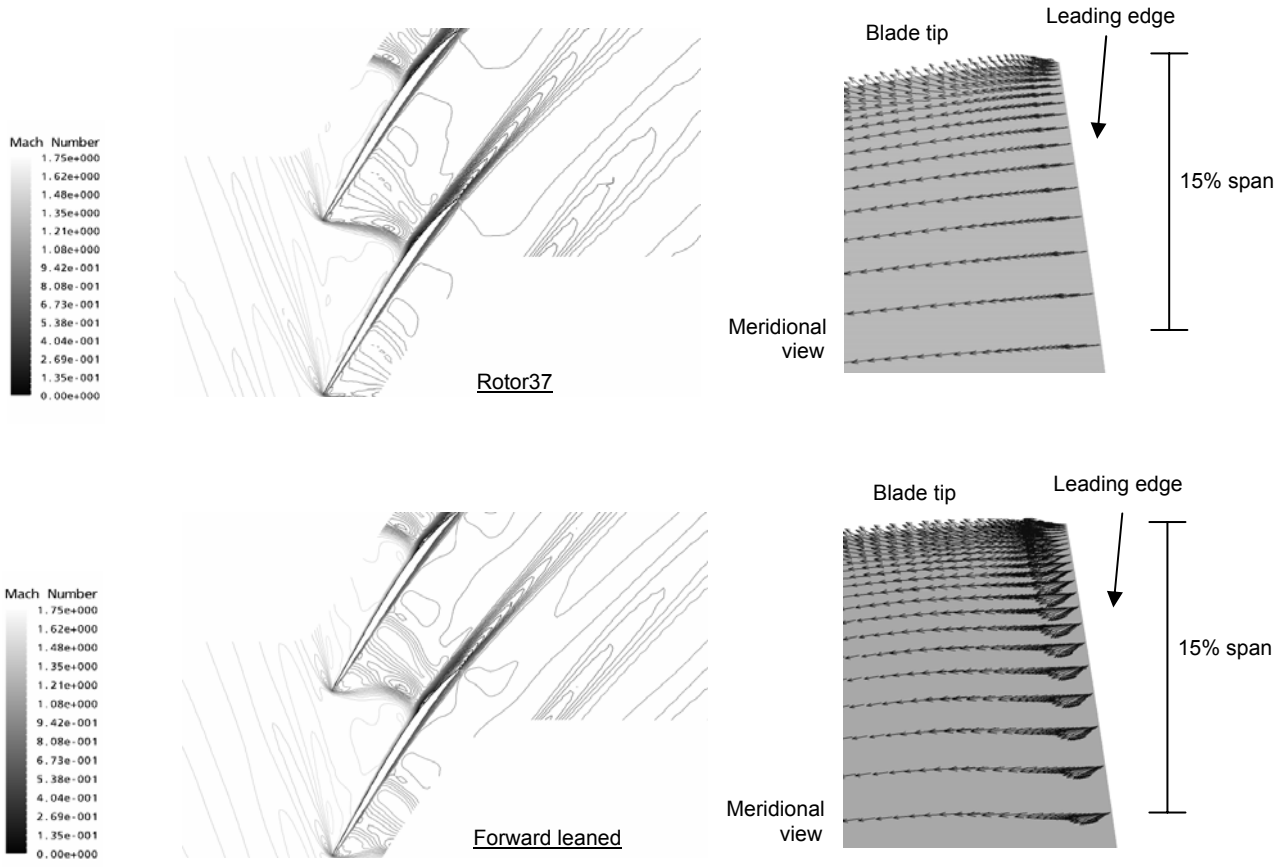

Fig. 4.19 Blade-to-blade relative Mach number distribution at 85% span (left) and relative velocity vectors near pressure side at leading edge – peak eff.

It is now interesting to understand the aerodynamic reasons for such a change in the shock structure.

The leaned rotor analyzed in this section, as well as any other leaned rotor considered in this work, was modeled starting from the Rotor 37 by changing only the circumferential curvature of the blade stacking line. Therefore, at each span both the baseline and the

leaned rotors have absolutely the same blade-to-blade section (same profile, same stagger angle etc.). Detailed investigations showed also that the relative Mach number upstream the blade is quite similar into the two rotors, as well as the relative flow direction. Therefore, on the basis of a quasi-three-dimensional (Q3D) blade-to-blade calculation, the shock structure should be comparable in the two cases (the shock structure depends on the imposed deviation and the upstream Mach number only). For that reason, the change in the shock structure must be associated with a three-dimensional flow feature. This was confirmed by Figure 4.19 (right), which shows the relative velocity vectors near the blade pressure side at the outer span (where the blade is leaned). While in the baseline rotor the flow moves around the leading edge without any evident spanwise velocity component, in the leaned rotor the flow clearly deviates radially inward. This changes the flow pattern

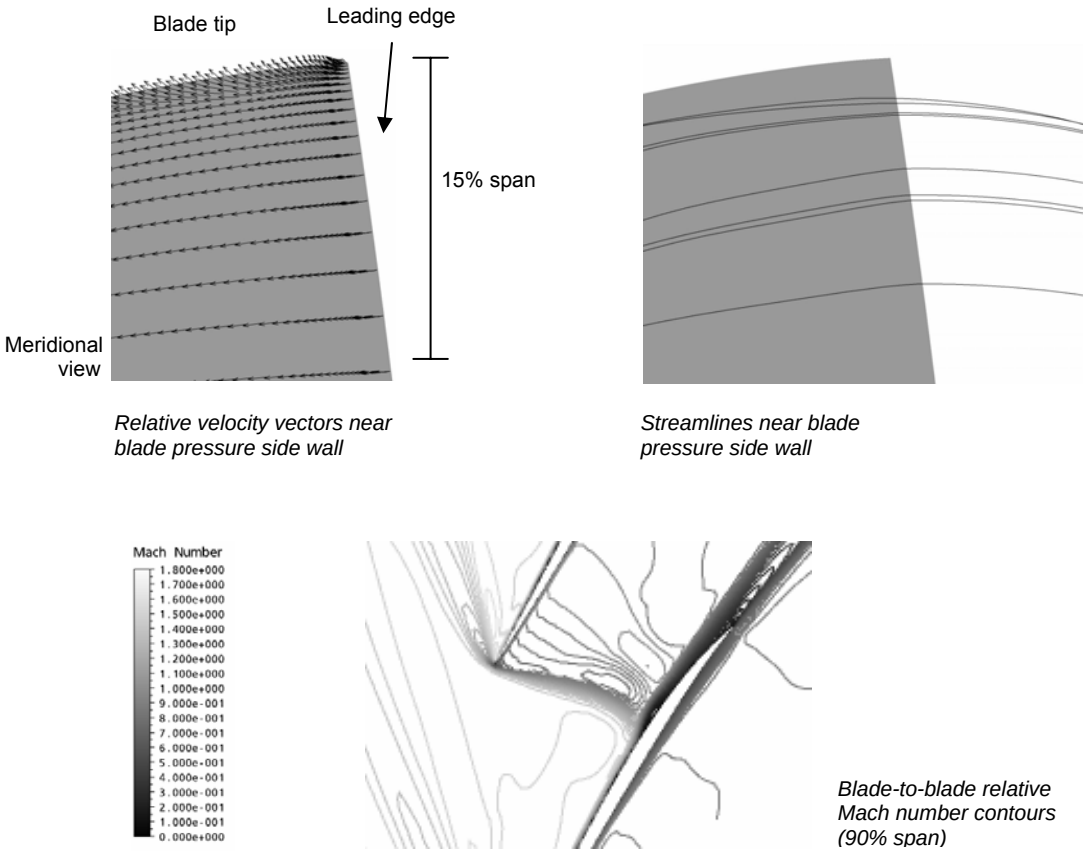

Fig. 4.20(a) Rotor 37 – 98% of choking mass flow rate.

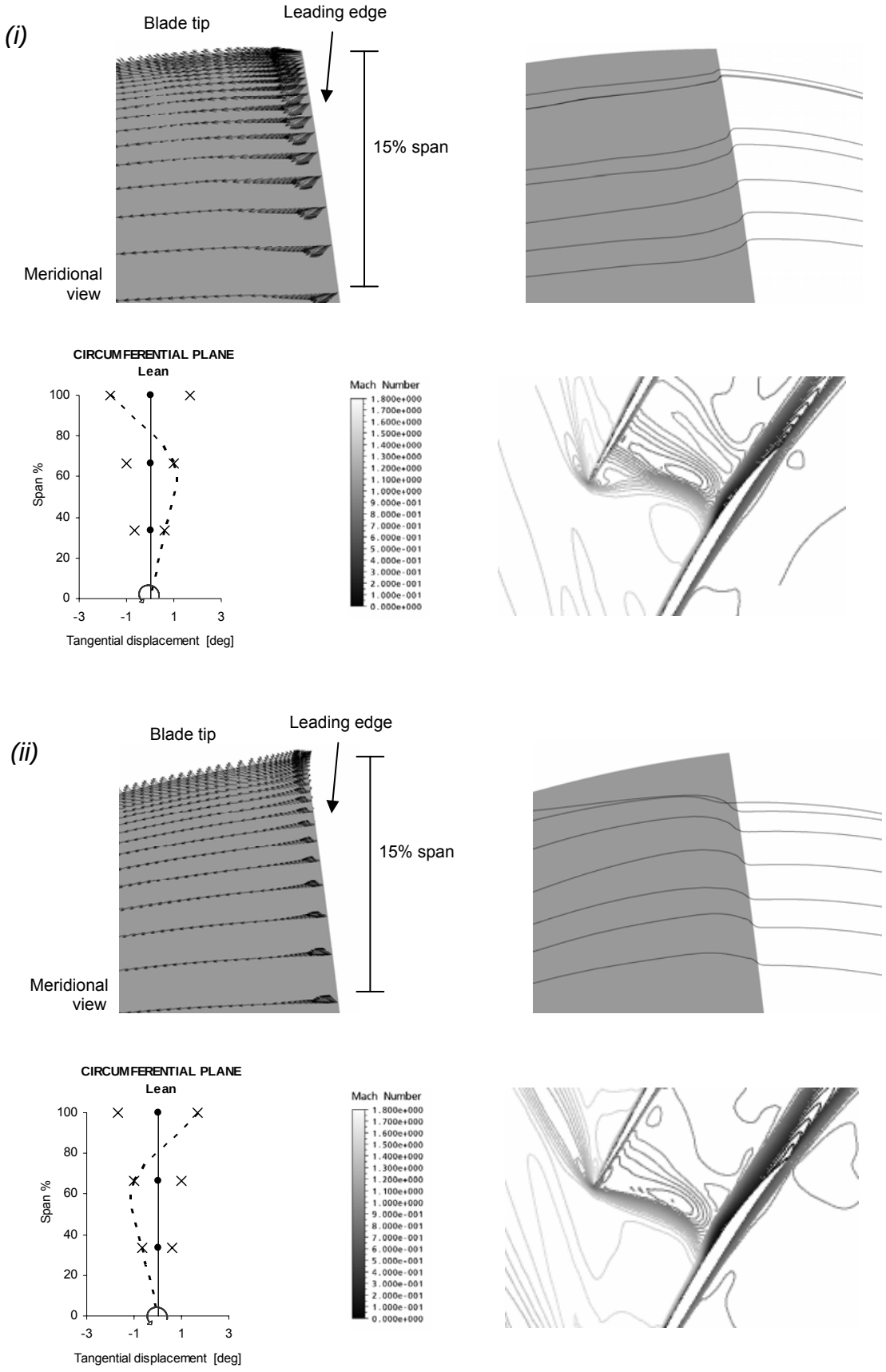

Fig. 4.20(b) Leaned rotors – 98% of choking mass flow rate.

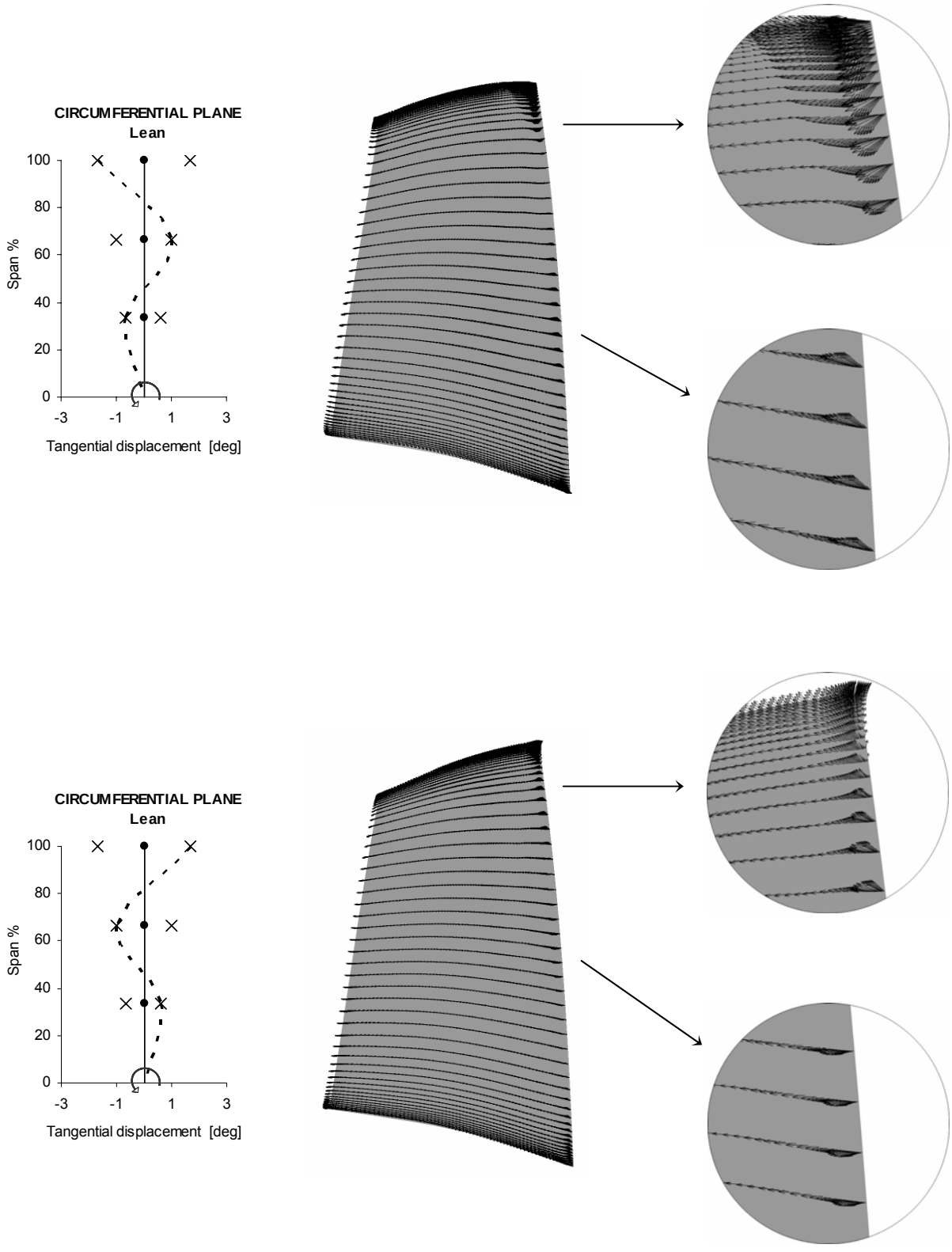

Fig. 4.21 Local impact of lean on flow pattern at leading edge (pressure side). (98% choking mass flow)

around the blade and, consequently, the deviation imposed by the blade pressure side wall to the flow, with a unavoidable impact on the shock structure.

All the forward leaned rotors gave the same flow feature at the blade leading edge (see, for instance, case (*i*) of Figure 4.20(b)). The backward leaned rotors, instead, gave the flow an outward spanwise velocity component at the blade leading edge near the pressure side, as shown by case (*ii*) of Figure 4.20(b); this led to a stronger shock and, consequently, to higher shock losses and stronger interactions between the shock and secondary flows, with a negative impact on the overall rotor efficiency.

More in general, it was observed that where the blade is inclined toward the direction of rotor rotation the flow is deviated radially inward by the pressure side leading edge, while where the blade is curved contrarily the flow is induced to move radially outward, as clearly shown in Figure 4.21.

4.1.4 Concluding remarks

All the aft swept rotors developed in this work showed an aerodynamic behavior similar to that gave by the aft swept rotors analyzed in detail in this chapter, as well as all the forward leaned rotors showed the same flow features observed in the forward leaned rotors considered above. On the basis of that, the impact of aft sweep and forward lean on the aerodynamic behavior of Rotor 37 can be summed up as follows.

Aft sweep showed clearly an impact on the shock structure as far as its shape on the meridional view, in consequence of the impact of sweep on the blade leading edge shape. However, this did not show a great effect on the overall rotor performance. The efficiency improvements gave by all the aft swept blades are mainly associated with a less detrimental blade wake development, thanks to a reduction of the radial outward flow migration which arises inside the blade suction side boundary layer after the interaction with the shock. It was observed, in fact, that a downstream blade curvature can help to reduce such radial fluid flow, with a positive impact on the boundary layer thickness and blade wake development.

Forward lean impacted considerably and prevalently on the three-dimensional shock structure. All the forward leaned blades showed a shock front more inclined downstream

than the baseline radially-stacked blade, both in the blade-to-blade and meridional views. This helps to reduce the shock strength and, consequently, the entropy generation and the aerodynamic losses associated with the shock. It was observed that this is due to a change in the flow incidence in consequence of an unusual flow pattern around the blade leading edge. A blade curved toward the direction of rotor rotation seems to induce the flow to move radially inward when reaches the blade pressure side leading edge.

A last observation is needed as far as lean effects. Lean showed some impacts also on the strength of the above mentioned radial outward flow of fluid particles inside the blade suction side boundary layer. In particular, such flow phenomenon seems to be relieved using forward lean. This is the reason for the thin wake shown by the leaned rotor of case (*ii*) in Figure 3.9(e) at 94% span (where the blade is curved toward the direction of rotor rotation). Backward lean, instead, seems to increase the strength of such fluid flow migration. It was observed, however, that in leaned rotors this effect is of lesser importance than in swept rotors (in the case of forward leaned blades, in particular, it does not aid significantly in changing the rotor performance) and for that reason it was not argued here.

4.2 Rotor stability enhancement using forward lean

In this section, a study on the possibility to widen the working range of a transonic compressor rotor using blade curvature was carried out. As mentioned in Chapter 1 (Section 1.2), it seems that stall in these rotors is associated with the interaction between the tip clearance vortex and the passage shock. Interacting with the shock, the vortex is subject to a sudden and strong deceleration; at lower flow operating conditions vortex breakdown can occur, generating a low momentum fluid blocking the passage and inducing rotor stall. As observed by Kablitz *et al.* (2003), vortex breakdown occurs when the relative total pressure in vortex core is lower than the static pressure downstream of the shock. After reaching a local minimum, the relative total pressure inside the vortex core is increased by a mixing process between the low momentum core and the higher momentum outer parts of the vortex and also with the main flow. It depends on the axial distance which is available for this “reenergization” whether it remains possible for the vortex to get

past the passage shock. On the basis of numerical observations made up to now, forward lean can help to increase the axial distance between the vortex start point and the shock-vortex interaction point, since it induces the shock to move downstream at the outer span. Therefore, forward lean could be helpful for reenergizing the vortex core and increasing the rotor stability at throttled operating conditions.

However, all the forward leaned rotors previously investigated did not show a higher stall margin compared to the baseline rotor (see, for instance, Figure 3.8(b)). This could be due to numerical reasons (numerical instabilities of solver in the computing of the flow field toward stall condition using a steady-state model) or, alternatively, the above considerations could be ill founded. With the aim to make clear on the effects of forward lean on the stability of a transonic compressor rotor, the impact of a promising forward leaned blade curvature on the tip endwall flow field of Rotor 37 was investigated in detail.

Investigated rotor geometry and numerical model

Figures 4.22 and 4.23 show the blade geometry of the rotor analyzed in this section. Just as all previous leaned and swept rotors were obtained, the new rotor considered here was modeled starting from the Rotor 37 by changing the shape of the original stacking line. In this case, however, the stacking line was modified both in the meridional and circumferential planes. The circumferential shape (which gives the blade a forward leaned curvature) was given because promising from the aerodynamic point of view. The meridional shape, instead, was added for structural reasons.

FEM analyses showed a detrimental blade structural behavior when a noticeable forward leaned curvature is applied. It was observed, in particular, an intensification of blade structural stresses due to strong bending loads arising from the action of centrifugal forces (see Section 3.4 for details). The meridional curvature was added actually to verify the possibility of relieving the negative structural effects induced by forward lean, without impacting considerably on the aerodynamic performance. Figure 4.24 shows the structural benefits induced by the applied meridional curvature (it gives the Von Mises stress distribution on the blade pressure side due to the centrifugal loading in the case of baseline

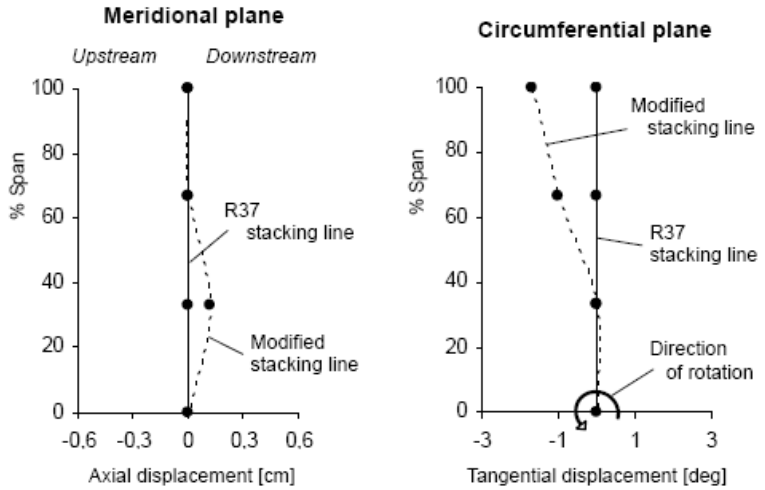

Fig. 4.22 Baseline (Rotor 37) and modified (new rotor) stacking lines.

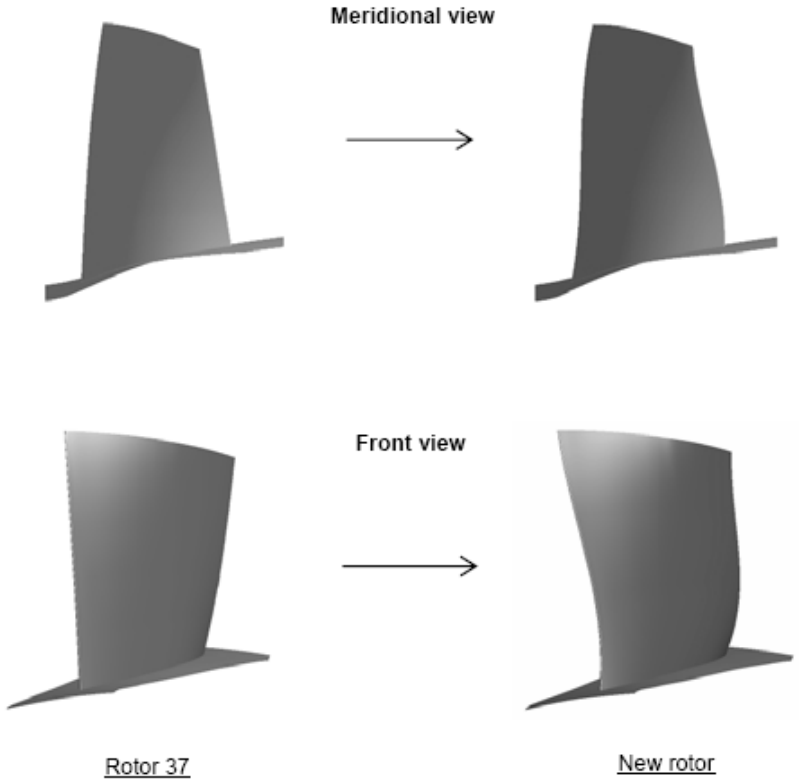

Fig. 4.23 Baseline (Rotor 37) and modified (new rotor) blades.

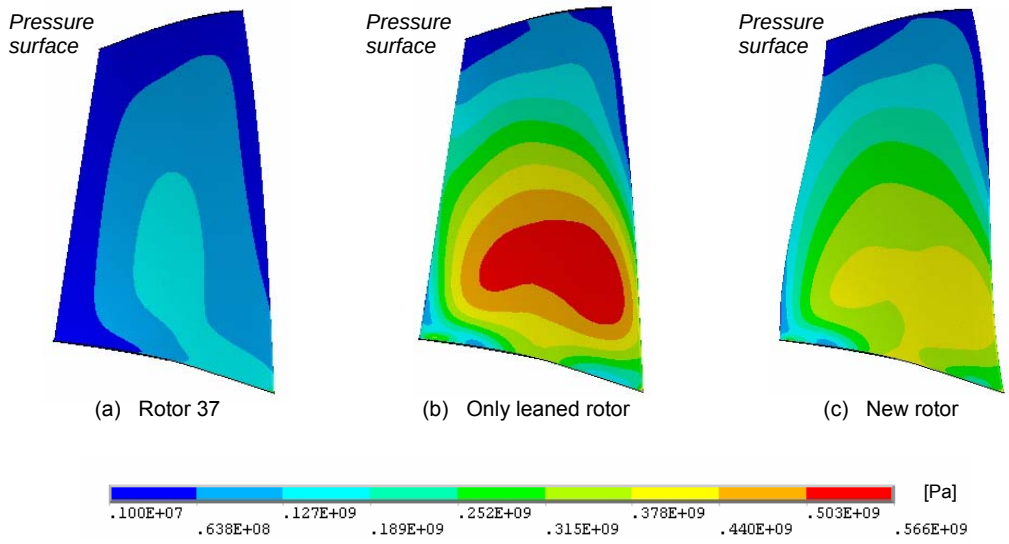

Fig. 4.24 Von Mises stress distribution due to wheel speed (1800 rad/s). (ANSYS Structural)

blade (a), the new blade without meridional curvature (b) and the new blade with meridional curvature (c)).

The aerodynamic behavior of the new rotor was calculated and compared to that of baseline configuration using a modified version of Model 3 (see Table 2.1). Steady-state simulations were carried out. With respect to Model 3, the model used here is characterized by a finer grid (about 1 million cells in all) at the outer span region for a more detailed prediction of the tip endwall flow field. In particular, to make the code able to solve accurately the wall boundary layer formed by the relative motion between the overtip leakage flow and the casing, which seems to have a considerable impact on the development of tip clearance flows (Van Zante *et al.*, 2000), the tip clearance gap was modeled using 20 (instead of 9 as in Model 3) radial grid points. The model was successfully validated against Rotor 37 experimental data, as shown in Figure 4.25. Similarly to Model 3, it gave a choking mass flow of 20.96 kg/s against the experimental value of 20.93 ± 0.14 kg/s.

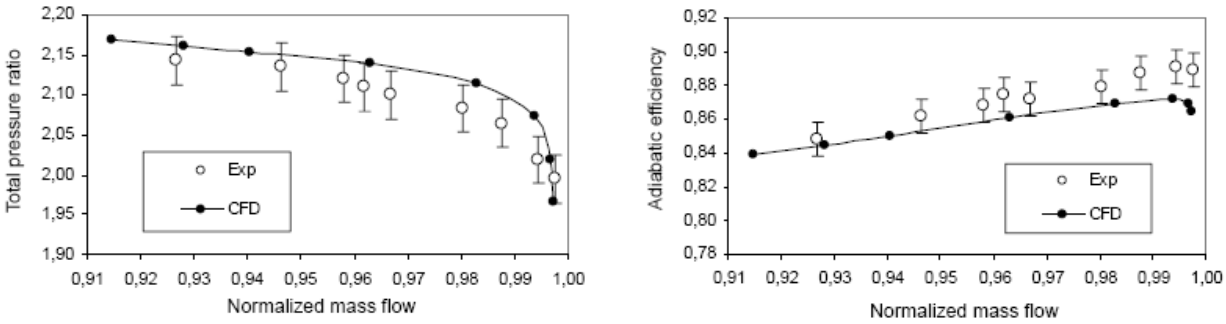

(a) Speed line.

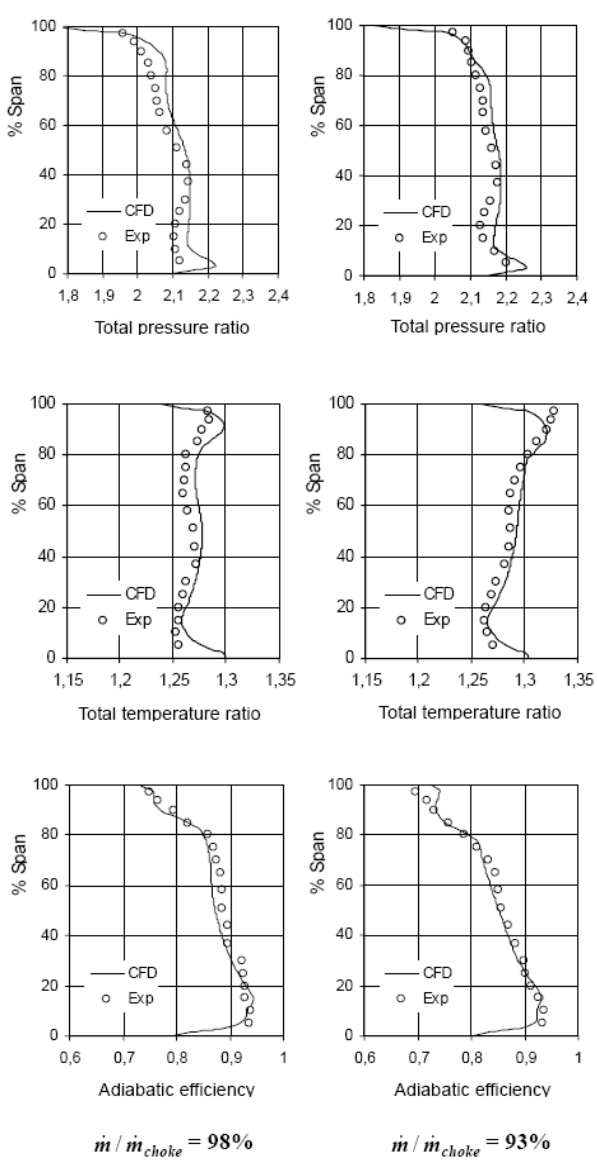

(b) Downstream performance profiles.

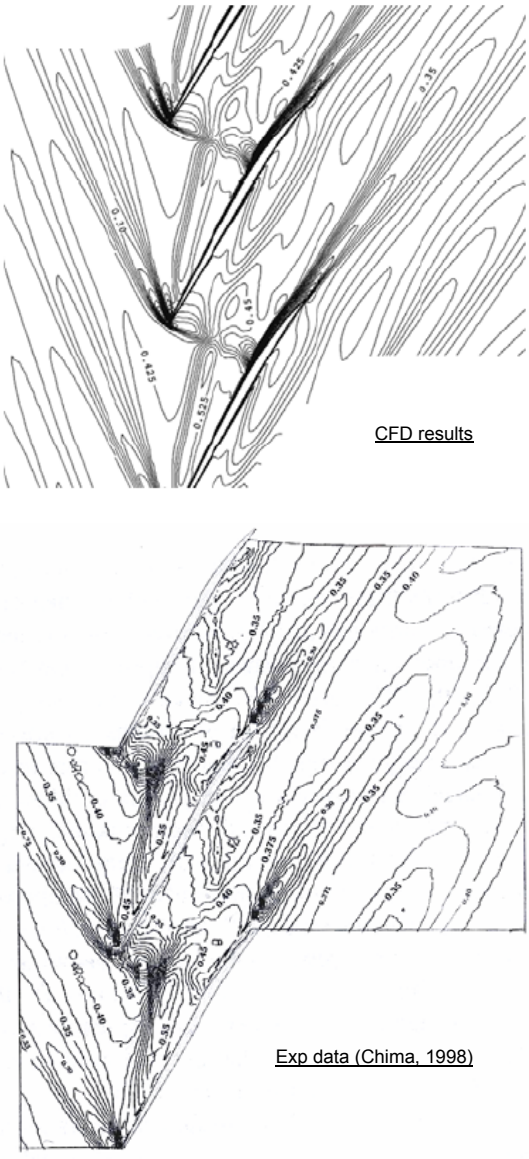

(c) Contours of normalized axial velocity. (95% span – 98% normalized mass flow)

Fig. 4.25 Numerical model validation (Rotor 37 – 1800 rad/s).

Flow analysis

Figure 4.26 compares the computed speed line of new rotor to that of baseline configuration. For each rotor, the calculated mass flows were normalized using the computed mass flow at choking condition (the new rotor gave a choking mass flow of 20.88 kg/s against 20.96 kg/s of Rotor 37). With respect to the baseline configuration, the new rotor gave a higher overall efficiency, a similar total pressure ratio and a lower operating range. The efficiency increment is of about 0.8 percentage points around the peak efficiency condition.

The flow fields of the two rotors were analyzed and compared at both the high efficiency and low flow working conditions indicated in Figure 4.26.

Figure 4.27 shows the spanwise profile of adiabatic efficiency calculated at the outflow boundary of the computational domain, for both the high efficiency and the low flow operating conditions. It will be considered later.

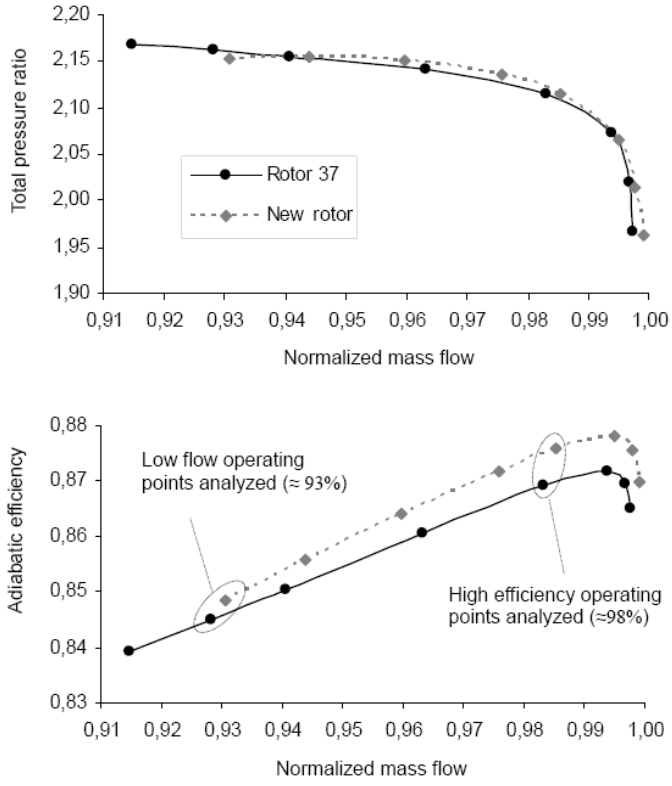

Fig. 4.26 Rotor 37 and new rotor calculated speed lines.

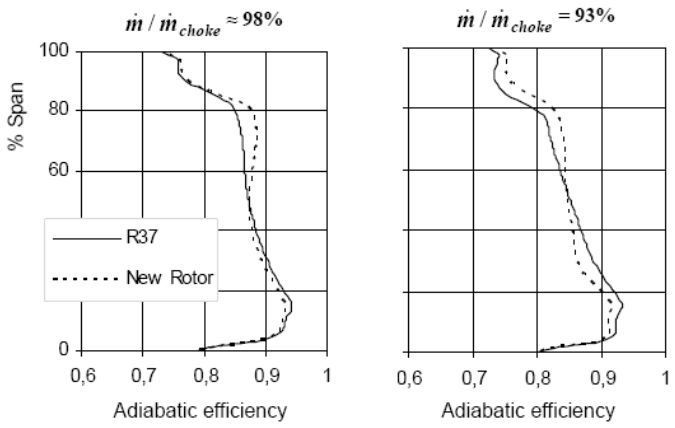

Fig. 4.27 Spanwise profiles of efficiency at the outlet.

As expected, the applied circumferential blade curvature induced the fluid to move radially inward near the pressure side of the blade leading edge (Figure 4.28(a)). This led to a change in the flow pattern (i.e. in the flow deviation imposed by the blade wall) influencing not only the blade-to-blade shock structure but also the blade loading. Compared to the radially-stacked rotor, at the outer span the new rotor gave a shock located more downstream and a lower blade loading at the leading edge (Figures 4.28(b) and 4.28(c)).

Figure 4.29 shows the relative Mach number distribution at the blade tip span (about 99.4% span) for the high efficiency operating condition. The black dashed line points out the tip clearance vortex core (or primary vortex core). Note that the shock-tip clearance vortex interaction point is located more downstream in the new rotor, thanks to the more oblique blade-to-blade shock front. However, while in the baseline rotor the vortex starts at the leading edge, in the new rotor it starts at about 10% chord, in consequence of the lower blade loading at the leading edge; therefore, the axial distance between the vortex start point and the shock-vortex interaction point is similar in the two rotors and the idea to increase the vortex core energy using forward lean failed at this working condition. Note that the low momentum region after the shock is almost the same in the two cases, in terms of both size and Mach number values, and that the efficiency is comparable near the casing (Figure 4.27, 98%). On the whole, the applied forward lean did not improve the tip endwall flow field at the high efficiency operating condition.

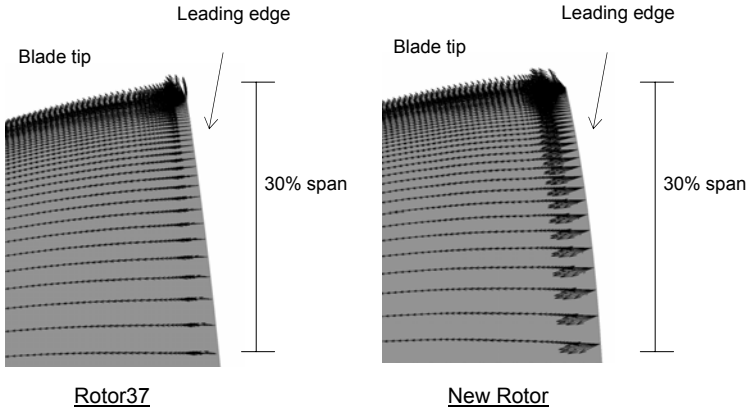

(a) Relative velocity vectors near pressure side.

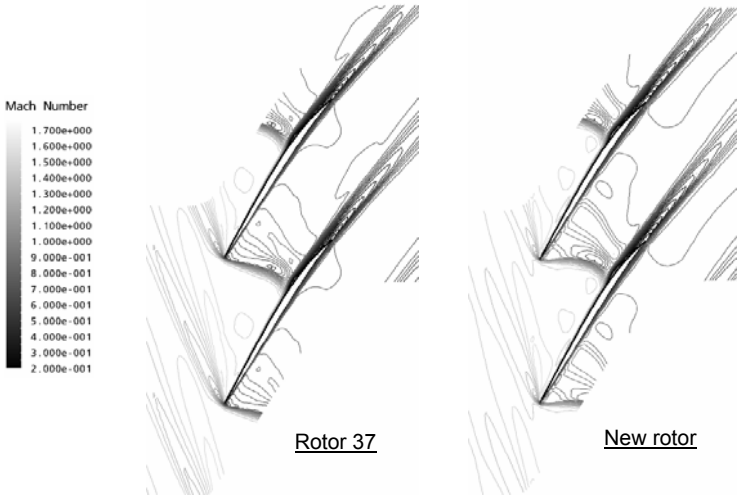

(b) Relative Mach number contours – 85% span.

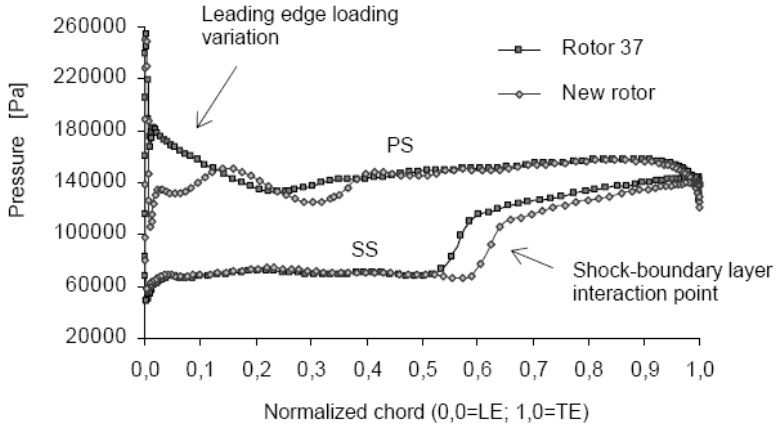

(c) Static pressure distribution around the blade – 85% span.

Fig. 4.28 R37 and new rotor comparisons – high efficiency condition.

A better aerodynamic behavior near the casing was observed in the new rotor actually at low flow operating conditions. Figure 4.30 shows the relative Mach number distribution at the blade tip for the 93% of choking mass flow (see Figure 4.26). At this operating condition, the tip clearance vortex starts at the leading edge in both rotors, but in the new rotor the shock front remains located more downstream (still attached to the blade leading edge). This led to a higher distance between the vortex start point and the shock-vortex interaction point and, as expected, to a less detrimental shock-vortex interaction (note the less unfavorable low momentum region after the shock developed by the new rotor).

Detailed numerical flow visualizations (not reported here) showed some interesting aspects concerning such low momentum region. It was observed that, at the blade tip span, it is formed mainly with fluid from the casing boundary layer, coming from the tip clearance gap (this was observed in both rotors). Therefore, it can not be considered as a consequence of the shock-vortex interaction only; it must be seen, more in general, as a consequence of the shock-tip clearance flows-casing boundary layer interaction. However, such low momentum fluid region has a spanwise dimension and flow visualizations showed that at lower span levels it is mostly formed with fluid coming directly from the vortex.

Figure 4.31 shows some three-dimensional streamlines released at midheight in the tip clearance gap, along with the relative Mach number distributions at blade tip span and 96% span. The tip clearance vortex (or primary vortex) is clearly visible. A secondary vortex arising after the shock can also be seen in both rotors. Being the streamlines released from the tip clearance gap, the secondary vortices shown in Figure 4.31 arise from the pressure difference between the pressure and suction blade side. Really, it was observed that they arise also from the radial outward migration of fluid particles which takes place inside the blade suction side boundary layer after the shock (see Section 4.1.2 for details on the mentioned radial fluid flow).

Compared to the new rotor, the low momentum region after the shock developed by the baseline rotor is considerably wider in the spanwise direction. As shown in Figure 4.31, at 96% span it is still visible inside the Rotor 37, while it does not appear in the new

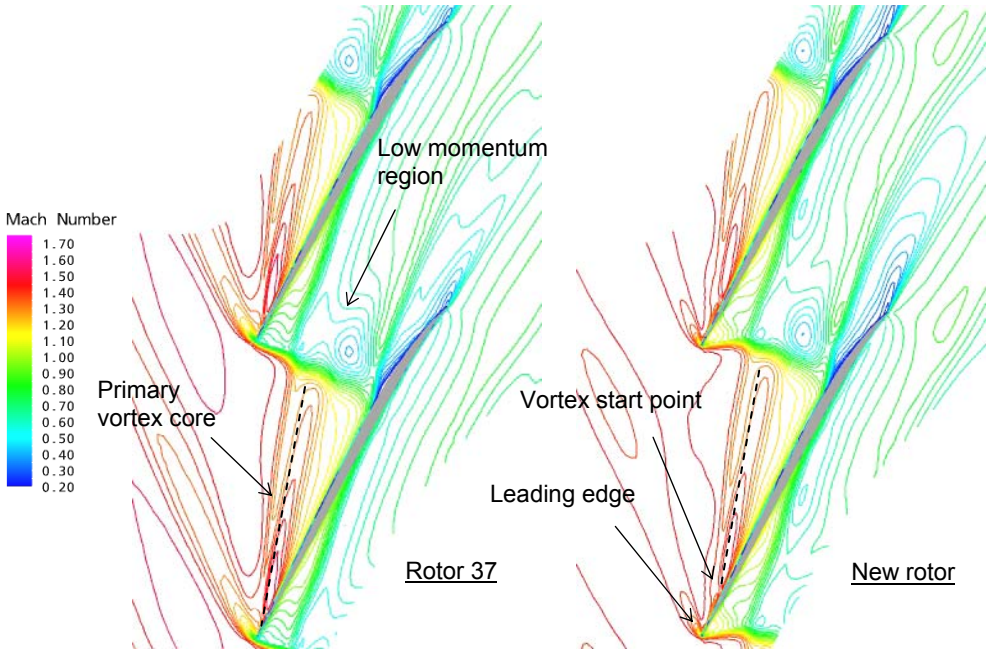

Fig. 4.29 Blade-to-blade relative Mach number distribution. (Blade tip span – high efficiency condition)

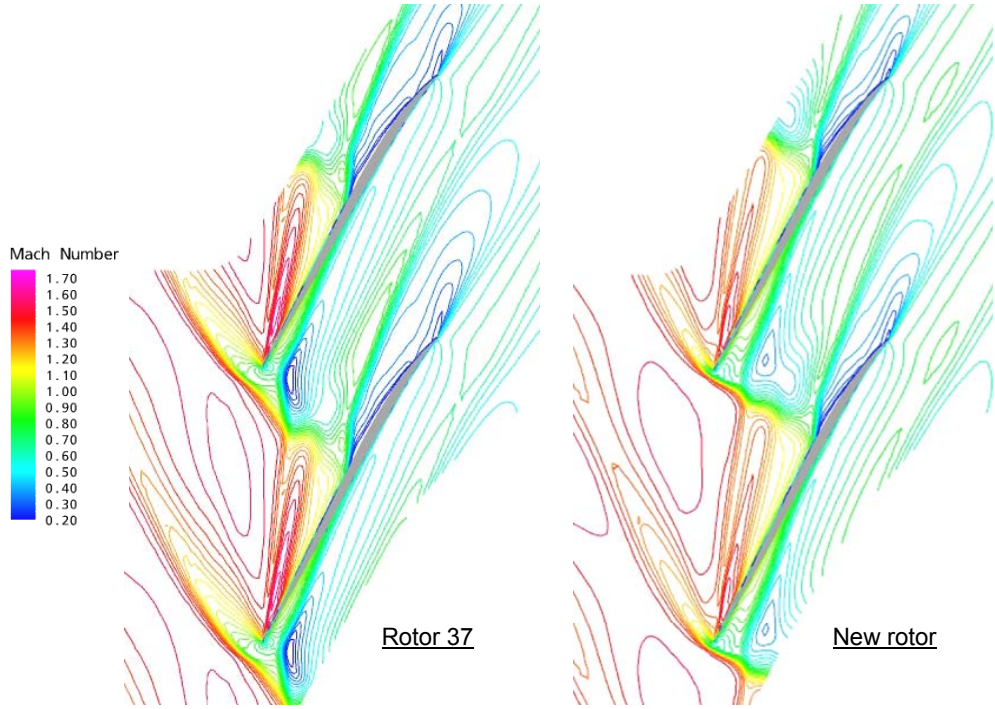

Fig. 4.30 Blade-to-blade relative Mach number distribution. (Blade tip span – low flow condition)

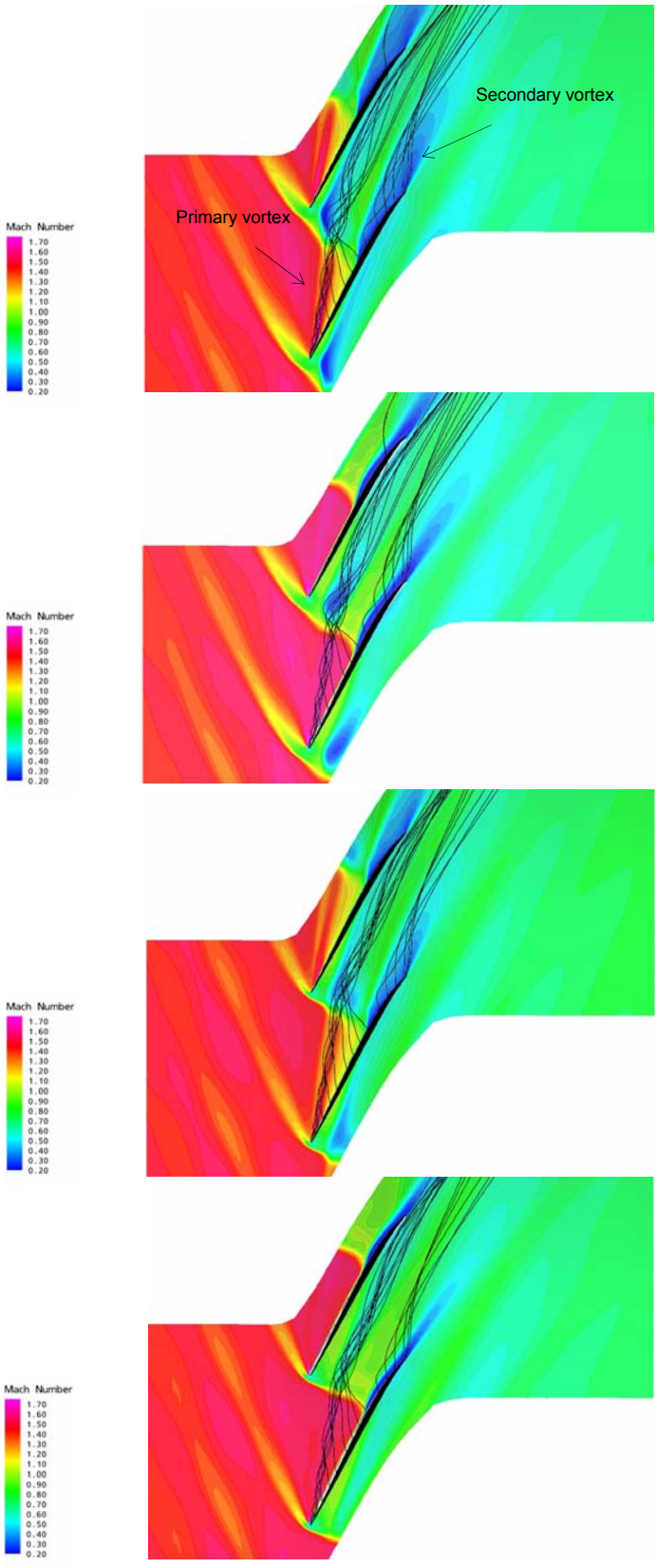

Rotor 37

Mach distribution at blade tip

Rotor 37

Mach distribution 96% span

New rotor

Mach distribution at blade tip

New rotor

Mach distribution 96% span

Fig. 4.31 Flow visualizations – 93% normalized mass flow.

rotor. It is also interesting to observe the difference in the blade wake development near the casing. The baseline rotor gave a considerably wider and deeper blade wake than the new rotor.

On the whole, at low flow operating conditions the new blade gave a better aerodynamic behavior at the tip endwall region compared to the baseline blade. As expected, the applied curvature led to a less detrimental shock-vortex interaction, along with a considerable reduction of local aerodynamic losses (see Figure 4.27 (93%)). Flow

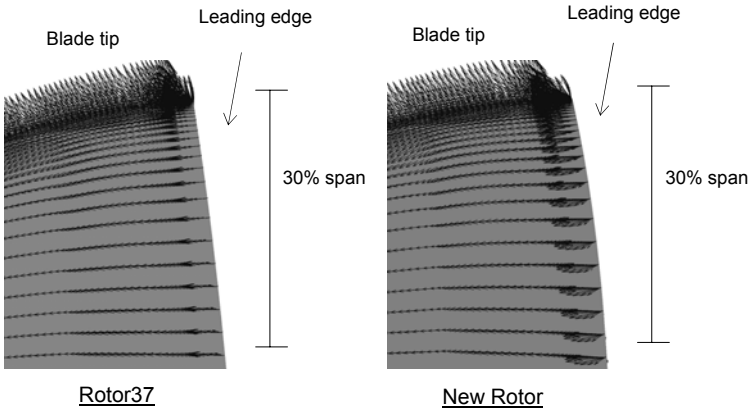

(a) Relative velocity vectors near pressure side.

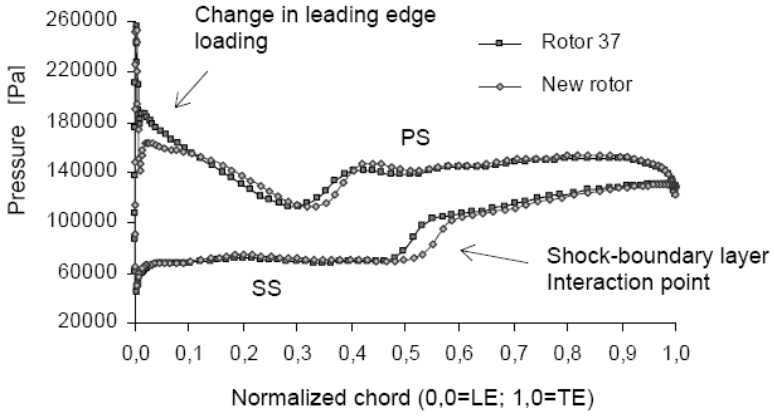

(b) Static pressure distribution around the blade – 85% span.

Fig. 4.32 R37 and new rotor comparisons – 98% normalized mass flow. (k-ω turbulence model)

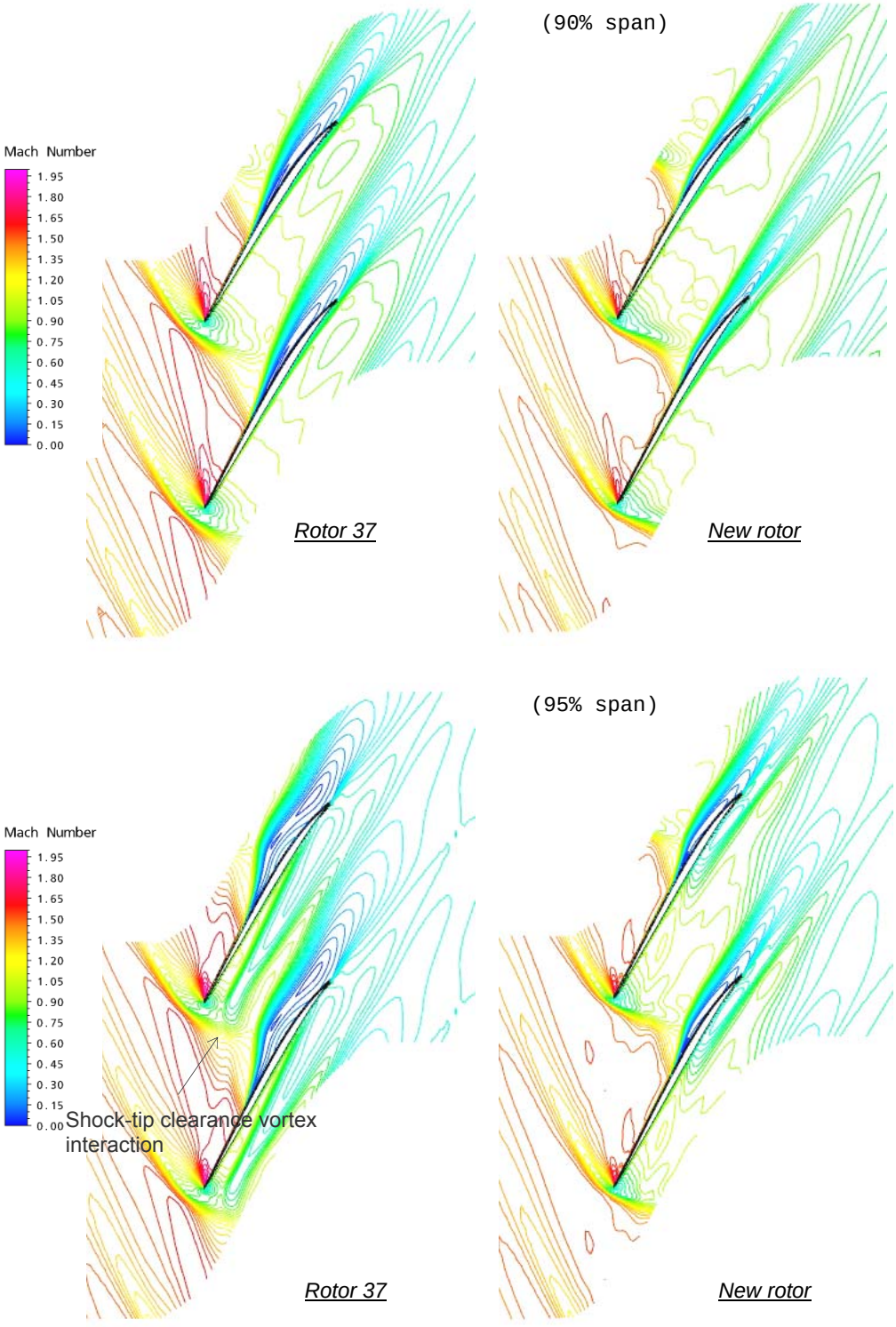

Fig. 4.33 R37 and new rotor comparisons – 92% normalized mass flow. (k-ω turbulence model)

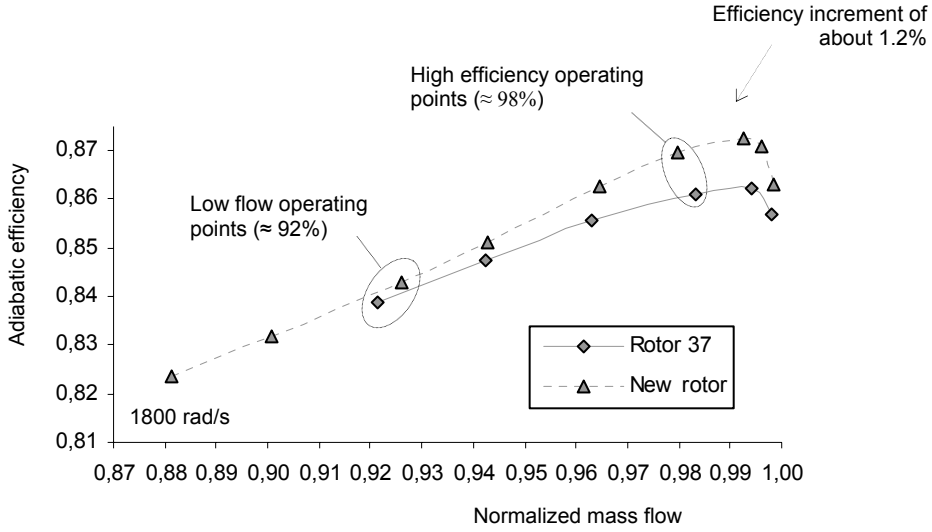

Fig. 4.34 Computed adiabatic efficiency.
(k-ω turbulence model)

visualizations showed a clear improvement in the peripheral flow stability. Despite of this, the new rotor gave an unjustified limited stable working range (see Figure 4.26). For both rotors, the lower mass flow operating point in the calculated speed line represents the last point for which the steady-state model implemented was able to converge. For lower mass flows the solver diverged or, more in general, was not able to give a converging solution. Generally, this is assumed as an indication of aerodynamic instability. In the case of the new rotor, however, the difficult of the model to converge at lower mass flows is unlikely compatible with a flow instability; it could be instead associated with a numerical instability. This was corroborated by the following analysis, where the use of a different numerical model confirmed the higher flow stability of the new rotor with respect to the baseline one and gave also a wider operating range.

Briefly, both the baseline and new version of Rotor 37 were simulated again using the more accurate Shear Stress Transport k-ω turbulence model instead of the k-ε turbulence model. In particular, Model 5 of Table 2.1 was used. Model 5 was accurately validated in Chapter 2 (Section 2.2.1), showing high-quality predictions of internal flow features.

Model 5 confirmed the impact of the applied blade curvature on the flow field. It predicted, for instance, the unusual flow pattern near the pressure side of the blade leading

edge (Fig. 4.32(a)), the displacement of the shock toward the rear and the change in the blade loading at the leading edge (Fig. 4.32(b)), the positive impact on the tip endwall flow field at low flow operating conditions (Fig. 4.33) etc. In addition, Model 5 confirmed the apparent higher stall margin of the new rotor giving a working range considerably wider than that of Rotor 37 (of about 50%), as shown in Fig. 4.34.

Concluding remarks

Besides the improvements in the overall efficiency, forward lean showed a positive impact also on the tip endwall region at low flow operating conditions, making it possible to increase the flow stability and, consequently, the stall margin.

The negative impact of forward lean on the structural behavior of the blade can be relieved adding a proper swept curvature without compromising the aerodynamic performance.

The steady-state model implemented (the modified version of Model 3) showed an unjustified limited operating range in the case of the new rotor, giving the last stable operating point at a mass flow rate for which the calculated flow field seems to have still stall margin. On the basis of this observation, the operating ranges of Figure 3.8 could be not realistic, as well as all the other ones computed here using the k-ε turbulence model.

Conclusions

An accurate numerical investigation on the influence of blade stacking line curvature on the performance of a transonic axial-flow compressor rotor was successfully undertaken. The main results can be summed up as follows.

CFD code validation

The investigation was carried out using the commercial code "ANSYS CFX". The capability of the code to compute the flow within a transonic compressor rotor was accurately validated. This was done by defining various steady-state 3-D RANS models of the well-known NASA Rotor 37 (a test case well representative of complex flow structures in transonic bladings) and by comparing predictions (computed overall performance and internal flow features) to the experimental data available in literature. The careful assessment of numerical consistency of different models led to a clear understanding of the impact of different choices in model definition (grid topology and density, discretization scheme etc.). Granted that the grid must be sufficiently fine to make the solver able to well capture the internal flow features, it was observed the following.

a) Grid topology and turbulence model showed a considerable influence on code predictions.

b) Grid topology revealed a great impact on the computing of choking mass flow and performance spanwise profiles, as well as on the shock spatial resolution. For instance, passing from the H/O-type grid to the less skewed and more stream aligned J/O-type grid and keeping all the other model features constant, the predicted choking mass flow changed from 20.64 kg/s to 20.96 kg/s against the measured value of 20.93 ± 0.14 kg/s, the calculated downstream radial profiles of flow parameters showed a considerably better agreement with experimental data and the blade-to-blade shock front resulted less smeared and better defined.

c) Turbulence model showed significant effects from every point of view (overall performance, flow features etc.). It was observed, in particular, that the k-ω turbulence model (well-known to give accurate predictions of boundary layer development under adverse pressure gradients) makes the code able to provide better calculations of Mach number distributions than the k-ε turbulence model (especially after the shock, where the computed Mach number depends greatly on the calculation of the blade suction side boundary layer thickness), leading to an optimal agreement with measurements.

During the work it was also observed what follows.

d) Some difficulties in predicting the stable working range of a transonic rotor using a steady-state model were observed. In some cases, with the k-ε turbulence model implemented, unjustified limited working ranges were calculated. The use of the k-ω turbulence model could lead to more reasonable results.

The careful evaluation of code CFD capabilities made it possible the definition of accurate 3-D RANS models for a fairly reliable prediction of the aerodynamic behavior of transonic compressor rotors (in terms of both overall performance and internal flow phenomena), providing an important tool for a better understanding of complex flow structures which take place in these machines (shock, shock-tip endwall flows interactions, shock-boundary layer interaction etc.) and to give insights on possible optimization techniques.

Sweep and lean impact

The aerodynamic impact of blade curvature in transonic compressor rotors was systematically investigated. This was done modeling a large number of new axially swept and tangentially leaned rotors starting from the radially-stacked NASA Rotor 37 and comparing their aerodynamic behavior to that of baseline configuration using the validated CFD code. The study revealed many interesting aspects which are believed to be very helpful to improve the overall performance of transonic rotors. Main observations are the following.

a) Compared to the baseline rotor, the forward leaned rotors (blade curved toward the direction of rotor rotation) and the aft swept rotors (blade curved downstream) gave a clear increment in the overall efficiency over the entire operating range. The first ones showed the higher increments, about 1 percentage point around the design operating condition. All the other new rotors gave a similar or lower efficiency compared to the baseline one.

b) Blade curvature impacted apparently on the three-dimensional shock structure, showing the possibility to handle the shock front shape using sweep and lean. In particular, sweep can help to influence the shock shape in the meridional plane, inducing the shock to assume the meridional curvature of blade leading edge. Lean seems helpful to change the blade-to-blade shock shape, inducing the shock to move downstream when the blade is curved toward the direction of rotor rotation and upstream when the blade is curved contrarily.

c) The change in the shock structure induced by lean can be associated with a change in the flow pattern near the pressure side of the blade leading edge. It was observed that lean induces the flow to move radially inward when the blade is curved toward the direction of rotor rotation and radially outward when the blade is contrarily curved (in the baseline rotor the flow moves around the blade leading edge without any evident spanwise velocity component). This leads to a change in the flow deviation imposed by the blade wall with respect to the baseline rotor and, consequently, to a change in the blade-to-blade shock structure.

d) The higher efficiency induced by forward lean can be associated actually with a more favorable three-dimensional shock structure at the outer span (where the shock strength reaches its maximum value). Compared to the baseline rotor, all the forward leaned rotors gave a shock front more oblique to the incoming

flow in the peripheral region, reducing the local entropy generation and the aerodynamic shock losses, with a positive impact on the overall efficiency.

e) Sweep showed a considerable impact on the radial outward migration of fluid particles which takes place inside the blade suction side boundary layer after the interaction with the shock. Compared to the baseline rotor, the code predicted a reduction of the strength of such detrimental secondary flow when the blade is curved downstream and an increment when the blade is curved upstream.

f) The higher efficiency shown by the aft swept rotors (up to 0.8% around the design working condition) can be associated actually with the reduction of the secondary flow mentioned in previous point. The flow phenomenon is harmful because obstructs the boundary layer development in the streamwise direction, leading to a thickening of blade wakes; a reduction of its strength helps to reduce the entropy generation and the aerodynamic losses associated with blade wake development.

The impact of sweep and lean was investigated also from the structural point of view (the FEM package "ANSYS Structural" was used). The analyses showed that the newly-designed curved blades are more stressed than the baseline radially-stacked blade, due to the arising of bending stresses induced from the action of centrifugal loading. Being the centrifugal loading particularly strong in these machines, the increment in structural stresses due to blade curvature can be considerable. This does not mean that the concepts of sweep and lean can not be used in transonic rotors, but that the aerodynamic design of a swept and/or leaned transonic rotor blade must be developed also from the structural point of view.

Performance enhancement using blade curvature

Finally, it was observed that blade curvature could help to increase also the stall margin of a transonic compressor rotor. In particular, forward lean seems to be very helpful in

this goal, showing the possibility to improve the aerodynamic behavior of these machines in terms of both efficiency and rotor stability using blade curvature only. A promising three-dimensional shaped curvature was applied to the blade of Rotor 37 and evaluated numerically. The original blade was both forward leaned at the outer half span and swept at about 30% span. Lean was applied because hopeful from the aerodynamic point of view while sweep was given to examine the possibility of relieving the negative structural impact induced by lean, without inducing negative effects from the aerodynamic point of view. The numerical analysis led to the following results.

a) Thanks to the applied forward lean, the new blade showed effectively a positive impact on the tip endwall flow region toward low flow operating conditions, inducing flow stability and reducing the local aerodynamic losses. In particular, a less detrimental shock-tip clearance vortex interaction was observed compared to the baseline rotor, probably due to the more downstream shock location.

b) Compared to the baseline blade, the new blade gave an efficiency increment of about 1.2% near the design working condition along with a wider working range of about 50%.

c) The possibility to improve the aerodynamic behavior of a transonic compressor rotor using blade curvature and overcome the induced structural drawbacks was observed. In this case, the negative structural impact due to the application of lean was fairly relieved adding a proper sweep and without compromising the rotor performance.

Future researches

A verification of these numerical results with experiments is needed. A proper test facility to house a lower scale (under the conditions established by the dynamic similitude)

of baseline and optimized versions of Rotor 37 has been designed and is now under construction.

If these numerical results should be confirmed by experimental tests, other numerical investigations could be carried out to ascertain their validity on other transonic compressor rotor geometries, as well as to investigate their applicability on transonic fans.

Bibliography

Abdelhamid, H. F., Shreeve, R. P., and Hobson, G. V., 1998, "*Sweep in a Transonic Fan Rotor: Part 2. CFD and Stress Analyses*," ASME Paper 98-GU-579, presented at the 43rd ASME Gas Turbine and Aeroengine Technical Congress, Exposition and User's Symposium, June 2-5, 1998, Stockholm, Sweden.

AGARD, 1998, "*CFD Validation for Propulsion System Components*," Agard-ar-355.

Ahn, C. S. and Kim, K.Y., 2002, "*Aerodynamic-Design Optimization of an Axial Compressor Rotor*," ASME Paper GT-2002-30445.

Beheshti, B. H., Teixeira, J. A., Ivey, P. C., Ghorbanian, K., and Farhanieh, B., 2004, "*Parametric Study of Tip Clearance-Casing Treatment on Performance and Stability of a Transonic Axial Compressor*," ASME Journal of Turbomachinery, Vol 126, pp. 527-535.

Beheshti, B. H., Ghorbanian, K., Farhanieh, B., Teixeira, J. A., and Ivey, P. C., 2006, "*A New Design for Tip Injection in Transonic Axial Compressors*," ASME Paper GT2006-90007.

Benini, E., 2004, "*Three-Dimensional Multi-Objective Design Optimization of a Transonic Compressor Rotor*," AIAA Journal of Propulsion and Power, Vol. 20 – No. 3 2004, pp. 559-565.

Bergner, J., Hennecke, D. K., Hoeger, M., and Engel, K., 2002, "*Darmstadt Rotor No. 2 – part II. Design of leaned rotor blades*," ISROMAC 9, Honolulu, Hawaii, USA, February 10-14, 2002.

CFX-TASCflow Theory Documentation, 2000, AEA Technology Engineering Software Ltd., Version 2.10, Waterloo, Ontario, Canada.

Chima, R. V., 1998, "*Calculation of Tip Clearance Effects in a Transonic Compressor Rotor*," ASME Journal of Turbomachinery, Vol. 120 – No. 1 1998, pp. 131-140.

Cumpsty, N. A., 1989, "*Compressor Aerodynamics*," Longman Group UK Ltd.

Denton, J. D., 1993, "*Loss Mechanisms in Turbomachines*," ASME Journal of Turbomachinery, Vol. 115, pp. 621-656.

Denton, J. D., 1996, "*Lessons from Rotor 37*," 3rd ISAIF Meeding, Beijing.

Denton, J. D. and Xu, L., 1999, "*The Exploitation of Three-Dimensional Flow in Turbomachinery Design*," Proc. I Mech E, Vol. 213, pp. 125-137.

Denton, J. D. and Xu, L., 2002, "*The Effects of Lean and Sweep on Transonic Fan Performance*," ASME Paper GT-2002-30327.

Fritsch, G., Hoeger, M., Blaha, C., and Bauer, D., 2000, "*Viscous Three-Dimensional Simulation of Transonic Compressor Stage on Parallel Hardware*," AIAA Journal of Propulsion and Power, Vol. 16, pp. 388-396.

Hah, C. and Reid, L., 1992, "*A Viscous Flow Study of Shock-Boundary Layer Interaction, Radial Transport, and Wake Development in a Transonic Compressor*," ASME Journal of Turbomachinery, Vol. 114, pp. 538-547.

Hah, C., Puterbaugh, S. L., and Wadia, A. R., 1998, "*Control of Shock Structure and Secondary Flow Field Inside Transonic Compressor Rotors Through Aerodynamic Sweep*," ASME Paper 98-GT-561.

Hah, C. and Loellbach, J., 1999, "*Development of Hub Corner Stall and its Influence on the Performance of Axial Compressor Blade Rows*," ASME Journal of Turbomachinery, Vol. 121, pp. 67-77.

Hathaway, M. D., 2000, "*An Improved Self-Recirculating Casing Treatment Concept for Enhanced Compressor Performance*," 22nd Army Science Conference, Baltimore, Maryland, Dec. 11-13, 2000.

Hathaway, M. D., 2002, "*Self-Recirculating Casing Treatment Concept for Enhanced Compressor Performance*," ASME Paper GT2002-30368.

Hofmann, W. and Ballmann, J., 2002, "*Tip Clearance Vortex Development and Shock-Vortex-Interaction in a Transonic Axial Compressor Rotor*," AIAA Paper 2002-0083.

Hutchinson, B. R. and Raithby, G. D., 1986, "*A Multigrid Method Based on Additive Correction Strategy*," Numerical Heat Transfer, Vol. 9, pp. 511-537.

Jang, C. M., Samad, A., and Kim, K. Y., 2006, "*Optimal Design of Swept, Leaned and Skewed Blades in a Transonic Axial Compressor*," ASME Paper GT2006-90384.

Kablitz, S., Hennecke, D. K., Passrucker, H., and Engber M., 2003, "*Experimental Analysis of the Influence of Sweep on Tip Leakage Vortex Structure on an Axial Transonic Compressor Stage*," ISABE-2003-1226.

Launder, B. and Spalding, D., 1974, "*The Numerical Computation of Turbulent Flow*," Comp. Math. in Appl. Mech. Eng., Vol. 3, pp. 269-289.

Menter, F. R., 1994, "*Two-Equation Eddy-Viscosity Turbulence Models for Engineering Applications*," AIAA-Journal, Vol. 32, pp. 1598-1605.

Moore, R. D. and Reid, L., 1980, "*Performance of Single-Stage Axial Flow Transonic Compressor with Rotor and Stator Aspect Ratios of 1.19 and 1.26, Respectively, and with Design Pressure Ratio of 2.05*," NASA TP 1659.

Povinelli, L. A., 1997, "*Current Lewis Turbomachinery Research: Building on our Legacy of Excellence*," Proc. 13th ISABE Conference, Chattanooga.

Qing, Y., Qiushi, L., and Ling, L., 2002, "*The Experimental Researches on Improving Operating Stability of a Single-Stage Transonic Fan*," ASME GT-2002-30640.

Rabe, D. C. and Hah, C., 2002, "*Application of Casing Circumferential Grooves for Improved Stall Margin in a Transonic Axial Compressor*," ASME GT-2002-30641.

Reid, L. and Moore, R. D., 1978, "*Design and Overall Performance of Four Highly Loaded, High-Speed Inlet Stages for an Advanced High-Pressure-Ratio Core Compressor*," NASA TP 1337.

Strazisar, A. J., Bright, M. M., Thorp, S., Culley, D. E., Suder, K. L., 2004, "*Compressor Stall Control Through Endwall Recirculation*," ASME Paper GT2004-54295.

Suder, K. L., 1998, "*Blockage Development in a Transonic, Axial Compressor Rotor*," ASME Journal of Turbomachinery, Vol. 120, pp. 465-476.

Suder, K. L. and Celestina, M. L., 1996, "*Experimental and Computational Investigation of the Tip Clearance Flow in a Transonic Axial Compressor Rotor*," ASME Journal of Turbomachinery, Vol. 118, pp. 218-229.

Suder, K. L., Chima, R. V., Strazisar, A. J., and Roberts, W. B., 1995, "*The Effect of Adding Roughness and Thickness to a Transonic Axial Compressor Rotor*," ASME Journal of Turbomachinery, Vol. 117, pp. 491-505.

Suder, K. L., Hathaway, M. D., Thorp, S. A., Strazisar, A. J., and Bright, M. B., 2001, "*Compressor Stability Enhancement Using Discrete Tip Injection*," ASME Journal of Turbomachinery, Vol. 123, pp. 14-23.

Thompson, D. W., King, P. I., and Rabe, D. C., 1997, "*Experimental Investigation of Stepped Tip Gap Effects on the Performance of a Transonic Axial-Flow Compressor Rotor*," ASME GT-97-7.

Van Zante, D. E., Strazisar, A. J., Wood, J. R., Hathaway, M. D., and Okiishi, T. H., 2000, "*Recommendations for Achieving Accurate Numerical Simulation of Tip Clearance Flows in Transonic Compressor Rotors*," ASME Journal of Turbomachinery, Vol. 122, pp.733-742.

Wadia, A. R. and Copenhaver, W. W., 1996, "*An Investigation of the Effect of Cascade Area Ratios on Transonic Compressor Performance*," ASME Journal of Turbomachinery, Vol. 118, pp. 760-770.

Wadia, A. R., Szucs, P. N., and Crall, D. W., 1998, "*Inner Workings of Aerodynamic Sweep*," ASME Journal of Turbomachinery, Vol. 120, pp. 671-682.

Wilke, I. and Kau, H.-P., 2004, "*A Numerical Investigation of the Flow Mechanisms in a HPC Front Stage with Axial Slots*," ASME Journal of Turbomachinery, Vol.126, pp. 339-349.

Wood, J. R., Strazisar, A. J., and Simonyi, P. S., 1987, "*Shock Structure Measured in a Transonic Fan using Laser Anemometry*," AGARD CP-401.

Yamaguchi, N., Tominaga, T., Hattori, S., and Mitsubishi, T., 1991, "*Secondary-Loss Reduction by Forward-Skewing of Axial Compressor Rotor Blading*," Proceedings of 1991 Yokohama International Gas Turbine Congress, Vol. 2.

Yi, W., Huang, H., and Han, W., 2006, "*Design Optimization of Transonic Compressor Rotor using CFD and Genetic Algorithm*," ASME Paper GT2006-90155.